The Low Energy Phenomenology of a Dark Force

CHRISTOPHER JAMES WALLACE

University of Durham

Institute for Particle Physics Phenomenology

Department of Physics

The Low Energy Phenomenology of a Dark Force

Chris J. Wallace

Primary Supervisors Prof. Jörg Jäckel and Dr. Michael Spannowsky

Secondary Supervisor Dr. Simon A. Gardiner

Chris J. Wallace

The Low Energy Phenomenology of a Dark Force

December 2014

Examiners: Dr. Steve Abel and Dr. Stephan Huber

Supervisors: Prof. Jörg Jäckel, Dr. Michael Spannowsky
and Dr. Simon A. Gardiner

University of Durham

Institute for Particle Physics Phenomenology

Ogden Centre for Fundamental Physics

Department of Physics

Durham

DH1 3LH

Abstract

This thesis investigates an area of beyond the Standard Model (BSM) phenomenology associated with the presence of additional light, "weakly interacting slim particles" (WISPs). Particular attention is given to the hidden photon, the gauge boson associated with an additional U(1) gauge group that mixes kinetically with hypercharge.

The theoretical foundation of the interactions studied lies in effective field theory, and the first part of the thesis investigates a so-far untested aspect of effective theories, namely effective non-locality in particle propagation.

There are no observable effects of hidden photons if they are massless. We investigate the impact on experimental signatures in the case that the hidden photon gets its mass during compactification from a higher dimensional theory.

WISPs make good dark matter candidates, and are especially compelling in light of the lack of observation of heavy WIMP ("weakly interacting massive particle") dark matter. Nonetheless, it is shown that if WIMP dark matter is composed of a Dirac fermion that couples to the SM only through a pseudoscalar, indirect detection may be our only experimental window, and that it may already be appearing as a gamma ray excess at the Galactic Centre.

There is considerable interest in dark matter searches at beam dump facilities, in particular for light dark matter coupled through a similarly light mediator particle. We investigate this set up in the context of the E613 beam dump experiment. Owing to the light mediator, the low-Q^2 kinematic region of deep inelastic scattering is especially important. We present a new treatment of dark particle scattering in this region via a light vector mediator (such as a hidden photon), and find that it enhances constraints.

The original research constituting this thesis has been previously presented in [1–4].

Declaration

This thesis was composed entirely by the author, and presents work performed solely by the author and his collaborators, unless otherwise indicated. No part of the author's work herein has been submitted as part of the requirement for any other degree at any institution.

Durham, December 2014

Chris J. Wallace

All Chapter quotations are from Heart of Darkness by Joseph Conrad.

Acknowledgements

Thanks to:

Jörg for not abandoning me. Michael for adopting me. Both for teaching me, not only about physics. Simon for enthusiasm for our weird little project. Hayley, Mam, Dad, Phil for love and support. More friends than I can name. Durham University. Heidelberg University. Silvia & Ruth for understanding and guidance in that difficult first year. My fellow conspirators: Céline Bœhm, Matt Dolan, Holger Gies, Chris McCabe, Davison Soper, Sabyasachi Roy and Tim Tait. The community at the Patras meetings – long may they continue.

Without these people, I would not have completed this thesis.

Dedication

To the memory of Sydney Oliver Craggs.

Contents

1 Introduction

> *There's no initiation either into such mysteries. He has to live in the midst of the incomprehensible . . .*
>
> **— Marlow**

1.1 Motivation

The high energy frontier of particle physics has expanded enormously in the last few years with the Run 1 LHC results. A new scalar boson has been discovered and looks alarmingly like a "vanilla" Standard Model Higgs boson [5–7]. The guiding symmetry principles by which the SM is constructed look as strong as ever and there is seemingly a complete lack of any Beyond the Standard Model (BSM) physics at $8\,\text{TeV}$.

It is nonetheless clear that neither experimental nor theoretical efforts have yet unearthed the full story. A handful of the problems that the Standard Model does not address are catalogued below.

- **Gravity**: While potential UV completions of the Standard Model are numerous, there is no theoretical consensus on the behaviour of gravity at Planck energies. This sits uncomfortably with the description of all other observed fundamental forces as gauged quantum field theories theories.

- **The hierarchy problem**: The difference between the Planck scale at which the strength of gravity becomes comparable to that of the other known fundamental forces, and the electroweak scale physics we commonly observe is extremely large, spanning more than ~ 16 orders of magnitude. An unnaturally precise cancellation of high scale physics would be required in order that a scalar boson coupling to the Standard model fermions could acquire a vacuum expectation value at the weak scale, and yet this is what we observe.

- **Dark energy**: Approximately $\sim 68\%$ of the observed total energy density is not accounted for by matter [8]. A massive, unknown source of energy is required to power the observed expansion of the Universe.

- **Dark matter**: Galactic rotation curves, structure formation, observations of the Bullet cluster, baryon acoustic oscillations and numerous other phenomena all point to the fact that the remaining $\sim 32\%$ of the energy density is composed of roughly 6 times more matter than we observe in baryonic matter [8], and that furthermore, the additional matter *cannot* be baryonic.

- **Neutrino masses**: Neutrino masses, bounded to be non-zero by observation of flavour oscillations, are not accounted for in the Standard Model. The essential nature of neutrinos is not known – they could be either Majorana or Dirac fermions – but it is quite possible that their masses originate with BSM physics.

- **The strong CP problem**: The Lagrangian describing QCD permits a CP violating term $\mathcal{L}_{\not{CP}} \propto \theta G^{\mu\nu}\tilde{G}_{\mu\nu}$, yet no CP violation is observed in the strong sector. One attempt to explain the unnatural smallness of θ is provided by the Peccei-Quinn symmetry, which gives rise to QCD axions. Further discussion of this is given below.

- **The muon anomalous magnetic moment**: The anomalous magnetic moment of the muon, a_μ, is truly anomalous, disagreeing with the SM predicted value by $\sim 3\,\sigma$ [9]. It is possible to explain this with the introduction of a new boson, such as the hidden photon we discuss.

Owing to the remarkable precision with which the SM accounts for observations of nature, it seems worthwhile to attempt to explain the above phenomena using the same principles and construct new theories (to say, particles and forces) in the language of gauge theory. Naturally doing so means there must be some interaction between any new theory and the existing SM: it is a pillar of theoretical particle physics that the Lagrangian density[1] describing a theory ought to include all gauge and Lorentz invariant terms – including any that mix old physics and new. Indeed if we are to solve any of the outstanding issues in physics, we had better ensure that our new theory interacts with existing physics – if not, it cannot be affecting the results of observations. Whether or not this interaction is observable is determined by nature, though one may be pragmatic and focus on those theories that have some hope of observation[2]. The raison d'être of beyond the Standard Model physics then is to provide an explanation, in terms of fundamental particles, of results for which the SM does not account, without perturbing the phenomenology of the SM sufficiently to be in conflict with other experimental results.

[1] Henceforth, we conform to the general convention of referring to the Lagrangian density simply as the Lagrangian.

[2] For example, it is possible that dark matter interacts with baryonic matter *only* gravitationally, in which case the prospect of an experimental discovery vanishes. Of course this does not mean that one should not search for non-gravitational interactions of dark matter experimentally.

While all the listed phenomena, and others, have engendered interesting physics, probably the problem that has attracted the most attention is dark matter, to which we turn now. First we present some preliminaries, followed by a general outline of the searches for dark matter, which are related by a complementarity exhibited by 4-particle scattering processes. The dominant paradigm in particle dark matter has long been that of the weakly interacting massive particle (WIMP) – we present some theory relating to this paradigm and motivate the introduction of an alternative: WISPs, or weakly interacting slim particles. After introducing WISPs and the surrounding theory, we turn to the experimental hunt for this kind of particle, in particular focusing on models with a hidden photon, which is central to some of the work in this thesis.

1.2 Dark matter

Substantial evidence has accrued that the baryonic matter in the Universe cannot be a full account of the total energy density. Based on observations of the gravitational interactions of nearby galaxies, and accepting that gravity persists unmodified at galactic scales, approximately five times the baryonic energy density must be added from an additional, unknown, source to reconcile theory and observation. No such source is visible to astrophysics (except through gravity) and SM neutrinos are thoroughly ruled out as the principal component (or even a large one) of the missing energy density, being far too relativistic to allow structure formation. A promising direction is to consider the missing component to be some sort of non-luminous *dark* matter, which interacts only weakly with the SM.

1.2.1 Preliminaries

While in general very little is known about dark matter, there are some particular properties to which it must conform (within the generally established framework of ΛCDM cosmology). Let us briefly consider the role of dark matter in the thermal history of the Universe.

The early Universe may be usefully described in the language of thermodynamics and we may write a Boltzmann equation for the number density of a single simple WIMP species,

$$\frac{dn}{dt} = -3Hn - \langle \sigma v \rangle_{\text{ann.}} (n^2 - n_{\text{eq.}}^2). \tag{1.1}$$

The Hubble parameter, $H = \dot{a}/a$, measures the expansion rate of the Universe, and a is the scale factor describing the relative size of the Universe (ranging from 0 at the Big Bang to 1 in the present day). It is defined by the Friedmann-Robertson-Walker (FRW) metric for a homogeneous and isotropic Universe, which, schematically, has line element $ds^2 = dt^2 - a^2(t)d\vec{x}^2$. The expression $\langle\sigma v\rangle_{\text{ann.}}$ indicates the cross-section multiplied by the the Møller velocity (i.e. relative velocity between annihilating particles[3]) and thermally averaged over a Maxwellian distribution, where σ is the effective annihilation cross-section for two DM particles to two SM particles. n is the present time number density of DM particles, and $n_{\text{eq.}}$ the equilibrium number density ($n_{\text{eq.}} = g(mT/2\pi)^{3/2}\exp(-m/T)$ for a non-relativistic Maxwell-Boltzmann distribution). Then the first term on the r.h.s. of Eq. (1.1) encodes the dilution of the dark matter number density due to the expansion of the Universe, and the second term the effect of dark matter annihilating into SM particles.

With the aim of calculating properties of the present day Universe, one important quantity is the interaction rate per particle,

$$\Gamma = n\sigma v. \tag{1.2}$$

We can compare this to the Boltzmann equation above and see that while the expansion rate of the Universe is approximately equal the interaction rate of a particle species, $H \sim \Gamma$, the particles are in thermal equilibrium with the Universe. When H becomes substantially larger than Γ, particle freeze-out occurs, corresponding to the particles no longer being likely to interact due to their rapidly increasing spatial separation.

Observation informs us that the Universe is, to a very good approximation, flat. A very important constraint on dark matter arises from this, as it must decouple to leave a sufficient density that Universe is not convex, but must also not be over dense, which would result in a concave Universe. The density parameter Ω is defined,

$$\Omega \equiv \frac{\rho}{\rho_{\text{crit.}}} = \frac{8\pi G}{3H^2}\rho, \tag{1.3}$$

where ρ is the density, $\rho_{\text{crit.}}$ is the critical density for a flat (Euclidean) Universe, and the r.h.s of the equation arises from Einstein's field equations for a FRW metric (G is Newton's gravitational constant). Note that the density parameter given above accounts for *all* matter, baryonic and dark, in the Universe (as well as the dark energy that is powering expansion), but may be considered component-wise by the insertion of the appropriate density ρ.

[3] $v = v_{\text{Møl}}$ is defined as $v_{\text{Møl}} = \frac{\sqrt{(\vec{v}_1-\vec{v}_2)^2-(\vec{v}_1\times\vec{v}_2)^2}}{1-\vec{v}_1\cdot\vec{v}_2}$, such that the annihilation rate per unit velocity and time $\frac{dN}{dtdV} = \sigma v n_1 n_2$ is frame independent.

The density parameter is often quoted multiplied by the Hubble parameter squared, Ωh^2 ($h = (H_0/100)\,\mathrm{km\,s^{-1}\,Mpc^{-1}}$, where H_0 is the present time Hubble parameter). Then $\Omega h^2 \sim 0.45$ is the density parameter of a flat Universe. Formally one must solve the Boltzmann equation to find an expression for the relic density of dark matter. However, accounting for the measured energy density, a useful approximation exists for a thermal WIMP [10],

$$\Omega_{\mathrm{DM}} h^2 = \frac{m_{\mathrm{DM}} n_{\mathrm{DM}}}{\rho_{\mathrm{crit.}}} \simeq \frac{3 \times 10^{-27} \mathrm{cm^3\,s^{-1}}}{\langle \sigma v \rangle_{\mathrm{ann.}}}. \tag{1.4}$$

where $\rho_{\mathrm{crit.}} \simeq 10^{-5}\, h^2\,\mathrm{GeV\,cm^{-3}}$ and m_{DM} and n_{DM} are the WIMP mass and number density respectively. Note though that the above result is subject to several assumptions. For example, it requires modification if there are any species in the early Universe that interact with the WIMP and are also approximately degenerate in mass with it, due to the resonant effect of co-annihilations [11].

With the above considerations in mind, we may make a few generic statements about dark matter that we expect to hold true relatively model independently.

- It must interact sufficiently weakly with the SM to have thus far escaped all but gravitational detection (modulo some potential astrophysical "hints" discussed later). The best current limits on WIMPs from direct detection experiments are shown in Figs. 1.2 and 1.3.

- To allow structure formation, the dominant component of dark matter must be cold (non-relativistic). In our galaxy, this has an average local velocity in the region of $\bar{v} \sim 200 - 300\,\mathrm{km/s}$ relative to Earth, subject to a significant uncertainty [12, 13].

- The particle comprising dark matter must be stable w.r.t SM decays on cosmological time scales, having a lifetime $\tau_{\mathrm{DM}} \gtrsim \mathcal{O}(10^{17} s)$.

- The local density of dark matter, at the Sun's location in the Galaxy, is $\rho_\odot \sim 0.4\,\mathrm{GeV/cm^3}$ [14, 15].

- The relic density of cold dark matter is $\Omega h^2 \sim 0.12$, approximately 27% of the total energy density of the Universe [8].

As mentioned above, a popular paradigm in constructing models of Cold Dark Matter (CDM) is that of the Weakly Interacting Massive Particle (WIMP). It turns out that for a single species of thermally produced particles with a mass in the 10s to 1000s of GeV range and a weak scale cross section, the relic abundance matches that experimentally observed with very little to no fine tuning. In order to do so, the thermally averaged cross section for pair annihilation into SM particles must fall in the region of $\langle \sigma v \rangle_{\mathrm{ann.}} \sim 3 \times 10^{-26} \mathrm{cm^3 s^{-1}}$, based on the estimate in Eq. (1.4).

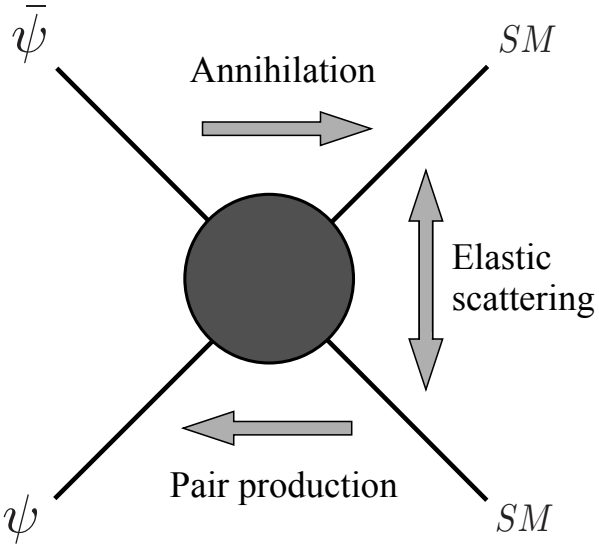

Fig. 1.1.: Schematic $2 \to 2$ processes, where ψ and $\bar{\psi}$ represent some dark matter field and its conjugate (it may be self-conjugate, $\psi = \bar{\psi}$).

We'll now turn to experimental and theoretical approaches to dark matter.

1.2.2 Experimental approaches

Based on the known interactions of the SM and the requirements for gauge and Lorentz invariance of the Lagrangian, it is not unreasonable to expect particle dark matter (hence simply "dark matter") to scatter in a $2 \to 2$ process featuring two SM particles and two dark particles. In such a scattering process there arises a natural complementarity between search techniques, paralleling a crossing symmetry in the process itself. Fig. 1.1 shows a sketch of the scattering process, which may proceed along three directions, corresponding to SM-dark matter scattering, DM-DM annihilation into SM and pair production of DM particles via SM-SM annihilation. The blob in the sketch represents some interaction which could, for example, be a 4-point effective vertex resulting from the presence of a heavy mediator particle. These three processes are vital to the experimental search for dark matter, each corresponding to one of the three canonical search techniques: direct detection (scattering), indirect detection (annihilation) and collider studies (pair production). We'll discuss the salient features of each in turn here.

Direct detection: $\mathrm{DM} + \mathrm{SM} \rightarrow \mathrm{DM} + \mathrm{SM}$

From observations of galactic dynamics, we know that dark matter is clustered around the Milky Way in a roughly spherical distribution [16]. The Earth's rotation around the Sun must then necessarily create some relative motion between the dark matter and the Earth, and we may search for an annual modulation in the signal of a suitable detection experiment. While there is some uncertainty in the absolute velocity distribution of galactic dark matter relative to Earth, this uncertainty is much reduced in the annual modulation signal, since the unknown velocities cancel over the course of one Solar orbit [17].

Several experiments are underway to search for this phenomenon, and there exists a pronounced tension between their reported results and those looking directly for WIMP interactions. The most stringent constraints on the interactions of potential WIMPs (currently from the LUX collaboration [18], which is directly searching for dark matter interactions via nuclear recoil) rule out the claimed annual modulation from the CoGeNT [19] and DAMA [20] collaborations. The CDMS experiment finds no sign of an annual modulation [21], but does report three WIMP candidate events with an expected background of only $0.41^{+0.20}_{-0.08}(stat.)^{+0.28}_{-0.24}(syst.)$ events, resulting in the preferred region shown in Fig. 1.2. CRESST also detected candidate events, resulting in the corresponding preferred region [22]. There have been numerous attempts to resolve the conflict, and there exist proposals for several non-exotic (SM) explanations of the apparent annual modulation [23, 24][4].

The current generation of direct detection experiments operate on the basis of nuclear recoil, which limits their region of sensitivity to masses of a GeV and above (though this can be extended to lighter masses, $\mathcal{O}(\text{few MeV})$ by looking for ionisation [29]). In the xenon-based detectors presently providing the most sensitive probes for spin independent interactions, a DM particle striking a nucleus with sufficient energy in an elastic collision causes both scintillation and ionization. The time delay in detection (with photomultiplier tubes) between the photons created by the initial scintillation (the "S1" signal) and the later scintillation of the ions ("S2"), which are accelerated, allows for positional and directional determination of the initial DM interaction.

The constraints on the DM-nucleon interaction cross-section resulting from this method have the advantage of being relatively model agnostic. Typically, the interaction is described by an effective theory that integrates out the particle mediating the WIMP-nucleon interaction.

[4] All of which are refuted by the DAMA collaboration [25–28].

Due to the very low energy of the collisions (WIMPs in the halo are non-relativistic, and recoil energies are on the order of 10s of keV), and correspondingly low 4-momentum exchange, the mass of the mediator need not be too high in order that it is not resolved: even $\mathcal{O}(\gtrsim \text{GeV})$ is safe.

The cross-section for WIMP scattering depends strongly on whether the interaction is spin dependent or not. In the case that it is, for example for interactions mediated by pseudoscalar exchange, the cross-section is suppressed by the non-relativistic velocity of the WIMPs, and the constraints from direct detection experiments are weakened by a factor of $v^2 \sim 10^{-6}$ ($c = 1$) relative to the spin independent case. We explore the difference between spin dependent and spin independent scattering further in Chapter 4.

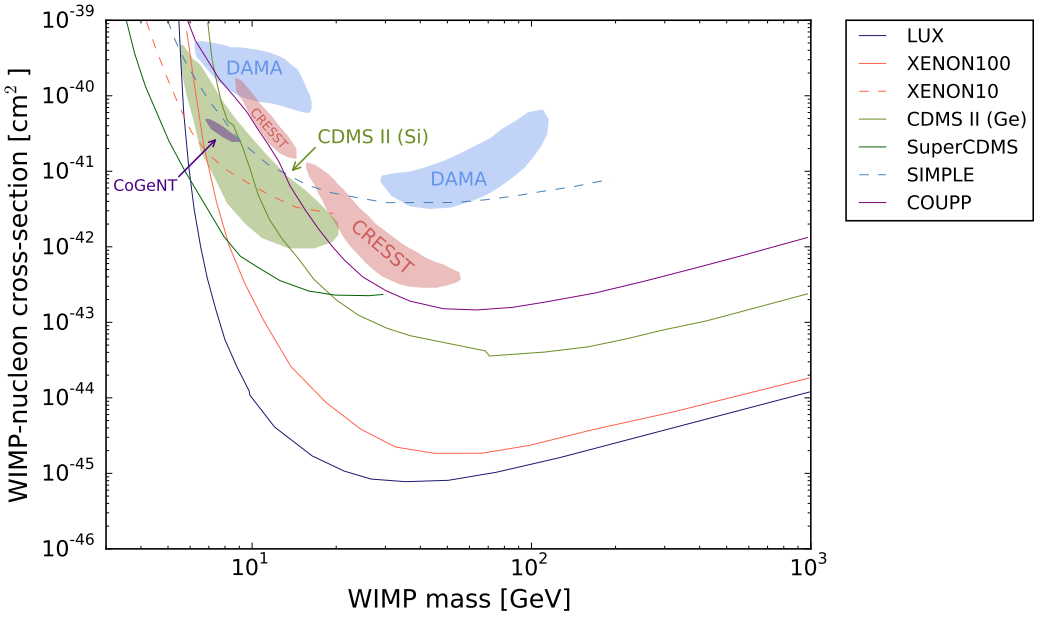

Fig. 1.2.: Exclusion limits on spin independent scattering of WIMPs with nucleons. Isospin symmetry between protons and neutrons is assumed. Combination given in [30], showing the constraints of [22, 31–41] with the more recent LUX [18] and SuperCDMS constraints [42] added.

Indirect detection: $\text{DM} + \text{DM} \to \text{SM} + \text{SM}$

Should the WIMP interact with the Standard Model through any means that is not gravitational, there are numerous astrophysical environments that make for promising hunting grounds. In particular, the galactic potential well, strongest in the centre, can act as an amplifier for dark matter annihilations (the rate grows with the square of the density, $\Gamma_{\text{ann.}} \propto \rho^2_{\text{DM}}/m^2_{\text{DM}}$), the products of which can be searched for in terrestrial and space based

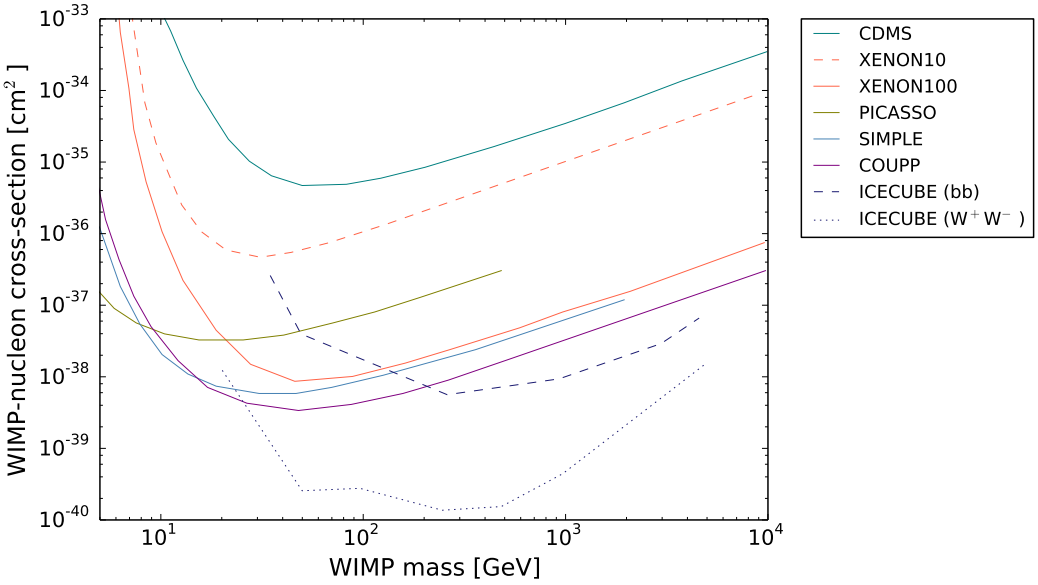

Fig. 1.3.: Exclusion limits on spin dependent WIMP scattering with a proton [34, 35, 43–46]. The results of IceCube are model dependent, representing limits on annihilation to the indicated particle pairs. The neutron limits are similar [30], though XENON100 is strongest, and IceCube present no constraint.

gamma- ray telescopes, positron and anti-proton telescopes and neutrino telescopes [16]. The annihilation products of dark matter are model dependent, but commonly result in a continuous photon spectrum from secondary decays/annihilations and synchrotron radiation from the propagation of charged annihilation products.

If the dark matter annihilates through an on-shell mediator, this would give rise to a distinctive peak in the photon spectrum. A strong line with no astrophysical explanation would be a smoking gun signal of dark matter annihilating into photons. Otherwise, one may expect some particle abundances to be enhanced in high density regions of the galaxy, corresponding to the product of dark matter annihilations.

There are several such astrophysical "hints" of dark matter, including a $\sim 3.5\,$keV line in the x-ray spectrum of some galaxy clusters [47], an excess of $511\,$keV gamma rays originating in the galactic central bulge [48], an overall gamma ray excess from the galactic centre [49], a $\sim 130\,$GeV line from the galactic centre [50] and an anomalously high positron abundance in cosmic radiation [51]. The soft x-ray spectrum of the Earth was recently reported to show seasonal variation, consistent with the conversion of meV mass Solar axions [52].

Further details of indirect detection – in particular regarding the observation of a galactic centre excess [49] by the Fermi satellite's Large Area Telescope – will be discussed in Chapter 4.

Collider: $\mathrm{SM} + \mathrm{SM} \to \mathrm{DM} + \mathrm{DM}$

The LHC has pushed the frontier of understanding to a new mass scale, and will do so again in coming years. While the LHC is not responsible for the highest energy interactions ever observed (that title is held by cosmic rays), it is the highest luminosity controlled source of TeV scale collisions by a very large margin. When searching for dark matter at or below TeV masses, one could expect that there may be signatures at the LHC.

The standard LHC search for dark matter particles (at least, WIMPs) has long been the monojet [53–55], whereby a single jet appears in the detector with no corresponding particle detection to balance transverse momentum, through interactions of the type $pp \to \bar{\chi}\chi + \mathrm{jet}$. Example Feynman diagrams for the process are shown in Fig. 1.4. Another promising channel for dark matter searches is a single photon plus missing transverse energy, or monophoton events [56, 57]. The two searches share a common operating principle. BSM particles must be weakly interacting in order to have evaded detection, so once produced, they are unlikely to interact again inside the detector, unless they decay near instantly to SM particles. This signal has a neutrino background, a feature common to dark matter searches, since the neutrino is also extremely weakly interacting and can bypass shielding designed to isolate detectors from SM particles. The ATLAS and CMS detectors are both multipurpose, and other searches for exotic phenomena will be made reference to throughout this thesis.

For some models of dark matter, LHC searches are competitive with, or exceed, the exclusion limits of direct detection experiments. However, they are reliant upon an effective 4-point interaction which is not valid in all regimes, and fails in particular if the particle mediating the interaction of the DM and SM particles is light. We return to this point below.

Complementary to the LHC, there are also a host of experiments employing a single particle beam (p or e^-) incident upon fixed targets, whose results may be adapted to place constraints on the interactions of dark particles [58–63]. The centre of mass energy of fixed target experiments scales as $E_{\mathrm{CoM}} = \sqrt{2E_{\mathrm{beam}}m_p}$ (where $m_p \sim 1\mathrm{GeV}$ is the proton mass), meaning that even with a high energy beam, such facilities will never compete with the CoM energy

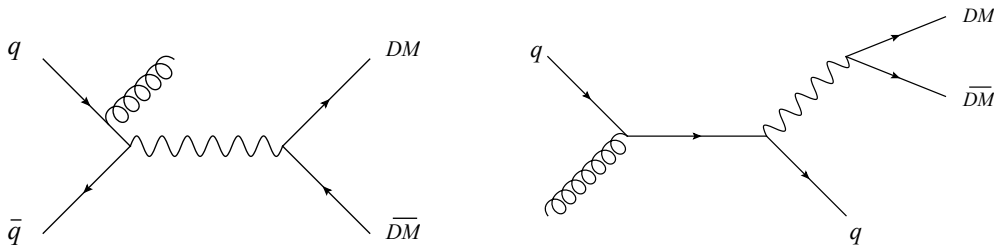

Fig. 1.4.: Simple monojet processes of the type that could contribute to an LHC signal. The DM particles (which here interact with quarks through a vector mediator) do not interact with the detector and contribute to a missing transverse energy signal, whereas the radiated gluon and final state quark form QCD jets.

attainable at the LHC, which scales linearly with the beam energies. The great advantage of fixed target facilities is in the large luminosity and well controlled backgrounds. The latter may be achieved due to the large spatial separation of the target and detector, allowing, for example, magnetic shielding to filter charged particles out of the beam. This makes them uniquely suited to neutrino production, but also production of any other stable, neutral particles with the appropriate couplings. In Chapter 5, we will extend the reach of the Fermilab E613 proton beam dump experiment by a detailed treatment of dark particle scattering, particularly considering QCD effects at low momentum transfer.

1.2.3 Theoretical approaches

Recent searches for dark matter, in particular at the LHC, have employed effective field theories for a hypothesized $2 \to 2$ interaction [64], as schematically shown in Fig. 1.1. These methods rely upon the assumption that the mediating particle – for example a new vector boson associated with a hidden U(1) gauge group – is heavy, i.e. its mass is sufficiently above the interaction energy (where sufficient is determined in part by how accurate we demand the predictions of the effective theory to be).

The canonical example of an effective field theory, Fermi's theory of weak interactions, includes a four-fermion vertex, where we now know a W boson mediates the interaction. The effective Lagrangian for charged current neutrino scattering is,

$$\mathcal{L}_{\mathrm{CC}} = 2\sqrt{2} G_F \left(\bar{\ell}\gamma^\mu P_L \nu\right) \left(\bar{u}\gamma_\mu P_L d\right) + \mathrm{h.c.} \tag{1.5}$$

P_L is the left projection operator, $P_L = (1 - \gamma_5)/2$, reflecting the chiral nature of weak interactions. When the full theory is resolved, we realise that the coupling, G_F, the Fermi constant, is inversely proportional to the W boson mass squared, $G_F = \frac{g^2}{2^{5/2}} \frac{1}{m_W^2}$, where g

is the weak coupling constant. The effective coupling constant G_F actually encodes the effect of the W boson propagator in the limit of small momentum compared to the W boson mass.

Our modern understanding of the SM as itself an effective theory suggests that it is possible that even this is not a complete description of the same scattering process, but the effects of additional dynamics are simply too small to notice at currently accessible energy scales.

While there are undeniably some desirable features in this framework, in particular the easy classification of all combinations of vector, scalar, axial-vector, etc. dark matter particles and interactions, the utility of such models is contingent upon the interaction originating at a sufficiently high scale.

Schematically, the Lagrangian term for an effective 4-point interaction between Dirac fermions ψ and χ looks like,

$$\mathcal{L} \supset \frac{g^2}{\Lambda^2}\bar{\psi}\Gamma_1\psi\bar{\chi}\Gamma_2\chi, \tag{1.6}$$

where Λ is the scale associated with new physics. The Γ encode the nature of the interaction between the Dirac field bilinears i.e. the properties of the mediator particle that has been integrated out in the effective Lagrangian:

$$\Gamma_{\{1,2\}} = \begin{cases} 1 & \text{scalar} \\ i\gamma^5 & \text{pseudoscalar} \\ \gamma^\mu & \text{vector} \\ \gamma^\mu\gamma^5 & \text{axial vector} \\ \sigma^{\mu\nu} & \text{tensor} \end{cases} \tag{1.7}$$

and it is implicit that the Lorentz indices are contracted across the two field bilinears in the Lagrangian. Mixed axial and non-axial interactions, for example $\psi\gamma_\mu\bar{\psi}\chi\gamma^\mu\gamma^5\bar{\chi}$, where Γ_1 is vector-like and Γ_2 is axial in nature are permitted, though such interactions would violate CP symmetry. In [64], 24 possible operators coupling Dirac fermions and real and complex scalars to SM quarks and gluons are enumerated, and have since been adopted by both CMS [65] and ATLAS [66] in their respective presentations of dark matter search results. While the advantage of a unified framework and notation is clear, there are limitations to this approach [67], not least of which is that it does not encompass the scenario in which mediator masses are lighter than TeV scale. There are several motivations to consider an alternative framework.

As illustrated above with the example of the weak force, 4-point interactions of the sort described by Eq. (1.6) originate from the elimination of a mediator particle from a theory. In order that the effective theory is valid at LHC energies, the scale Λ suppressing the interaction must be sufficiently large compared to the momentum exchange that the latter may be ignored in the propagator for the removed mediating particle. The suppression by a potentially very high scale Λ lowers the cross section for processes involving the operator, but it is possible that this is compensated by a high value of the coupling constant. Owing to the large momentum exchange interactions at the LHC, one can find that even for the maximum allowed perturbative coupling ($g \sim \sqrt{4\pi}$ for an expansion in α), the suppression scale must be so large that the resulting cross sections are too small to result in a sufficient event rate. Additionally, in the case that the mediator is light, such effective operators may actually underestimate the cross section by not accounting for resonant production of dark particles via on-shell mediators.

That dark matter can be detected at the LHC at all is not a requirement nature imposes. However, in the case of thermal WIMPs, if the mediator is heavy and the coupling is not too large the dark matter may not annihilate efficiently enough, overclosing the Universe (i.e. resulting in a much higher than observed relic density), so there is reason to hope that the LHC may yet discover a candidate. However, as discussed in Chapter 4, there are viable models of even light particle dark matter that could be accessible to us only through their astrophysical signs at present. Fortunately, we will see below that the WIMP paradigm is not the only candidate.

The alternative approach: simple models

The great advantage of the effective theories, in the region where they are valid, is that they are relatively model independent (modulo the assumptions necessary to allow the use of effective theories). If one introduces lighter mediators, the interaction may be resolved, and one must specify the theory in greater detail[5].

Interest in simple models has recently been revived in light of the above criticisms of applying a purely effective operator approach [68–70]. One complication of resolving a more fundamental theory, i.e. replacing the 4-point interaction with space-time-separated 3-point

[5]Note that the result is likely still to be an effective field theory, but the scale at which the effective theory is not valid has been raised. It is the modern view that any field theory, at least below the Planck scale, may be considered fundamental only in so far as its short distance interactions have not been probed

interactions connected by an intermediate state, is the introduction of new parameters. In the effective view, the unknown couplings and mass scale by which an operator is suppressed may be combined into a single Wilson coefficient. This is not the case if the interaction is resolved (though couplings may still be combined multiplicatively if the mediator width is unimportant), but it is nonetheless possible to characterise some interaction types with relatively few parameters.

The Lagrangians specified in [68] give simple models of vector and axial vector mediated scattering of dark Dirac fermions,

$$\begin{aligned}\mathcal{L}_{\text{vector}} &\supset g_{\text{DM}} V_\mu \bar{\chi}\gamma^\mu \chi + \sum_q g_q V_\mu \bar{q}\gamma^\mu q \\ \mathcal{L}_{\text{axial}} &\supset g_{\text{DM}} \tilde{V}_\mu \bar{\chi}\gamma^\mu\gamma_5 \chi + \sum_q g_q \tilde{V}_\mu \bar{q}\gamma^\mu\gamma_5 q,\end{aligned} \tag{1.8}$$

where the vector V_μ, axial vector $\tilde{V}_\mu$ and dark fermion χ have standard mass terms and the sum runs over all SM quark species. We see that either model depends on only a few parameters: (i) the mass m_{DM} of the dark matter particle, (ii) the mass m_{med} of the mediating particle, (iii) the coupling g_{DM} of the dark particle to the vector mediator and (iv) the coupling g_q of the mediator particle to the SM quarks. If we assume a flavour universal mediator-quark coupling, the parameters number only four. One could in principle allow for an arbitrary coupling to each quark flavour, increasing the number of free parameters. Often though, there will be some inherent structure to the coupling scheme; for example, with a scalar or pseudoscalar mediator instead of vectors, one may take inspiration from the Standard Model and couple to quarks with a Yukawa hierarchy. Then, though each quark has a different coupling, the number of model parameters remains low. In the limit that m_{med} is large, these models in any case reproduce the same phenomenology as the corresponding effective 4-point vertex (though in the case of the Lagrangians above no CP-violating interactions are present, and as such they do not represent the full complement of the 4-point interactions of [64]).

There is no reason to expect that nature in reality conforms to a simple structure. Indeed, it may be a little naïve, given the rich structure of the SM, to hope that dark matter or other BSM phenomena can be explained with the introduction of a single, arbitrary, new particle species or two. Nonetheless, the hope is that by studying such models, we can learn something of the full structure, if it extends beyond our first guess. This has the advantage

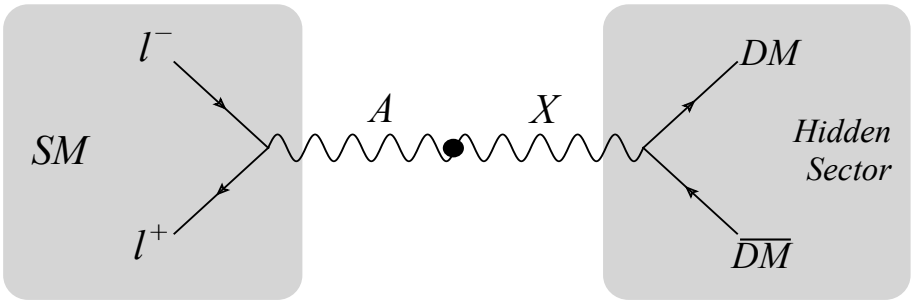

Fig. 1.5.: Sketch of the communication of the hidden and visible sectors through a mediator particle, or portal. In this instance the mediator is the hidden photon (which we discuss below in Section 1.3.2), which interacts with dark matter in the hidden sector, and communicates with the SM through a kinetic mixing operator with the photon (here represented with a black dot).

of being computationally simpler, in part by not introducing a large spectrum of new states[6]. The "WISPy" models presented below conform well to the principles of simple models.

1.3 WISPs

Given the rich structure of the Standard Model matter and gauge fields that account for only approximately 5% of the observable energy density of the Universe, it does not seem unreasonable that dark matter also has a nontrivial field content. Nonetheless, following a "bottom up" approach and beginning with the phenomenology of BSM physics, we ought to start with simple field configurations, and see what we can learn. The historical tactic for discovery of new physics has been to probe ever higher masses. There is at least one orthogonal direction to probe in the search - that of weak couplings. We will see that light, weakly coupled hidden sectors of physics can provide solutions to BSM problems that are as compelling as their heavier cousins. By hidden sector, it is meant that there exist distinct sets of fields that are not charged under the Standard model SU(3)$\times$SU(2)$\times$U(1) gauge group. Such models arise naturally in brane constructions, where distinct sectors of physics may be located on branes that are spatially separated in higher dimensions. Constructing models in such a way also provides the mechanism for achieving the requisite extremely weak couplings [71–79]. In order that a hidden sector can interact with the SM fields at all,

[6] The clear allusion here is to the comparatively 'complicated' (meaning having many free parameters) supersymmetry (SUSY) and its many variants and extensions. This is not to be derided for its complexity, however, since the principal reason for introducing SUSY was not explaining dark matter. There are a host of good motivations to extend the space time symmetry group, including a solution to the hierarchy problem, unification of the SM coupling constants in the UV regime and indeed providing a WIMP candidate in the lightest supersymmetric particle (LSP). Further discussion of SUSY lies beyond the scope of this thesis.

there must exist some mediating particles that interact with both sectors. Numerous possible portals exist, for example [80],

- Vector[7] $\sim \chi B^{\mu\nu} X_{\mu\nu}$.
- Axial/pseudoscalar $\sim \frac{a}{f_a} F^{\mu\nu}\tilde{F}_{\mu\nu}$, $\frac{\partial_\mu a}{f_a}\bar{\psi}\gamma^\mu\gamma^5\psi$.
- Scalar $\sim (\mu S + \lambda S^2) H^\dagger H$.
- Neutrino $\sim y_n L H N$.

This thesis will be concerned principally with the vector portal, though Chapter 4 investigates the phenomenology of a pseudoscalar mediated interaction in the context of astrophysical hints of dark matter. First though, let us review the case for light, weakly interacting particles, by way of introducing the WISP "zoo".

1.3.1 Axions

QCD provides a theoretically sound and phenomenologically successful framework for strong interactions, but still hides several mysteries. The non-perturbative regime at small Bjorken-x, for example, is poorly understood (something we revisit in the context of dark matter scattering in Chapter 5). Strikingly, the CP-violating term in the QCD Lagrangian,

$$\mathcal{L}_{\rm QCD} \supset \frac{\theta}{32\pi} G^{\mu\nu}\tilde{G}_{\mu\nu} \tag{1.9}$$

where θ is in principal non-zero and $G^{\mu\nu}$ is the gluon field strength tensor (with dual $\tilde{G}^{\mu\nu}$), appears to be vanishing, or at least unnaturally small. No CP-violating interactions have been observed in the strong sector, so that the limit (from measurements of the neutron electric dipole moment, which would be generated by CP-violating strong interactions) on the magnitude of θ is that it is at least 10 orders of magnitude smaller than would be expected naïvely.

One possible solution to the problem of an anomalously small θ is to introduce a new symmetry: Peccei and Quinn introduced an approximate global U(1) symmetry [81, 82]. The symmetry (which is already anomalously broken by the QCD vacuum) is spontaneously

[7] Up until now we have used χ to represent a non-SM fermion. We avoid this notation here and in the remainder of this thesis, to prevent confusion with the kinetic mixing parameter intended here.

broken, and the resulting pseudo-Goldstone boson acquires a mass. The potential that this generates sets the natural value of the CP violating term to zero, by a cancellation between the θ term and the expectation value of the axion field ($\langle a \rangle = f_a \theta$), which has a Lagrangian term,

$$\mathcal{L}_{\not{CP}} = \frac{a}{f_a} G^{\mu\nu} \tilde{G}_{\mu\nu}, \tag{1.10}$$

suppressed by the mass scale f_a at which the Peccei-Quinn symmetry was spontaneously broken.

The axion also has a gauge invariant two photon interaction, which is key to many searches for the (so far, completely) elusive particle. If one has a pseudoscalar with a two photon coupling that does not solve the strong CP problem, it is often referred to as an axion-like-particle (ALP), and is subject to many of the same constraints.

1.3.2 Hidden photons

We may attempt to reconcile the success of the Standard Model with the necessity of additional physics by introducing new matter and forces in such a way that the essential structure of the SM is not changed, but perhaps appended to. We'll here give considerable attention to the simplest possible addition, which underpins much of the present thesis.

Consider the extension of the SM gauge group to include an additional Abelian symmetry [71, 72, 74–78, 83–92], becoming SU(3)×SU(2)×U(1)×U(1)′, before electroweak symmetry breaking. After symmetry breaking, so that the gauge bosons have mass, the electroweak gauge part of the SM Lagrangian, with an additional U(1)′ gauge field is,

$$\begin{aligned}\mathcal{L} = &-\frac{1}{4} B^{\mu\nu} B_{\mu\nu} - \frac{1}{4} X^{\mu\nu} X_{\mu\nu} - \frac{1}{4} W^{a,\mu\nu} W^a_{\mu\nu} - \frac{1}{2} \chi_Y B^{\mu\nu} X_{\mu\nu} + \frac{1}{2} m_X^2 X^\mu X_\mu \\ &+ \frac{1}{2} \frac{m_W^2}{g^2} (g W^{3,\mu} - g' B^\mu)^2 + \frac{1}{2} m_W^2 (W^{1,\mu} W^1_\mu - W^{2,\mu} W^2_\mu).\end{aligned} \tag{1.11}$$

Assuming no SM matter fields are charged directly under the U(1)′, the principal interaction comes from the the kinetic mixing of the new gauge boson with hypercharge, with mixing angle χ_Y. Considering only the Abelian portion of the Lagrangian at energies sufficiently below the electroweak scale that we can ignore the heavy electroweak gauge bosons, the terms consistent with gauge and Lorentz invariance are:

$$\mathcal{L} = -\frac{1}{4} F^{\mu\nu} F_{\mu\nu} - \frac{1}{4} X^{\mu\nu} X_{\mu\nu} - \frac{1}{2} \chi F^{\mu\nu} X_{\mu\nu} + \frac{1}{2} m_X^2 X^\mu X_\nu + j^\mu A_\mu. \tag{1.12}$$

The $j \cdot A$ term couples hypercharge to the electromagnetic current and the additional term $\propto m_X^2$ is a mass for the gauge boson associated with the new field, X^μ (with field strength tensor $X^{\mu\nu} = \partial^\mu X^\nu - \partial^\nu X^\mu$). Such a mass term can arise from either a Higgs or Stueckelberg mechanism – we return to the question of mass generation below and in Chapter 3, where we will consider the impact of the U(1)′ being extra-dimensional, such that initially massless hidden photons generate a massive Kaluza-Klein tower upon compactification. The direct mixing with the photon described by Eq. (1.12) is valid so long as $m_X \ll m_Z$. For hidden photon masses comparable to or larger than m_Z, the additional mixing of the hidden photon with the hypercharge component of the Z boson must also be included. The kinetic mixing parameter in Eq. (1.12) relates to the kinetic mixing with hypercharge as $\chi = \chi_Y \cos\theta_W$, corresponding to the factor $\cos\theta_W$ relating the hypercharge and photon gauge fields[8].

The kinetic mixing between the two gauge fields is the novel feature that generates interesting phenomenology for hidden photon models, but let us try to remove it, and bring the Lagrangian into a more familiar form. This may be accomplished with either of two field redefinitions. Consider first redefining the hidden gauge field as such: $X^\mu \to X^\mu - \chi A^\mu$. Note that terms of order χ^2 and above will be ignored – we are interested in small values of χ, which justifies the approximation. In the case that the new gauge field is massless, $m_X = 0$, this decouples the two fields entirely - the SM phenomenology would not be impacted at all. However, in the presence of a mass term, we find that the result of the shift is simply to change basis, diagonalising the kinetic term and moving the mixing to the mass terms,

$$\mathcal{L} = -\frac{1}{4}F^{\mu\nu}F_{\mu\nu} - \frac{1}{4}X^{\mu\nu}X_{\mu\nu} + \frac{1}{2}m_X^2(X^\mu - \chi A^\mu)^2 + j^\mu A_\mu. \tag{1.13}$$

Instead of shifting the hidden field, we could have shifted the SM photon field as $A^\mu \to A^\mu - \chi X^\mu$. The resulting Lagrangian,

$$\mathcal{L} = -\frac{1}{4}F^{\mu\nu}F_{\mu\nu} - \frac{1}{4}X^{\mu\nu}X_{\mu\nu} + \frac{1}{2}m_X^2 X^\mu X_\mu + j^\mu(A^\mu - \chi X^\mu), \tag{1.14}$$

is diagonal in the kinetic terms, as before. Now, instead of creating a mixing in the mass terms for A^μ and X^μ, there is a direct coupling between the SM electromagnetic current and the new field X^μ.

[8] The mixing parameter χ (and the hypercharge equivalent) is in fact a mixing angle, and the prefactor to the mixing terms $\sin\chi$. In practice, we are mostly (and entirely, throughout the present work), interested in small values of χ, so the distinction makes no difference.

It must be emphasised that the physical pictures corresponding to the two field redefinitions above – that of photon-hidden photon oscillation and that of a direct coupling between the electromagnetic current and the hidden photon – are completely equivalent. Which picture is used depends only upon what is convenient when computing the impact on a given physical phenomenon: all observables take the same value regardless of the picture used[9].

We have derived a mass mixing, analogous to that of neutrinos, that allows the oscillation of photons (after EWSB) into the new gauge boson, the so-called hidden photon. Having done so by beginning with the Lagrangian (1.12), it is worth asking how we got a mixing angle in the first place. The answer is that the Lagrangian represents an effective quantum field theory, assumed to be valid only to a finite energy scale. The interaction that leads to mixing between the gauge fields involves some heavy particles that cannot be accessed at low energies, but whose existence facilitates the mixing interaction. Though the origin of the interaction does not affect the low energy phenomenology of the theory, it is instructive to see how such a mixing arises. We will consider the case of two Dirac fermions (though

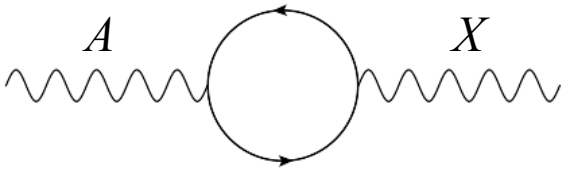

Fig. 1.6.: Loop diagram resulting in the mixing of the SM U(1) with a hidden U(1) gauge group. In the presence of multiple high scale fermions, the contributions of all fermions to the process must be accounted for.

this is not a unique choice) described by the Lagrangian,

$$\mathcal{L} = \sum_n \left(i\bar{\Psi}_n \gamma^\mu \partial_\mu \Psi_n - m_n \bar{\Psi}_n \Psi_n - i g_n A^\mu \bar{\Psi}_n \gamma_\mu \Psi_n - i g'_n X^\mu \bar{\Psi}_n \gamma_\mu \Psi_n \right) \tag{1.15}$$

where the two species of fermion are indexed by $n = 1, 2$. The interaction leading to mixing is a fermion loop (shown in Fig. 1.6), similar to the leading order diagram for the photon self-energy (leading to charge renormalisation) in QED. To evaluate the diagram, thus χ, one must integrate over the loop momentum. For a single fermion,

$$i\mathcal{M} = (-1) \int \frac{d^4k}{(2\pi)^4} (-ig_h)(-ig'_h) \mathrm{tr} \left[\gamma^\mu \frac{1}{\gamma \cdot k - m} \gamma^\nu \frac{1}{\gamma \cdot (p+k) - m} \right]. \tag{1.16}$$

[9] In the course of this thesis, both pictures will be used and made reference to. In most cases, it will not be explicitly stated which physical picture is envisaged, though it should be apparent from the situation being considered.

This integral is at least logarithmically UV divergent, even when dimensional regularisation is applied. We can extract (after some work) the divergent part, and find,

$$\chi \propto g_h g'_h \log \frac{m}{\Lambda}. \tag{1.17}$$

If we add the contribution of the second fermion, we find the problem is not alleviated unless the diagrams enter with relative sign, so that the divergences are cancelled. One means to accomplish this structure is presented in Appendix A, where U(1)×U(1)′ kinetic mixing is derived from a spontaneously broken SU(2)×U(1)′ gauge theory. The charge structure under (U(1),U(1)′) resulting from the spontaneous breaking of SU(2)→U(1), is $Q = (1, 1)$ for the first fermion and $Q = (1, -1)$ for the second, so the diagrams add destructively, as required. As such, we find the logarithmic divergence is tamed to $\log m_1/m_2$, and mixing can only result so long as the masses m_1, m_2 are non-degenerate.

It is important to note that the diagram in Fig. 1.6 is fundamentally divergent. The necessity of two fermions generating the loop here is entirely manually inserted to make the diagram calculable, which is not a restriction that nature imposes.

Beyond the considerations in some string constructions (e.g. [71, 72, 89]), there is little to *a priori* specify the allowed values of any of the coulings g_h, g'_h or masses $m_{1,2}$, so we find that the kinetic mixing parameter can take practically any value.

It was noted earlier that in the absence of additional hidden matter charged under the U(1)′, if the hidden photon is massless, it decouples from the SM, which can be seen by a simple field shift. The following sections consider two means of generating a mass for the hidden photon.

A hidden Higgs?

Taking inspiration from the Standard Model, the first mechanism for generating masses for hidden photons we will consider is to invoke a hidden Higgs [93]. In the presence of a suitable potential,

$$V_{\rm h} = -\mu_{\rm h}^2 |\varphi_{\rm h}|^2 + \lambda_{\rm h} |\varphi_{\rm h}|^4, \tag{1.18}$$

the hidden Higgs field $\varphi_{\rm h}$ acquires a vacuum expectation value, $\langle \varphi_{\rm h} \rangle = \frac{v_{\rm h}}{\sqrt{2}} = \frac{1}{\sqrt{2}} \sqrt{\frac{\mu_{\rm h}^2}{\lambda_{\rm h}}}$. Assuming the hidden Higgs is initially charged (0, q_X) under U(1)$_{\rm EM}$×U(1)′, upon spon-

taneous symmetry breaking the Higgs-hidden photon interaction term becomes a hidden photon mass term,

$$\mathcal{L} \supset q_X^2 g_X^2 |\varphi_\mathrm{h}|^2 X^\mu X_\mu \xrightarrow{\mathrm{SSB}} q_X^2 g_X^2 \frac{v_\mathrm{h}^2}{2} X^\mu X_\mu. \tag{1.19}$$

Performing a change of basis for the X^μ or A^μ field, as described previously, results in either of the physically equivalent pictures of hidden photon mass mixing with the photon, or a direct coupling to the electromagnetic current. However, in addition to the standard hidden photon phenomenology that results from the non-zero mass, there is a dynamical Higgs field, $h = \frac{1}{\sqrt{2}}(v_\mathrm{h} + \varphi_\mathrm{h})$.

This additional field changes the phenomenology of the model substantially. In fact, the hidden Higgs field picks up a fractional electromagnetic charge $-\chi(g_X/e)q_X$ from its interactions with the Abelian fields, acting as a minicharged particle [94] (further described later in this Chapter), and the same constraints, shown in Fig. 1.8, apply. Additionally, the new scalar may interact, unsuppressed, with the SM Higgs field, inducing a so-called "Higgs portal" [95] between the SM and hidden sectors. Even without addition of hidden photons from an extra U(1)′, Higgs portal models present a rich phenomenology themselves (for example [59, 95–97]).

The Stueckelberg mechanism

Since the hidden photon arises from an Abelian symmetry, an alternative, Stueckelberg, mechanism can generate the hidden photon mass necessary for observable phenomenology [98]. Consider the following Lagrangian for an Abelian gauge field,

$$\mathcal{L}_\mathrm{Abelian} = -\frac{1}{2}\partial_\mu A_\nu \partial^\mu A^\nu + \frac{1}{2} m^2 A_\mu A^\mu, \tag{1.20}$$

which results in the equation of motion,

$$(\partial^2 + m^2) A_\mu(x) = 0. \tag{1.21}$$

In order to restore gauge invariance to Eq. (1.20), an additional field must be introduced: Stueckelberg's B field. The field obeys the same equations of motion as the Abelian gauge field,

$$(\partial^2 + m^2) B(x) = 0, \tag{1.22}$$

following from the Lagrangian terms,

$$\mathcal{L}_{\text{Stueckelberg}} \supset \frac{1}{2}\partial_\mu B \partial^\mu B - \frac{1}{2}m^2 B^2. \tag{1.23}$$

The gauge transformations of the two fields are:

$$\begin{aligned} A_\mu(x) &\to A'_\mu(x) = A_\mu(x) + \partial_\mu \Lambda(x) \\ B(x) &\to B'(x) = B(x) + m\Lambda(x) \end{aligned} \tag{1.24}$$

The gauge function $\Lambda(x)$ (which is complex) obeys the same equations of motion as the gauge and Stueckelberg fields, $(\partial^2 + m^2)\Lambda(x) = 0$, a feature not present in standard QED, but which is necessary to lower the total degrees of freedom for our massive vector field to three (in addition to a condition that the free field annihilation operators of the combination $\partial^\mu A_\mu(x) + mB(x)$ must annihilate a physical state – without the Stueckelberg field, $\partial^\mu A_\mu(x)$ alone must do the same).

Under the gauge transform (1.24), the Lagrangian (1.20) is gauge invariant, permitting a mass term for an Abelian field. We can see the mass generation more explicitly by rewriting the whole Stueckelberg Lagrangian (i.e. the sum of equations (1.20) and (1.23)), which is, up to total derivatives,

$$\begin{aligned} \mathcal{L}_{\text{Stueckelberg}} = -\frac{1}{4}F^{\mu\nu}F_{\mu\nu} + \frac{m^2}{2}\left(A^\mu - \frac{1}{m}\partial^\mu B\right)\left(A_\mu - \frac{1}{m}\partial_\mu B\right) \\ - \frac{1}{2}\left(\partial^\mu A_\mu + mB\right)\left(\partial^\nu A_\nu + mB\right). \end{aligned} \tag{1.25}$$

The trick here has been to realise that a spin one representation can be built from a scalar field with the application of the momentum operator. In essence, the Stueckelberg mechanism is a version of the Higgs mechanism, where the particle excitation of the field – the boson – is infinitely massive and so decouples. Consider parametrising the Higgs field in polar coordinates, $\phi = (v + h)e^{i\theta/v}$. Taking the boson, h, mass to be infinite, it can be integrated out and decouples from all processes in the theory. Then θ is analogous to the Stuckelberg field $B(x)$.

We have considered two HP mass generation mechanisms. In Chapter 3, we consider a third: the hidden photon field exists in higher spacetime dimensions, and mass is generated upon compactification to the four dimensions of our common experience. The idea is inspired by the fact that both hidden photons and additional spatial dimensions arise frequently in

string theory, though we employ only a toy model, with the aim of investigating the salient features of the resulting phenomenology.

1.3.3 Minicharged particles

Axions and hidden photons are both viable dark matter candidates in themselves. Nonetheless, there is much phenomenological interest in pseudoscalar and vector (and many other) portals to more extended hidden sectors. In part, this relates to the fact that an additional mediator particle allows one to tune the annihilation cross-section of a thermally produced dark matter candidate, to be discussed later in this Chapter.

As a first example of a simple but non-minimal model, we may consider a theory with a simple hidden sector, to say a group of fields completely uncharged under the SM gauge groups. For example, the hidden sector could consist of a single species of Dirac fermion, ψ, that interacts with the visible (SM) sector only through the kinetic mixing of a hidden U(1)$'$ group – under which the hidden fermion is charged (with coupling constant g_h) – with the SM hypercharge. The Lagrangian describing such a theory is

$$\mathcal{L}_{\rm BSM} = -\frac{1}{4}F^{\mu\nu}F_{\mu\nu} - \frac{1}{4}X^{\mu\nu}X_{\mu\nu} - \frac{1}{2}\chi F^{\mu\nu}X_{\mu\nu} + i\bar{\psi}\gamma^{\mu}\partial_{\mu}\psi - ig_h X^{\mu}\bar{\psi}\gamma_{\mu}\psi - m\bar{\psi}\psi. \tag{1.26}$$

Performing the same field redefinition designed to diagonalise the kinetic terms as earlier, $X^{\mu} \to X^{\mu} - \chi A^{\mu}$, the interaction terms of the hidden fermion become,

$$\mathcal{L} \supset -ig_h X^{\mu}\bar{\psi}\gamma_{\mu}\psi + i\chi g_h A^{\mu}\bar{\psi}\gamma_{\mu}\psi. \tag{1.27}$$

The latter term is precisely analogous to the coupling between photons and electrons, with with electric charge e replaced by a combination of the kinetic mixing and hidden gauge charge, χg_h. Since the kinetic mixing is not assumed to be quantised, and is likely to be small, this results in the hidden fermion appearing to the SM fields exactly as if it were in possession of an electromagnetic charge of size $\epsilon = \frac{\chi g_h}{e}$ (in units of the electron charge). Notice that in contrast to our earlier observation, in the presence of an extended hidden sector charged under the U(1)$'$ even a massless hidden photon can present interesting phenomenology.

1.3.4 Generalised hidden sectors

The example of minicharged particles is representative of a much larger class of BSM models, with some matter occupying a hidden sector and the interaction with the SM mediated by an additional new particle. Various combinations of particle can be considered for both the hidden sector and the mediator, each with its own characteristic experimental signatures, birthing a broad search [80]. Typically, the mediator is considered to be light, such that it can be resolved by the collider experiments employed in searches for this variety of model, rather than relying on an effective 4-point vertex. A possibility of particular interest for us later (see Chapter 5) is a *secluded* scenario [99], whereby the mediator is lighter than the dark matter, so that annihilation into the SM is allowed, but the mediator cannot decay into dark matter.

The presence of a mediator allows even thermally produced MeV – GeV mass dark particles to act as dark matter, since the mediator mass and couplings can regulate the dark matter annihilation rate [100]. So long as the rate is not too small, the dark matter does not freeze out too early (in which case it would remain relativistic, inhibiting structure formation), and even light particles can be a good CDM candidate. We discuss an alternative to thermal production for light dark matter in the next Section.

Light dark matter scenarios involving a hidden sector coupled by some mediator particle are apt for exploration at fixed target facilities, such as those used as neutrino factories [4, 61, 62, 101, 102].

1.3.5 WISPs as dark matter

The dominant paradigm in particle dark matter has long been that of the weakly interacting massive particle (WIMP), which when produced thermally in the early Universe with weak scale interactions, almost automatically produces the correct relic density [10]. The standard lore is that dark matter candidates that are too light violate the Lee-Weinberg bound [103], resulting in a relic density that is far too high. However, this assumes both thermal production and interaction through a heavy mediator (e.g. electroweak boson), and actually motivates the introduction of new, light bosons as messengers between the visible and dark sectors. Light particles also pose a problem for structure formation as the light particle is less likely to be trapped in a potential well (to say, light particles have higher free-streaming lengths

than heavy particles). In order that light dark matter be viable, an alternative production mechanism must be in place – a good substitute exists in the misalignment mechanism.

Consider the equation of motion of a scalar field on a Friedmann-Robertson-Walker (FRW) background metric,

$$\ddot{\phi} + 3H(t)\,\dot{\phi} + m^2\phi = 0. \tag{1.28}$$

Recognising that this resembles a damped harmonic oscillator, we break the solution into two regimes: overdamped and underdamped. In the overdamped stage, for early times, $H(t) \gg m$, so there is essentially no oscillation, $\dot{\phi} = 0$. As the Universe expands the Hubble constant decreases, so that at some time $H(t_{\rm crit}) \sim m$ and the field begins to oscillate. Note that before oscillation, the mass term is negligible compared to H, and there is no reason to expect the field value to be zero. It should be noted that m is not constant during the evolution of the Universe, since it receives corrections from thermal processes.

The misalignment mechanism works in much the same way for vector fields as for (pseudo) scalars, like the axion. In order to fully reproduce the scalar behaviour with the spatial components of a vector, however, a non-minimal coupling to gravity is required [104, 105]. Here we explicitly derive the equations of motion governing the vector field.

Again assuming a FRW metric with scale factor $a(t)$ (for notational elegance, we will hence suppress the time dependence of a),

$$ds^2 = dt^2 - a^2\delta_{ij}dx^i dx^j. \tag{1.29}$$

The action describing the dynamics of a massive vector field in this background is,

$$S = \int dx^4\,\sqrt{-g}\left(-\frac{1}{4}F^{\mu\nu}F_{\mu\nu} + \frac{1}{2}m^2A^\mu A_\mu\right) \tag{1.30}$$

The equations of motion for the A^μ field are arrived at by taking the functional derivative of the action with respect to the same field. It is easiest to present the result component-wise, splitting the time component of the field from the spatial components,

$$\begin{aligned} -\frac{1}{a^2}\partial_i^2 A_0 + m^2 A_0 + \frac{1}{a^2}\partial_i\dot{A}_i &= 0 \\ \ddot{A}_i + \frac{\dot{a}}{a}\dot{A}_i - \frac{1}{a^2}\partial_i^2 A_i + m^2 A_i - \partial_i\dot{A}_0 - \frac{\dot{a}}{a}\partial_i A_0 + \frac{1}{a^2}\partial_i(\partial_k A_k) &= 0 \end{aligned} \tag{1.31}$$

One can make the assumption of spatial homogeneity and treat the first derivative of the field w.r.t. any of the spatial components as negligible, $\partial_i A^\mu \sim 0$. Then it follows from the equations of motion above that the time component of the field $A_0 = 0$.

We arrive at an equation of motion for the spatial components of the A_μ field, A_i,

$$\ddot{A}_i + H\dot{A}_i + m^2 A_i = 0, \tag{1.32}$$

where $H = \dot{a}/a$ is the Hubble constant (which is, via a, a function of time).

Since the spatial components of the metric are all preceded by a factor of a^2, we may redefine the vector field to absorb it, making the computation of the energy density later straightforward. We introduce the field $B_i \equiv A_i/a$, and can rewrite the equation of motion as,

$$\ddot{B}_i + 3H\dot{B}_i + (m^2 + 2H^2 + \dot{H})B_i = 0 \tag{1.33}$$

From the above, we can see that for sufficiently late times, when $m \gg H$, the spatial components of the vector field behave like independent scalars. However, during the early Universe, the additional potential terms, $\propto 2H^2$, $\dot{H}$ are dominant. These terms enter as prefactors to the field B_i, so, the hidden photon is subject to a large effective mass, which causes problems with the standard inflationary paradigm (the "slow rollover" period requires a relatively flat potential). One way to mitigate this effect, without introducing fine tuning, is to introduce a non-minimal coupling to gravity, $\mathcal{L}_{\rm grav} = \frac{R}{12} A^\mu A_\mu$. Since, for a FRW metric, $\frac{R}{6} = -(2H^2 + \dot{H})$, this term precisely cancels the geometric contribution to the vector mass. More generally, one could parametrise the strength of the non-minimal coupling with a prefactor κ to the Lagrangian term, as in [106], and find that the geometric mass term is proportional to $(1 - \kappa)$. It would be interesting to study the effect in cases where $\kappa \neq 1$.

For late times, the Hubble terms become negligible and oscillation modes of the field may be interpreted as particles, which are non-relativistic (cold), providing a suitable dark matter candidate.

1.4 The low energy frontier

The three primary experimental approaches utilised in the search for WIMP dark matter (outlined in Section 1.2.2) may also be applied to WISP dark matter. As we have seen

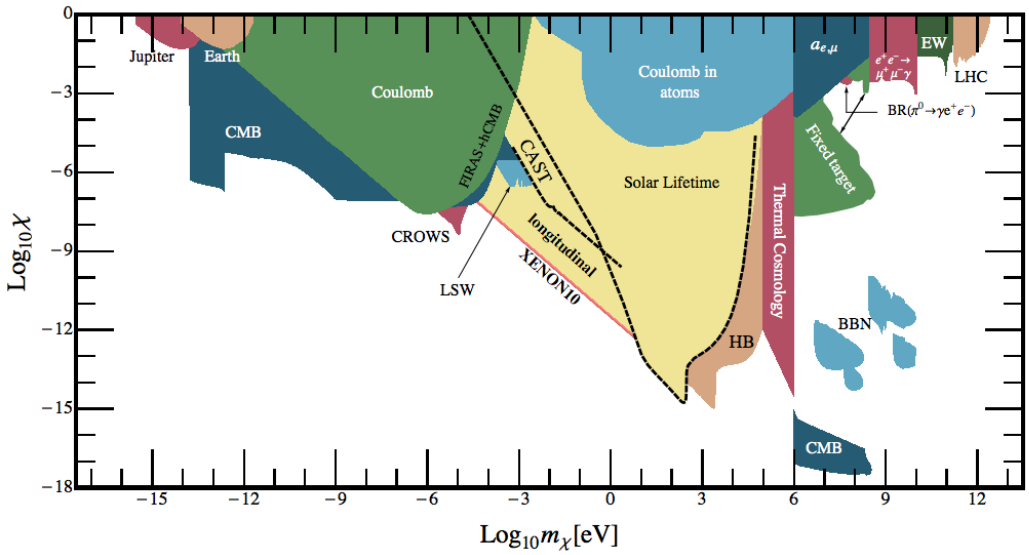

Fig. 1.7.: Current best constraints on HP parameter space, updated from [107]. See text for details.

though, some WISP candidates are motivated by considerations other than dark matter, and may not comprise a sufficient fraction of the relic density to be susceptible direct or indirect detection searches. Additionally, the light masses of WISPs open up avenues for exploration in low-energy, precision experiments. The experimental search for new light particles has engendered much innovation and novelty. Here we outline some of the experimental techniques employed to search for WISPs. As in the preceding theoretical section, our primary focus will be hidden photons and dark sectors coupled via kinetic mixing, reflecting the content of the following Chapters in this work.

The search for hidden photons benefits from parallel and complementary searches for axions and ALPs. In some cases, experiments designed to search for axions may be reinterpreted in the context of hidden photon models, a prime example being the CERN Axion Solar Telescope (CAST) [108] bounds [109, 110], now part of the established canon of hidden photon searches. The CAST constraint is shown as an extension to the solar lifetime constraint in Fig. 1.7, but has since been eclipsed by the solar lifetime constraint itself, owing to the inclusion of previously neglected effects from longitudinal modes [111, 112].

Certainly, the established astrophysical searches for, and theory surrounding, axions can be used as a guide to construct similar constraints for hidden photons, e.g. [58, 113–115].

1.4.1 Hidden photon searches

The strongest current bounds on the hidden photon (m_X, χ) parameter space are shown in Fig. 1.7. Clearly the space is large, with constraints spanning 29 orders of magnitude in mass and 18 in the mixing parameter. There are no concrete predictions for either parameter, though some string models make broad statements about the expected ranges. However, if the hidden photon is to act as cold dark matter, the mixing must be of order $\sim 10^{-7}$ or below in order that a sufficient amount can survive to the present day.

To bound the mass from below, one may consider the structure formation of compact galaxies [116], with typical length scales on the order of a single kilopasec (kpc) and masses of order $2 \times 10^{11} M_\odot$. In order that the structure formation can occur, the Compton wavelength of the particles involved must clearly be shorter than the size of the galaxy, since otherwise the uncertainty in the particle's position does not allow it to be localised to the galaxy. This can provide a rough estimate of the minimum allowable mass for a cold dark matter hidden photon [117],

$$\begin{aligned} 1\text{kpc} > \Delta x = \frac{\hbar}{2\Delta p} &= \frac{\hbar}{2 m_X v_{\text{esc}}} \\ \Rightarrow m_X > \frac{\hbar}{2\,\text{kpc}\, v_{\text{esc}}} &\sim 2.5 \times 10^{-25}\text{eV}. \end{aligned} \tag{1.34}$$

In practice this is not a restrictive bound, since our experimental and observational reach ceases some ten orders of magnitude higher than this mass.

The bounds of Fig. 1.7:

- **Planetary magnetic fields.** Many of the constraints on hidden photons arise from the modification to Maxwell's equations that ensue from the addition of a massive photon. This modification can be probed by many experiments, but also in astrophysical environments, such as the magnetic fields of the Earth and Jupiter [118]. Planetary magnetic fields allow us to probe small mass scales as a result of the large distances involved.

- **Cosmic Microwave Background.** Accurate measurements of the CMB allow us to calculate the effective number of light particle species during recombination (photon decoupling, the time at which the CMB formed), $N_\nu^{\text{eff}} = 3.30 \pm 0.27$ [8]. Combining this with measurements of Large Scale Structure (LSS) and supernovae [113, 114]

allows bounds to be placed on the hidden photon, which would contribute additional relativistic degrees of freedom, increasing N_ν^{eff}.

- **Light Shining Through Walls & Helioscopes.** Exploiting the phenomenon of photon-hidden photon oscillations would in principle allow light to pass through an otherwise opaque wall. This can be exploited in several setups, including fixed target colliders (discussed below) and much lower energy setups, for example coupling two, e.g., Fabry-Pérot cavities [119–122]. The latter rules out a small but interesting regime, and extension of the idea to microwave frequency cavities has proved fruitful [123–126]. This novel technique is discussed further in Chapter 2. Applying the same principle of photon regeneration after an opaque wall, but sourcing the hidden photons from the Sun, describes a helioscope. Note that no cavity set up can be employed by helioscopes, and in any case would not help, as solar hidden photons would be emitted with a broad spectrum of energies – there is no resonant mode. Though now eclipsed by other constraints, CAST generated a substantial exclusion region [109, 110] and designs for a successor experiment, the International Axion Observatory (IAXO) are underway [127].

- **Stellar evolution.** The evolution of stars is a reasonably well understood process [128]. If additional particle species (such as HPs) are introduced and produced in sufficient quantity in stellar interiors, the contribution to the energy loss of stars must be calculated. If this loss is too high, no stellar model can be constructed that would allow, for example, the Sun to survive to the present day. Even if the energy loss is curtailed by reabsorption of the new particle species, constructing a viable model can be rendered impossible by the contribution to non-local energy transfer within the star. Observation of the Sun and horizontal branch stars provide constraints on the maximum allowed mixing of HPs with photons [109]. Recently, the importance of longitudinal modes was noticed, which increases the strength of the bound in the low mass region considerably [111, 112].

- **Electron fixed target experiments.** Hidden photons produced in bremsstrahlung from an electron beam incident on a fixed target can traverse the beam lines of such facilities easily. Their low interaction cross-section allows HPs to pass through the shielding that stops all SM particles except neutrinos. This gives rise to a novel signature: pairs of electrons reaching the detector. The SLAC E137 and E141 experiments, and Fermilab E774, have all been used to place limits on the mass and

kinetic mixing of hidden photons via simple event counting [58]. Some additional past electron fixed target experiments have since had their results mapped to the hidden photon plane [129]. These constraints all borrow somewhat from the light-shining-through-walls principle, as the hidden photon can propagate through layers of rock and shielding that would otherwise stop the electron beam. There are several purpose built experiments running that instead search for a resonance from the hidden photon decay in the dielectron invariont mass spectrum [130–133]. The two approaches are very complimentary, with the LSW-flavoured beam dump experiments probing smaller mixings but unable to constrain the higher mixings that would result in the produced HPs decaying before reaching the detector. The mass peak searches are sensitive to higher mixing angles, and also slightly higher masses.

- **LHC.** For high mass hidden photons, the only viable controlled production environment is the Large Hadron Collider. One could look for missing transverse energy caused by HPs leaving the beam line without interacting, but the more promising signal turns out to be a dilepton event, caused by the decay of a HP into an e^+e^- or $\mu^+\mu^-$ pair [134]. However, the LHC is ill suited to search for WISPs in general, since their mass spectrum spans many orders of magnitude below the high energies the LHC is designed for and they are extremely weakly interacting. High luminosity fixed target experiments cover a larger, but complementary, area of parameter space.

- **IDPB.** Hidden photons may also be sought in the Intergalactic Diffuse Photon Background, where their decays would create an excess of photons over that expected from background processes [135, 136]. This constraint is contingent upon the hidden photons surviving until the present day, and also requires that they are not sufficiently massive to decay to electron pairs. When this is the case, the fermion-loop-induced three photon decay dominates, resulting in a photon excess.

- **Atomic spectra.** HPs need not be produced on-shell to contribute to physical observables. The Lamb shift in the hydrogen atom, for example, receives a contribution from the hidden photon as an insertion into the photon propagator. By comparing a theoretical prediction of the HP-adjusted spectra of atomic transitions with the experimental error on such transitions, constraints can be placed on the HP parameter space [137–139].

- **Coulomb potential.** The HP insertion to the photon propagator creates a Yukawa-like modification to the Coulomb potential, $\delta V(r) \propto -\chi^2 e^{-m_X r}/r$ [140–142]. This can be bounded by precise, tabletop experiments, specifically designed to search for long range forces that would manifest in such a way.

Several of the above constraints will be discussed in more detail in Chapter 3, when we derive constraints on a hidden photon in the presence of large extra dimensions.

1.4.2 Proton beam dumps

The WISP paradigm represents a low energy approach to theory beyond the standard model, and we have already described some of the experimental techniques employed to search for hidden photons. Among those techniques, the use of high luminosity, relatively low energy beam dump experiments best generalises to the search for more extended hidden sectors.

Proton beam dump facilities – where a proton beam is fired directly into a suitable metal target – used to generate neutrinos for long baseline experiments also make excellent production factories for some classes of hidden sector models [4, 61, 62, 101, 102]. In particular, when the hidden sector matter is light and connected to the standard model by a light mediator.

Assuming a coupling to quarks, the light mediator also facilitates plentiful production in relatively low energy collisions by a direct Drell-Yan process and in the decays of mesons produced from the pN collisions. The advantage of these facilities is the high luminosity, with, for example, MiniBooNE, MINOS and T2K each delivering on the order of $\sim 10^{21}$ protons on target to date [61].

The MiniBooNE experiment is currently delivering a dedicated run searching for low mass dark particles coupled through a vector portal [143] (such as kinetic mixing). Project X (under consideration) also has the potential to search for numerous light dark matter and/or WISP scenarios [144]. In light of the increasing interest in this experimental approach, it is important that we understand the interactions of dark particles in such an environment thoroughly. The specific interactions are of course model dependent. In Chapter 5 a thorough treatment of dark fermion scattering through a vector portal is given (a popular paradigm, in part owing to the connection to the hidden photons and minicharged particles discussed previously), in particular accounting for novel QCD effects at low momentum transfer. This is

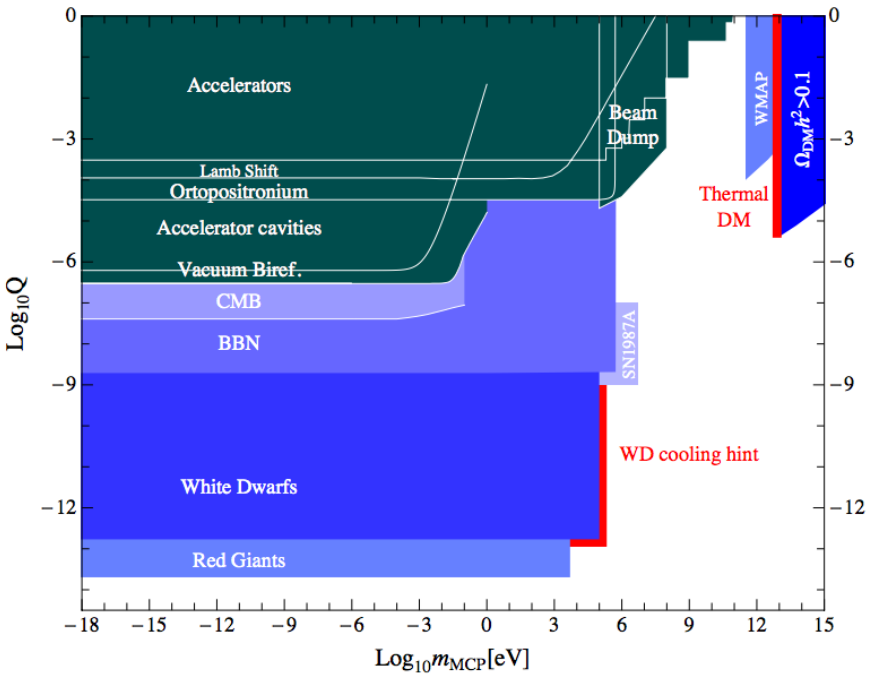

Fig. 1.8.: Exclusion limits on the minicharge as a function of mass from numerous experiments and astrophysical considerations. Figure from [80], see references therein.

especially important for light particles, where the low momentum transfer region dominates the cross-section.

The novel formalism of Chapter 5 will be used to enhance the constraint on minicharged particles from the E613 beam dump experiment. This is a small contribution to the exclusion limits on minicharged particles, as there has been considerable experimental effort devoted to the search already, resulting in the exclusion limits shown in Fig. 1.8. However, the applicability of the same formalism to other scenarios makes even the small increase in sensitivity it grants significant.

1.5 Thesis structure

This content of this thesis is built around four publications [1–4]. Each of Chapters $2-5$ will detail the work of one publication. As such, the Chapters are relatively self contained, though there are some common themes running throughout. The Chapter contents are as follows.

Chapter 2

In Chapter 2 we explore the notion of effective theories a little further, particularly in light of low energy experiments. Taking motivation from light-shining-through-walls searches for WISPs, we construct a toy quantum optics setup that may realise a novel tunnelling phenomenon dubbed "Tunnelling of the 3rd kind". Such a phenomenon would be a smoking gun for WISPy physics if observed with fundamental particles, but in the quantum optic setup, actually allows one to test the effective non-locality present in effective theories. To the author's knowledge no other test of this phenomenon has been devised.

I was involved in all stages of (and calculations in) the work, which has been previously presented in [1]:

Tunnelling of thc 3rd Kind: A Test of the Effective Non-locality of Quantum Field Theory
Europhys.Lett. 101 (2013) 61001

Chapter 3

In this Chapter we move on to WISPs proper with a study of hidden photons in the presence of large extra dimensions. This string-inspired set up provides an alternative mass generation mechanism worth exploring, even in light of the recent discovery of a SM Higgs boson.

We review the work already presented in [3]. This project was the basis of a previous thesis by Sabyasachi Roy [145], who performed many of the bound calculations. There have been several developments since then, including the addition of the effects of longitudinal modes in stellar constraints, bounds from the LHC and much of the perturbativity discussion. All the bounds have been reproduced independently by myself, but I am indebted to Sachi for his work. While some of the content of the Chapter is standard formalism, the novel aspects are weighted towards my own contributions.

Hidden Photons with Kaluza-Klein Towers
arXiv:1408.0019 [hep-ph]

Chapter 4

Here I present [2]:

Extended gamma-ray emission from Coy Dark Matter
JCAP 05 (2014) 009

Having investigated a WISP scenario in detail in the previous Chapter, we now divert ourselves to the WIMP paradigm. Counter to the essential message of this thesis – that WISPs are a fruitful and worthwhile class of models to study – we show that the WIMP paradigm is not without merit. A simple model of WIMP dark matter is able to fit the Galactic Centre excess while leaving no trace in either direct detection or collider experiments. This effect originates in the axial nature of the interaction, which serves to highlight the importance of understanding dark matter scattering.

I was instrumental in initiating this project and performing the first calculations, including setting up rudimentary versions of the monojet and Fermi-LAT analyses. However, much credit is due to Matt Dolan and Chris McCabe for the final code and plots used in the paper.

Chapter 5

Beam dump experiments have been used in BSM searches since their inception. With increasing interest in light dark matter scenarios, it is timely to investigate theoretical issues surrounding the scattering of light particles in some depth. Here we present a treatment of the scattering of low mass dark Dirac fermions, interacting through a light vector portal, from lead nuclei in the E613 beam dump experiment [4]. The treatment is novel in dealing with QCD effects at low-Q^2 and low Bjorken-x. These effects are negligible in the case of a heavy mediator particle, but become important in BSM scenarios where this is not guaranteed. As with the Coy Dark Matter study, this reinforces (albeit, in a subtler way) the importance of investigating the interactions of dark matter carefully.

I was involved in, and responsible for, all calculations within the paper, of course with extremely valuable contributions and validation from the other authors.

Scattering of Dark Particles with Light Mediators

Phys. Rev. D 90 (2014) 115005

Chapter 6

Finally, I conclude with a short summary bringing together the themes of the thesis, namely: the utility of effective theories and simple models in BSM physics, the good physics case for light, WISPy hidden sectors and the potential of low energy experiments for the discovery of such states.

2

Tunnelling of the Third Kind

> *For a time I would feel I belonged still to a world of straightforward facts; but the feeling would not last long. Something would turn up to scare it away.*
>
> **— Marlow**

The modern understanding of the Standard Model of particle physics is that it represents an *effective* theory of the fundamental forces and matter content of nature. By effective, it is implied that the theory does not hold to arbitrarily high energy scales, but rather represents only a low energy description. This view reconciles the apparent excellent agreement between the Standard Model and experiment in many areas with its clear inadequacy in explaining some phenomena at all: the physics explaining the remaining "BSM problems" is generated at a high energy scale, of which the observed SM is perhaps only an effective description. Note that this does not imply that there are no other signals of the higher energy theory at accessible scales. In particular we detailed in the previous Chapter the possibility that very light, weakly coupled particles are responsible for gravitational observations of dark matter.

Among the interesting phenomena associated with effective field theories, there is a general property of non-locality. To obtain an effective theory, one integrates out virtual degrees of freedom from the more fundamental (to say, valid at higher energy scales) theory. This produces some novel effects, such as allowing seemingly forbidden interactions (e.g. 4-photon), or a generating a contribution to the effective potential between particles. These phenomena account for the effects of the virtual particles that were integrated out. In fact, owing to quantum corrections, a non-locality is induced in the propagation of the remaining particles, through, at first order, a one-loop diagram. It is this effective non-locality we will investigate in this chapter. First though, we give some context to the study, with reference to the hidden photons so prevalent in this thesis.

2.1 Effective field theories

It is noted by Howard Georgi in a review of effective field theory [146] that "*One of the most astonishing things about the world in which we live is that there seems to be interesting physics at all scales*". While a unified theory of physics encompassing all matter and its interactions remains the pipe dream of the particle physics effort, it is clearly impractical to simply observe all phenomena to which we have access and attempt to dream up a single all-encompassing model. Effective theories are extremely useful tools to isolate the phenomena that are relevant in a given regime. In the case of fundamental particle physics, the regime may be determined by a single parameter - the energy (or, equivalently, length) scale. Heavy particles associated with higher energy regimes naturally have a very short range, so constructing an effective theory of physics in some regime involves consideration of the minimum length that can be probed in that regime. One can then neglect all interactions that occur exclusively at shorter length scales, and include these effects, if they are important at all, as corrections to the effective theory.

An effective quantum field theory is so named for being a description of quantized (i.e. particulate) field interactions that is supposed only to be valid up to a certain energy. Above this boundary the theory is not valid, owing to the availability of additional degrees of freedom that can be excited. If the effective description is a good one, these degrees do not sufficiently impact the theory at low energies for it to be worth explicitly including their dynamics in computations. There is generally no lower boundary on the energy regime to which an effective theory is valid, but it may be that the description provided by the effective theory can be replaced by an even simpler effective theory at lower energies.

Novel Light Effects

The existence of virtual particles is fundamental to the modern understanding of quantum field theory, and their effects must be factored in to any relativistic scattering calculation. Additionally, virtual particles give rise to a host of novel phenomena, that would not be possible without their existence. An early example of this is the Euler-Heisenberg Lagrangian,

which includes the first order quantum correction to photon propagation, permitting light-by-light scattering,

$$\mathcal{L}_{\mathrm{E-H}} = -\frac{1}{4}F^{\mu\nu}F_{\mu\nu} - \frac{\alpha^2}{m_e^4}\left(c_1(F^{\mu\nu}F_{\mu\nu})^2 + c_2(F^{\mu\nu}\tilde{F}_{\mu\nu})^2\right) + \mathcal{O}(\alpha^3) \tag{2.1}$$

$\tilde{F}$ is the dual to the field strength tensor, $\tilde{F}^{\mu\nu} = \frac{1}{2}\varepsilon^{\mu\nu\rho\sigma}F_{\rho\sigma}$. The Euler-Heisenberg Lagrangian serves as an example of an effective field theory. Here an electron loop has been integrated out to give rise to an effective four-photon interaction. We see that the corresponding interaction terms in the Lagrangian are suppressed by the fourth power of the electron mass, one power for each electron propagator in the full diagram (there are correspondingly four powers of the electron charge e encoded in α^2). The constants $c_{1,2}$ must be determined by matching to the full theory, i.e. QED[1]. Note, for the context of tunnelling of the third kind that we introduce shortly, that the operators in the Lagrangian (2.1), while higher dimensional, are entirely local.

2.1.1 Light shining through walls

The search for WISPs has engendered many novel techniques. One class of experiments is that of laser based light-shining-through-walls [119]. This kind of experiment exploits the oscillation of photons into hidden photons (or, in a magnetic field, axions) to search for light in an otherwise dark cavity separated from a laser cavity by a reflective wall. The only particle capable of producing such a signal in the Standard Model is the neutrino, which, in the presence of a magnetic field, could be produced on one side of the wall and pass through unhindered, before being detected on the other (indeed, this is the operating principle of long baseline experiments, where the "wall" is many kilometres of Earth). However, in order that the neutrinos are produced by a laser, and detected as photons, a loop diagram and electroweak boson exchange is required on both sides of the wall, within the confines of the cavity. The probability of this is so prohibitively small that even if one were to shine every photon in the universe at the wall, perhaps no photons would pass through in this channel [119, 147].

The advantage the light-through-walls approach in a laser set up (over a beam dump type set up, for example) is that photon-WISP oscillations can be coherent if the phase velocities of the photon and the WISP are close. In this case, the amplitudes for conversion all interfere

[1] The calculation is relatively involved, but yields the simple, if seemingly arbitrary result $c_1 = 1/90$ and $c_2 = 7/360$.

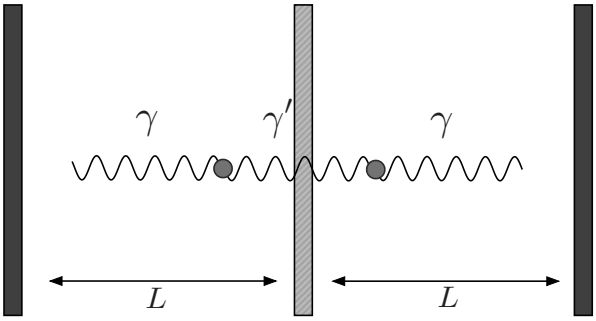

Fig. 2.1.: Schematic experimental setup for light shining through walls cavity experiment.

constructively, greatly enhancing production. Additionally, in an optical cavity with reflective walls, photons can be "recycled" (i.e. make a pass of the cavity) $\sim 10^5$ times, enabling the easy production of high luminosity experiments.

A schematic of a typical setup in shown in Fig. 2.1 (in this case, without a magnetic field that would be uniformly applied across the cavity).

2.1.2 Tunnelling of the third kind

Taking the idea of light shining through walls to the extreme, whereby the wall is traversed not by real particle oscillation, but by an off-shell virtual particle, we arrive at a new phenomenon - tunnelling of the third kind[2] (T3K). The idea is that photons initially trapped in one cavity may traverse a wall (much like a light-shining-through walls setup) by fluctuating into a virtual particle-antiparticle pair, before regenerating in an adjacent cavity. Since neutrinos carry no electrical charge, there are no known fundamental particles for which this is possible at the 1-loop level. (Neutrinos can be used beyond the 1-loop level, but the probability is small enough that there is zero chance of observing the effect over the lifetime of the Universe). It would thus be a smoking gun signal of BSM physics.

Motivating investigation of the phenomenon from a bottom up perspective, in the correct experimental set up, tunnelling of the third kind can enhance existing constraints on minicharged particle (MCL) scenarios. Fig. 2.2 shows the region of parameter space accessible by applying a strong magnetic field ($B = 5$ T) rotated at various angles to the polarisation of the cavity photons. Notice that magnetically amplified T3K can actually improve on cosmological constraints in the low mass MCP region.

[2]We identify the first kind of tunnelling to be the non- relativistic quantum tunnelling of a particle through a potential barrier and the second kind to be transition via a real particle conversion, i.e. the light-shining-through-walls effect.

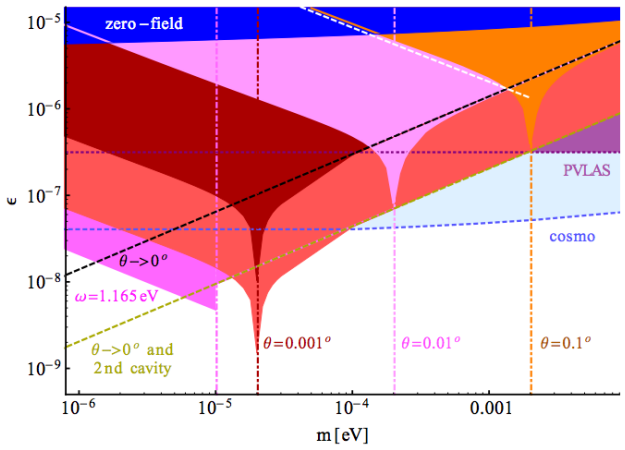

Fig. 2.2.: The probe-able minicharged particle parameter space with the application of a strong magnetic field to a tunnelling of the third kind experiment [148].

The technique was in fact originally proposed [149] as a means of searching for minicharged particles. Here we depart temporarily from BSM physics and explore a novel phenomenon inherent to effective quantum field theories – effective non-locality. We describe a potentially realisable quantum optical set up that could exhibit T3K.

2.2 A test of effective non-locality

2.2.1 Lagrangian approach

We begin with the foundation of most quantum field theories, a classical local action.

$$S = \int d^4x\, \mathcal{L}, \tag{2.2}$$

where $\mathcal{L}$ is the Lagrangian of the theory in question and contains all renormalisable interactions permitted by Lorentz and gauge symmetry. The process we will investigate can be neatly formalised with a classical field theory for three scalar fields and their local interactions, described by,

$$S_{\text{int}} = \int d^4x \frac{\lambda}{\hbar^2 c^2} \phi_a(x) \phi_b^*(x) \phi_c(x) + \text{h.c.}, \tag{2.3}$$

where $\phi_{a,b}$ are complex and ϕ_c is real (the choice of complex or real may seem arbitrary, but is justified in the following). Notice that the interactions of Eq. (2.3) (which, for simplicity,

does not include any couplings to external potentials) and the accompanying kinetic terms are entirely local. In the non-relativistic limit, and with only one spatial dimension plus time, also for simplicity, the theory is expressed as

$$S_{\text{eff}} = \iiiint dtdt'dxdx'\phi_a^*(x',t')\Big\{\delta(x-x')\delta(t-t')\times\Big[i\hbar\partial_t + \frac{\hbar^2}{2m}\partial_x^2 - V_a(x)\Big] - \Pi(x,x',t-t')\Big\}\phi_a(x,t), \quad (2.4)$$

with the corresponding equation of motion,

$$i\hbar\partial_t\phi_a(x,t) = -\frac{\hbar^2}{2m}\partial_x^2\phi_a(x,t) + V(x)\phi_a(x,t) + \iint dx'dt'\Pi(x,x',t-t')\phi_a(x',t'). \quad (2.5)$$

This is a non-local version of Schroedinger's equation for the field $\phi_a(x,t)$. The non-locality is manifest in the function $\Pi(x,x',t-t')$, which implies that the evolution of $\phi_a(x,t)$ depends not only on its value at space-time coordinates (x,t), but also on its value at a spatially and temporally separated point (x',t') (so long as $\Pi(x,x',t-t')$ is not proportional to $\delta(x-x')$).

We can test this effective non-locality by realising a "tunnelling of the third kind" experiment. Tunnelling processes (say, between two square well potentials) in non-relativistic quantum mechanics rely upon a finite barrier height; the tunnelling rate is vanishing in the limit that the barrier height goes to infinity. However, quantum field theory introduces non-particle number conserving processes not present in single particle ("regular") quantum mechanics. This allows the real particle ϕ_a to split into a pair of virtual ϕ_b and ϕ_c particle states. Tunnelling of the third kind can be achieved if these virtual states interact sufficiently weakly with the (infinite) barrier potential to pass through it. The states must, as they are virtual, recombine into a real ϕ_a particle. If they have traversed the barrier, then the particle ϕ_a has crossed a region that is forbidden to it both classically and quantum mechanically, a clearly non-local phenomenon. This is induced explicitly by the non-particle number conserving property of quantum field theory. The non-locality is only an effective one, resulting from eliminating the intermediate states from the description when we write the effective Schrödinger equation, Eq. (2.5), for the particle ϕ_a.

As mentioned, there are no suitable fundamental particles to realise T3K in the SM, but a realisation may be possible by exploiting the behaviour of atomic excited states. We outline a toy quantum optical configuration that is a suitable analogue to directly test the non-locality inherent to effective field theories.

The set up will consist of two potential wells separated by an infinite potential barrier, with an atom **A** in the ground state localised to the left hand well. The T3K process then consists of the atom entering a virtual excited state $\mathbf{A}^*$ by the emission of a virtual photon and passing the barrier into the right hand well before recombining. It is assumed that neither the photon nor the excited state are subject to the barrier potential, but both remain bounded within the overall potential well. Such a situation is realisable with excited atomic states, which often occupy different potential surfaces to the ground state. As a practical consideration, we will place the whole arrangement within a cavity that allows only a single resonant mode of the photon (but ensure the potentials in which the atoms are trapped are such that there is no possibility of collision with the cavity walls).

We can investigate the effect of the effective non-locality on the rate of tunnelling between the two potential wells (which, in the absence of the virtual state, would be zero). In the eigenbasis expansion, $\phi_a(x,t) = \sum_n c_n^{(a)}(t)\varphi_n^{(a)}(x)$ where $\varphi_n^{(a)}(x)$ are the eigenstates of the unperturbed system, we explicitly separate the time dependence of the field from its spatial dependence. The unperturbed eigenstates are the solutions to the (local) Schroedinger equation,

$$\left(-\frac{\hbar^2}{2m}\partial_x^2 + V_a(x)\right)\varphi_n^{(a)}(x) = E_n^{(a)}\varphi_n^{(a)}(x). \tag{2.6}$$

We can use this expansion to write the effective action (2.4) in energy space,

$$\begin{aligned} S_{\text{eff}} = &\sum_n \int dt \left[c_n^{(a)*}(t)\left(i\hbar\frac{d}{dt} - E_n^{(a)}\right)c_n^{(a)}(t)\right] \\ &- \sum_{n,n'} \iint dtdt' \left[c_n^{(a)*}(t)\Pi_{n,n'}\delta(t-t')c_{n'}^{(a)}(t')\right], \end{aligned} \tag{2.7}$$

where $\Pi_{n,n'}(t-t') \equiv \iint dxdx'\varphi_n^{(a)*}(x)\Pi(x,x',t-t')\varphi_{n'}^{(a)}(x')$ and we assume short lived virtual intermediate states, such that we can make the approximation $\Pi_{n,n'}(t-t') \approx \Pi_{n,n'}\delta(t-t')$. Note that this approximation is not valid in the resonant case, where the energy of the photon in the intermediate state equals the energy difference between the ground and excited state. The assumption that this is not the case is justified a posteriori by the agreement between the Lagrangian and Hamiltonian calculation we will perform. The resulting equations of motion are,

$$0 = \frac{\delta S_{\text{eff}}}{\delta c_n^{(a)*}(t)} = \left(i\hbar\frac{d}{dt} - E_n^{(a)}\right)c_n^{(a)}(t) - \sum_{n'}\Pi_{n,n'}c_{n'}^{(a)}(t), \tag{2.8}$$

which we can cast as a matrix equation

$$i\hbar\frac{d}{dt}\begin{pmatrix} c_S(t) \\ c_A(t) \end{pmatrix} = \begin{pmatrix} E_S & 0 \\ 0 & E_A \end{pmatrix}\begin{pmatrix} c_S(t) \\ c_A(t) \end{pmatrix} + \begin{pmatrix} \Pi_{SS} & 0 \\ 0 & \Pi_{AA} \end{pmatrix}\begin{pmatrix} c_S(t) \\ c_A(t) \end{pmatrix}. \quad (2.9)$$

In writing the matrix equation, we have assumed the potential V_a to be symmetric around the central barrier. We have further ignored all but the lowest two energy eigenstates of ϕ_a, allowing us to cast them in a symmetric (subscript S) and antisymmetric (subscript A) basis.

Parity enforces that $\Pi_{AS} = \Pi_{SA} = 0$, and the symmetry between the two wells sets means $E \equiv E_S = E_A$ (the parity operator commutes with the Hamiltonian, so energy eigenstates are also parity eigenstates, and parity must be conserved). Π_{SS} is the energy shift caused by the creation of virtual particles coupling two symmetric states (and similarly for the antisymmetric case).

We are investigating the tunnelling between two adjacent potential wells, and there is a natural basis that reflects that. Let $c_L \equiv (c_S + c_A)/\sqrt{2}$ and $c_R \equiv (c_S - c_A)/\sqrt{2}$ define amplitudes for the left and right hand wells respectively. We localised the atom in the ground state (a) to the left hand well at $t_0 = 0$, so we can apply the initial condition $c_L(0) = 1$, $c_R(0) = 0$, to get $c_R(t) = [e^{-i(E+\Pi_{SS})t/\hbar} - e^{-i(E+\Pi_{AA})t/\hbar}]/2$. Then the tunnelling probability is simply the probability to find the atom in the right hand well at a time $t > t_0$.

$$P_{\text{T3K}}(t) = |c_R(t)|^2 = \sin^2([\Pi_{AA} - \Pi_{SS}]t/2\hbar), \quad (2.10)$$

This result displays the expected feature that the tunnelling rate is determined by the energy shift $\delta E = \Pi_{AA} - \Pi_{SS}$.

2.2.2 Hamiltonian approach

The Lagrangian formulation has the advantage of making the non-locality manifest, and is a familiar language for high energy physics. However, in this instance, the equivalent Hamiltonian formulation, more often applied to non-relativistic quantum mechanics, proves computationally easier.

To set up the framework, we must define the potentials involved in the problem. The first is an overall trapping potential to localise all particles to an infinite square well, which we define to have length $2\ell + d$,

$$V_b(x) = \begin{cases} 0 & \text{for} \quad -\ell - d/2 \leq x \leq \ell + d/2, \\ \infty & \text{for} \quad |x| > \ell + d/2. \end{cases} \tag{2.11}$$

Additionally, we must define a central "wall" potential that will be felt by the ground state atom, but not the excited state or virtual photon. We give it width d, so that each side of the well has width ℓ,

$$U(x) = \begin{cases} \infty & \text{for} \quad -d/2 < x < d/2, \\ 0 & \text{for} \quad |x| \geq d/2. \end{cases} \tag{2.12}$$

The "bare" frequencies for atoms in a, b states are,

$$\omega_j^{(a)} = \Omega_a + \frac{\hbar\pi^2 j^2}{2m\ell^2}, \qquad \omega_j^{(b)} = \Omega_b + \frac{\hbar\pi^2 j^2}{2m(2\ell + d)^2}, \tag{2.13}$$

where $\hbar\Omega_{a,b}$ are the internal energies of the atom when in the ground and excited states. j indexes the energy eigenstate, and we again take only the lowest two spatial modes (corresponding to $j = 1$) for the atom in state a. The two modes are denoted $\varphi_L^{(a)}(x)$ and $\varphi_R^{(a)}(x)$, and we abbreviate $\omega_a \equiv \omega_1^{(a)}$. The excited atom, in state b, has spatial modes denoted $\varphi_j^{(b)}$. We initially assume that only a single cavity (photon) mode couples the a and b states, with energy $\hbar\omega_c$.

Can now write a complete Hamiltonian realising the desired features,

$$\hat{H} = \sum_{\sigma=L,R} \hbar\omega_a \hat{a}_\sigma^\dagger \hat{a}_\sigma + \sum_{j=1}^{\infty} \hbar\omega_j^{(b)} \hat{b}_j^\dagger \hat{b}_j + \hbar\omega_c \hat{c}^\dagger \hat{c} + \sum_{\sigma=L,R} \sum_{j=1}^{\infty} \hbar g_{\sigma j} (\hat{c} + \hat{c}^\dagger)(\hat{a}_\sigma^\dagger \hat{b}_j + \hat{b}_j^\dagger \hat{a}_\sigma). \tag{2.14}$$

The terms in the Hamiltonian form analogues to those in the Lagrangian description. The creation ($\hat{a}^\dagger$) and annihilation ($\hat{a}$) operators respectively create and annihilate an atom in state a, represented by the field $\varphi_\sigma^{(a)}(x)$ (and similarly for the b and c states).

The couplings (normalised to be real) $g_{\sigma j}$ are,

$$g_{\sigma j} = g \int dx \varphi_\sigma^{(a)}(x) \varphi_j^{(b)}(x) C(x), \tag{2.15}$$

where g represents some overall scaling of the couplings. It is usual in atomic optics to neglect terms in the Hamiltonian representing high frequency oscillations – the Rotating

Wave Approximation (RWA) [150] – but here our effect arises from precisely these beyond-RWA [151] terms, which are explicitly included.

For the simple set up we have described, with a single atom in either state a or b and n cavity photons (with $n \in \{0, 1\}$ for now), we can use the basis $\{|a, \sigma, n\rangle, |b, j, n\rangle\}$, with $\sigma \in \{L, R\}$ and $j \in \{1, 2, 3, \dots\}$. The result is a simple form for the probability of tunnelling of the third kind to occur,

$$P_{\text{T3K}}(t) = |\langle a, R, 0| \exp(-i\hat{H}t/\hbar)|a, L, 0\rangle|^2. \tag{2.16}$$

For a first approximation, we can consider only the lowest spatial modes of the a and b states and a single photon. We will see that this proves too naïve and correct it later. The matrix form of Hamiltonian is,

$$\hat{H} = \hbar \begin{pmatrix} \omega_a & \tilde{g} & 0 \\ \tilde{g} & \omega_b + \omega_c & \tilde{g} \\ 0 & \tilde{g} & \omega_a \end{pmatrix}, \tag{2.17}$$

with $\omega_b \equiv \omega_1^{(b)}$, $\omega_a \equiv \omega_1^{(a)}$ as defined in Eq. (2.13), and $\tilde{g} = g_{L1} = g_{R1}$ from Eq. (2.15). The lowest order solution is,

$$P_{\text{T3K}}(t) = \left|\sin(\tilde{g}^2 t/\delta) + 2(\tilde{g}/\delta)^2 e^{-i\delta t/2} \sin(\delta t/2)\right|^2, \tag{2.18}$$

where $\delta = \omega_b + \omega_c - \omega_a$ is defined for convenience. The solution contains both slowly and rapidly oscillating components (assuming that the coupling is sufficiently small, $|\tilde{g}| \ll |\delta|$). The slow oscillating term, frequency $2\tilde{g}^2/\delta$ dominates for large times. The second term is has high frequency, δ, oscillations, but is suppressed by the small factor $(\tilde{g}/\delta)^2$. Ignoring this second term shows the same time dependence as the result from the Lagrangian calculation, Eq. (2.10), when we recognise that the energy gap $\Pi_{AA} - \Pi_{SS} = 2\tilde{g}^2/\delta$ (which may be checked explicitly in second order perturbation theory). This agreement justifies the earlier claim that a short lived intermediate state (such that $\Pi_{n,n'}(t - t') \approx \Pi_{n,n'}\delta(t - t')$) was justified in the Lagrangian calculation.

Recall: 'regular' quantum tunnelling

It will be useful to quickly review the salient features of "regular" quantum tunnelling. Consider 2 1-D potential wells separated by a finite potential barrier of height V_0. For a particle initially localised to one side of the coupled wells, the probability to later find it in the opposite well is exponentially suppressed by the height of the potential barrier V_0, and the width d of the barrier. At the barrier, the particle wavefunction is a solution to,

$$-\frac{\hbar^2}{2m}\frac{\partial^2\psi(x)}{\partial x^2} = (E - V_0)\psi(x), \tag{2.19}$$

which takes the form,

$$\psi(x) \propto \exp\left(-\sqrt{\frac{2m(V_0 - E)}{\hbar^2}}x\right). \tag{2.20}$$

There is a problem with the result: it does not obey the Heisenberg uncertainty principle. Provided the energy of the excited state $|b, j, 1\rangle$ is greater than the ground state energy $|a, L, 0\rangle$, then analogy to regular quantum tunnelling with a finite barrier (where the "barrier" here is the energy required to enter the excited state), the Heisenberg uncertainty principle predicts that the tunnelling rate should be proportional to the exponential of the energy gap and the wall thickness (each to some power). This behaviour is not displayed by Eq. (2.18).

Additionally, the energy gap between the ground and excited state ($\sim \hbar\,\delta$) is usually larger than the energy splittings of the spatial modes of the b states, and one should realistically sum over all j. This requires an infinite dimensional matrix in the Hamiltonian, but with a suitable simplification, one can still obtain a result. The simplification is to make the cavity mode $C(x)$ slow varying with respect to the tunnelling time, such that the coupling $\tilde{g}_0 \equiv gC(x)$ may be taken constant. Then we can compute the energy difference again in second order perturbation theory. The calculation is presented in Appendix B, and results in the energy splitting;

$$\delta E = \Pi_{AA} - \Pi_{SS} = \frac{8\tilde{g}_0^2 m\xi\ell\sinh^2(\ell/\xi)\,\mathrm{csch}([2\ell + d]/\xi)}{\pi^2(1 + \ell^2/\xi^2\pi^2)^2}, \tag{2.21}$$

where we have defined a characteristic length scale $\xi = \sqrt{\hbar/2m|\Delta|}$ and $\Delta = \Omega_b + \omega_c - \omega_a$.

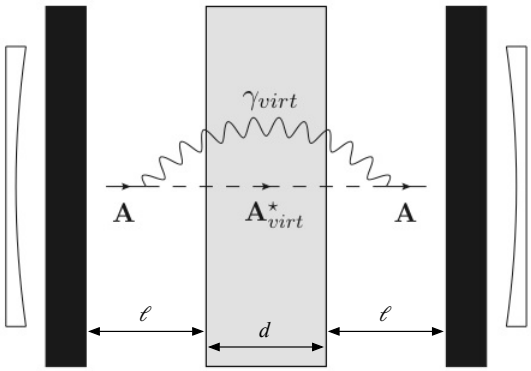

Fig. 2.3.: Schematic experimental setup for tunnelling of the third kind cavity experiment, realised with an atom $\mathbf{A}$ and it's virtual excited state $\mathbf{A}^{*}_{virt}$.

In the limit that $\ell \gg \xi$, we get the expected exponential suppression with the wall thickness,

$$\delta E \approx \epsilon \exp(-d/\xi), \tag{2.22}$$

as a function of a characteristic energy scale (that bounds δE from above),

$$\epsilon = 2\pi^2 \frac{\hbar \tilde{g}_0^2}{\Delta} \left(\frac{\xi}{\ell}\right)^3. \tag{2.23}$$

2.2.3 Experimental prospects

The approximate setup we want to imitate is shown in Fig. 2.3. The maximum barrier width for which tunnelling is feasible, corresponding to the length scale associated with the effective non-locality, is (from Eq. (2.22)) $d = \xi \ln(\epsilon/\delta E)$, which is clearly linearly dependent on ξ but only weakly dependent on $\epsilon/\delta E$. We can observe no tunnelling if the cavity decays faster than the tunnelling rate. To get a reasonable sample of events, we require that the tunnelling rate is much greater than the cavity decay rate, κ. This puts a further constraint on the barrier width,

$$d \ll \xi \ln\left(\frac{\epsilon}{\hbar\kappa}\right). \tag{2.24}$$

As an example feasibility study, let us consider circular Rydberg atoms in a cryogenically cooled superconducting microwave cavity. The two key characteristics of such a setup are the typical decay length (ξ) and typical transition frequency ($\epsilon/\hbar$). A reasonable Rabi frequency $\Omega/2\pi = 50\text{kHz}$ (for transition frequency between the a and b state of 51.1GHz), which maps to the coupling $\tilde{g}_0$ in our formulation, results in a cavity decay rate $\kappa/2\pi = 7.7\text{Hz}$, with

$\mathcal{O}(\text{seconds})$ atomic lifetimes [152]. Even making the optimistic assumption of $\ell \sim \xi$, the resulting characteristic length $\xi \sim 30\text{pm}$ is too small to realise with an optical setup, though the characteristic frequency $\epsilon/\hbar \sim 2\pi^2\tilde{g}_0^2/\Delta \sim 6\text{Hz}$ is of the same order as the cavity decay rate.

Fortunately the experimental situation is not completely without promise. We can consider a situation in which the initial state a is of higher internal energy than the intermediate $b+\gamma$ state. The modified energy gap is then,

$$\delta E = \frac{8\tilde{g}_0^2 m\xi\ell \sin^2(\ell/\xi)\csc([2\ell+d]/\xi)}{\pi^2(1-\ell^2/\xi^2\pi^2)^2}. \tag{2.25}$$

in which essentially all the Δ in Eq. (2.21) have been replaced with a negative quantity, $-|\Delta|$. This results in the replacements $\xi \to i\xi$, and the hyperbolic functions become trigonometric. Crucially this modification has removed the exponential suppression with d, making the system much easier to realise. With a negative energy gap between the a and b states, the real decay of the initial state becomes possible, but the cavity setup we have described does not permit $\Delta = 0$ (it is detuned from this resonance), so that only off-shell states may traverse the wall, and the process is fundamentally the same as in the $\Delta > 0$ case.

A simulation of light-shining-through-walls

If tunnelling of the third kind could be realised in a quantum optical set up, it would serve as a simulation of the light-shining-through-walls experiments searching for WISPs. The initial state a would represent a photon, with the excited state b representing a WISP (for example the hidden photon). The additional photon in the intermediate state of the quantum optical setup is superfluous, since the hidden photon can be produced by oscillation of the SM photon. In the case of an axion, a magnetic field would be required to facilitate production via its two photon coupling. In a real experiment, the initial state would not be a single photon, but a large number (N) of photons trapped in the cavity, enhancing the probability of the process by a factor N. Building a quantum optical set up to exhibit the LSW phenomenon (via a real rather than virtual intermediate state) could act as both a proof of principle for LSW and a first step towards realising a T3K experiment.

2.3 Conclusion

We have investigated the possibility of experimentally testing the effective non-locality in the propagation of particles in an effective theory in a quantum optical system. The realisation of a fully virtual transition across a potential barrier with atoms is difficult due to the extremely narrow barrier width required. Considering an internal state with lower energy than the initial state, the situation becomes more promising. An experiment to realise the barrier crossing phenomenon even with an on-shell intermediate state would serve as a simulation of LSW and represent a first step towards realising a full T3K experiment.

This Chapter has been something of a diversion from the primary BSM physics investigated in this Thesis, but illustrates that investigating BSM phenomena can lead to innovations in experiment applicable to SM (or even quantum optical) processes.

3 Hidden Photons from Large Extra Dimensions

> *. . . and got the dimensions back and front and every way, taking notes carefully . . .*
>
> **— Marlow**

Hidden photons, motivated in the Introduction, often arise in string compactifications (when higher degree gauge groups are broken upon compactification). In light of this, it seems worthwhile to consider, in a very general way, the effects that the necessary extra dimensions of string theories have on the phenomenology associated with hidden photons. In particular, a single additional Abelian gauge boson has no effect on the Standard Model (except an undetectable field redefinition) if it is massless and there is no hidden sector matter to which it couples. Therefore, if we are to have any hope that hidden photons could be detected, should they exist, we must provide the theoretical framework to generate their mass. In addition to the "standard" Higgs and Stueckelberg mechanisms, extra dimensional theories provide a novel means of mass generation, without the explicit introduction of additional scalar fields for this purpose. If we begin with a massless extra dimensional U(1) gauge field, a stack of massive Kaluza-Klein (KK) modes of the field are generated upon compactification.

This Chapter will discuss this idea in detail, and experimental and theoretical constraints on a toy model will be presented.

3.1 Introduction to LED

The hierarchy problem of particle physics may be phrased in multiple ways, and has attracted many and varied approaches to its resolution. Electroweak symmetry breaking occurs in the early Universe, the Higgs field gains a vacuum expectation value (VEV) and fundamental particles become massive. It is common to put the question of the hierarchy problem in terms

of the Higgs mass, which is particularly relevant in light of the recent discovery. In principle, loop corrections to the Higgs mass introduce an arbitrarily high scale. The correction due to a single fermion loop, for example, is $\delta m_h^2 \propto \Lambda^2 + c \log \Lambda$, where Λ is the high scale, usually taken in this context as the Planck scale. In order that the Higgs mass be at the electroweak scale then (which is required to regularize longitudinal vector boson scattering, but is also what we observe, both directly and in the masses of fermions), there must be some extraordinary cancellation across 16 orders of magnitude. Supersymmetric theories address this issue by providing a superpartner to every particle that contributes to quantum corrections – this analytically cancels the term (or would, if SUSY were unbroken). An alternative and orthogonal approach is to alleviate the problem by lowering the relevant fundamental scale.

Perhaps a simpler statement of the hierarchy problem, and one that cuts to the heart of the issue – a discrepancy of scales – is to ask "Why is gravity so much weaker than the other fundamental forces?"

The answer to this question is not known, but there are several compelling possibilities; among them is the idea of extra spatial dimensions. The idea is not new, dating back at least to the work of Kaluza [153] and Klein [154] in the 1920s, but was revived more recently by the introduction of viable models for large extra dimensions (LED) [155–157]. In such models, only a subset of the full field content of the model may propagate along the extra dimensions. Commonly, only gravity is permitted in the bulk space. Its strength is consequently diluted by the volume of the extra dimensions. Thus a solution to the hierarchy problem is provided by introducing a new, lower "fundamental" scale which is closer to the electroweak scale and associated with the full, $(4 + d)$-dimensional space. The alternative paradigm, that of universal extra dimensions (UED), in which all fields experience all dimensions, is subject to tighter experimental constraints on the size of the extra dimensions. In such a situation, every SM particle would have an associated tower of heavier states (so-called Kaluza-Klein excitations), none of which have yet been detected.

Models with LEDs may be further divided into two categories: those with flat extra dimensions and those with warped extra dimensions, per the work of Randall and Sundrum [158–160]. The latter case creates an exponential hierarchy between the weak scale and Planck scale by introducing a warping factor in the metric. The content of this Chapter will be concerned with the former, flat, case with a $(4 + d)$-dimensional Minkowski metric. Similar work has been previously performed for the warped case [161, 162] (though with a focus

primarily on high energy collider signals, rather than the low energy phenomenology we will detail here).

Large extra dimensions attempt to solve the hierarchy problem by lowering the fundamental scale, and having the observed high Planck scale be the result of compactification to 4 dimensions. We can see how this works by considering the Einstein-Hilbert action,

$$\mathcal{S}_4 = -M_{\text{Pl.}}^2 \int d^4x \sqrt{|-g^{(4)}|}\mathcal{R}^{(4)}. \tag{3.1}$$

Here $M_{\text{Pl.}}$ is the familiar 4-dimensional Planck mass and $\mathcal{R}$ is the Ricci scalar. The generalisation to $4+d$ dimensions is,

$$\mathcal{S}_{4+d} = -M_\star^{2+d} \int d^{(4+d)}x \sqrt{|-g^{(4+d)}|}\mathcal{R}^{(4+d)}. \tag{3.2}$$

We can first observe that when computed, the Ricci scalar doesn't change in higher dimensions, so $\mathcal{R}^{(4+d)} = \mathcal{R}^{(4)}$. The line element for the whole $4+d$ dimensional space, with $d\Omega_{(d)}$ representing the extra dimensional line element (and ignoring fluctuations of the metric) maybe parameterised as,

$$ds^2 = \eta_{\mu\nu}dx^\mu dx^\nu - R^2 d\Omega_{(d)}^2, \tag{3.3}$$

where $\eta_{\mu\nu}$ is the 4D Minkowski metric. One can see from this that the determinant of the metric obeys $\sqrt{|-g^{(4+d)}|} = R^d\sqrt{|-g^{(4)}|}$. This allows the full $(4+d)$-dimensional action to be expressed as,

$$\mathcal{S}_{4+d} = -M_\star^{2+d} \int d^4x d\Omega_{(d)} R^d \sqrt{|-g^{(4)}|}\mathcal{R}^{(4)}. \tag{3.4}$$

The factor $\int d\Omega_{(d)}R^d$ is precisely the extra dimensional volume, $V_d = (2\pi R)^d$. Comparing Eq. (3.4) to Eq. (3.1), we arrive at the desired relation between the 4-dimensional Planck scale $M_{\text{Pl.}}$ and the extra dimensional, *fundamental* scale $M_\star$,

$$M_{\text{Pl.}}^2 = V_d M_\star^{2+d}. \tag{3.5}$$

We note briefly that there are several means of arriving at this relationship [163]. One can now see that the fundamental scale and size R of the extra spatial dimensions are inversely correlated, since $M_{\text{Pl.}}$ is fixed. So in order that the fundamental scale is very low, say on order 1 TeV, the extra dimensions must be correspondingly large. In the case of a single extra dimension, the necessary size is on the order of 1 A.U. (astronomical unit, i.e. the Earth-Sun distance, roughly 10^{11} m). This would clearly modify the Newtonian dynamics of

d	$1/R = m_0$	$M_\star$
1	> 1.1 meV	$\gtrsim 3 \times 10^5$ TeV
2	> 4.6 meV (27 eV)	$\gtrsim 3$ TeV (230 TeV)
3	> 740 eV (12 keV)	$\gtrsim 3$ TeV (16 TeV)
4	> 290 keV	$\gtrsim 3$ TeV
5	> 10 MeV	$\gtrsim 3$ TeV
6	> 120 MeV	$\gtrsim 3$ TeV

Tab. 3.1.: Limits on the scale of extra dimensions. The $d = 1$ constraint arises from direct tests of the gravitational inverse square law [165, 166]. For $d = 2{-}6$ the scale is more strongly constrained by the minimum value of the extra dimensional (i.e. the fundamental) scale $M_\star$ provided by colliders [167, 168]. The values in brackets for $d = 2{,}3$ come from consideration of photon emission from KK gravitons produced in neutron stars [164], and are discussed further in the main text.

the solar system, so cannot be possible. If one wishes to lower the fundamental scale from the Planck scale to 1 TeV with flat extra dimensions, one must consider more than one extra dimension. In the case of two extra dimensions, the scale can be lowered to roughly 3TeV before coming into conflict with LHC bounds. The limits on the size of extra dimensions allowed by experiment for $d = 1 \ldots 6$ are given in terms of $M_\star$ and the corresponding $1/R$ in Table 3.1.

For $d = 2 - 3$ extra dimensions the strongest current bounds arise from the consideration of the photon spectrum due to KK graviton excitations decaying into photons after being produced in neutron stars [164]. These constraints are listed in brackets due to their reliance on astrophysical processes being well modelled - in general, collider processes are far better understood than those occurring in complex stellar environments. As such, while the neutron star bounds are far stronger, they are perhaps less reliable than those obtained with the LHC. In the exclusion plots shown later in the Chapter, the minimum KK mode mass will be taken at the LHC limit, but the neutron star limit will also be shown. It should be noted that the same reservations about bounds arising from astrophysical processes apply to the bounds derived in the work [3] this Chapter presents.

3.2 The toy model

In Chapter 1 we highlighted that in the absence of an extended hidden sector, massless hidden photons can have no observable effects. As such, two methods of mass generation were covered – a hidden Higgs mechanism and the Stueckelberg mechanism. It was noted that the presence of a hidden Higgs boson changes the constraints on the hidden photon

parameter space by providing new experimental signatures. Here we will present a toy model where the mass of the hidden photon originates from neither of the above mechanisms per se, but is the result of compactification from a higher dimensional theory.

We consider the simplest situation: a Minkowski bulk space with d extra spatial dimensions. The Standard Model fields are localised to a 3-brane, which we represent with an effective description. The brane is assumed to be infinitesimally thin, infinitely heavy and possessed of no intrinsic dynamics. In addition to the brane-localised SM, we include gravity and an additional $D = d + 4$ dimensional hidden photon gauge field (so that the number of extra spatial dimensions is d), both of which extend through the whole bulk space.

Our notation is perhaps best illustrated by considering the extra dimensional metric, which has the structure,

$$g_{MN} = \begin{pmatrix} g_{\mu\nu} & g_{\mu b} \\ g_{a\nu} & g_{ab} \end{pmatrix} \tag{3.6}$$

where $g_{\mu\nu}$ is the usual 4D metric (for Minkowski space, say), the indices M, N run over $0, \ldots, D-1$, and the indices a, b cover only the extra spatial components, $4, \ldots, D-1$. For notational transparency, a general extra dimensional spatial vector a_M has its components represented by $(x_0, \ldots, x_3, y_4, \ldots, y_{D-1})$, so that the y_a represent only the d extra dimensions. Note that since we are treating only flat extra dimensions perpendicular to the brane, the metric is a generalisation of 4D Minkowski space, so the off- diagonal terms $g_{\mu b} = g_{a\nu} = 0$.

The hidden photon mixes kinetically with hypercharge only on the brane (due to the localisation of the SM). Similarly, gravity interacts with the SM only on the brane, but may interact with the hidden photon field in the bulk (see Section 3.3).

Explicitly including only the mixing with the photon (after electroweak symmetry breaking, this is the most relevant part for the accessible phenomenology), the above is described by the action,

$$S_D = \int \mathrm{d}^D x \sqrt{g} \Big(-\frac{1}{4} F^{\mu\nu} F_{\mu\nu} \delta^d(\vec{y}) - \frac{1}{4} X^{MN} X_{MN} - \frac{1}{2} \chi_{\mathrm{D}} F^{\mu\nu} X_{\mu\nu} \delta^d(\vec{y}) \Big), \tag{3.7}$$

plus terms describing the remainder of usual SM.

It is experimentally clear that, for any number of extra dimensions in which gravity acts, the spatial extent of these dimensions cannot be large. For a single extra dimension the most

stringent constraint on this comes from tabletop tests of the inverse square law [165, 166]. For higher numbers of extra dimensions, constraints on the production of gravitons at the LHC provide a tighter bound [167, 168]. Thus, extra dimensions must necessarily be small enough that they have evaded these constraints. From a theoretical perspective, they must be compactified onto a finite manifold. In keeping with the philosophy of choosing the simplest model, we select a d-dimensional torus, $\mathcal{T}_d = \mathcal{S}_1 \times \mathcal{S}_1 \times \cdots \times \mathcal{S}_1$, as the compactification manifold, with each torus having equal radius R. Notice that each dimension here has a U(1) symmetry. This is emphatically not the same as the additional hidden photon U(1) gauge field.

Compactification then, is the process of enforcing the symmetries of the manifold on the field that is being compactified. In this simple case, it can be accomplished by Fourier expanding the hidden photon field along each of the extra dimensions.

$$X_M(x^\mu, y^a) = \frac{1}{(\pi R)^{d/2}} \sum_{|\vec{n}|\geq 0,\sigma} X_M^{(\vec{n},\sigma)}(x^\mu) \prod_{i=1}^{d} f_{\sigma_i}(n_i y_i). \tag{3.8}$$

Here σ indexes the nature of the Fourier modes, hence referred to as Kaluza-Klein (KK) modes, each of which may be either cosine ($+$) or sine ($-$). The mode associated with compactification along each extra dimension decomposes into both types, so that we should consider all combinations, and $\sigma = \{(+,\ldots,+,+),(+,\ldots,+,-),\ldots,(-,\ldots,-,-)\}$. The functions f are,

$$f_s(nx) = \begin{cases} \sqrt{2}\cos x & s = +, \quad n \neq 0 \\ \sqrt{2}\sin x & s = -, \quad n \neq 0 \\ 1 & s = +, \quad n = 0 \end{cases} . \tag{3.9}$$

Physically, only the modes that are nonzero at the brane location may interact with Standard Model fields. Since the brane is located, by choice, at $\vec{y} = 0$, this corresponds to the cosine modes in the Fourier expansion (denoted by $s = +$ above)[1].

Let us calculate the effective action of the 4D theory resulting from the compactification of d extra dimensions in our setup. We begin by Fourier expanding the extra dimensions along

[1]The choice of brane location is entirely arbitrary: shifting it would result in only a linear combination of sine and cosine modes interacting with on-brane physics

circles of radius R, corresponding to the chosen compactification manifold. Explicitly for the simplest case of a single extra dimension,

$$X_M(x^\mu, y^a) = \frac{X_M^{(0)}}{(2\pi R)^{d/2}} + \frac{1}{(\pi R)^{d/2}} \sum_{n>0} \left(X_M^{(n,+)}(x^\mu) \cos\left(\frac{ny}{R}\right) + X_M^{(n,-)}(x^\mu) \sin\left(\frac{ny}{R}\right) \right). \tag{3.10}$$

Inserting this into the action in Eq. (3.7), (and returning to the general case of d extra dimensions), we have,

$$S_{\text{eff}} = \int d^4x \left[-\frac{1}{4} F^{\mu\nu} F_{\mu\nu} - \frac{1}{4} X^{\mu\nu(0)} X^{(0)}_{\mu\nu} + \sum_{n>0,\sigma} \left(\frac{1}{4} X^{\mu\nu(n,\sigma)} X^{(n,\sigma)}_{\mu\nu} + \frac{1}{2} \frac{n^2}{R^2} X^{(n,\sigma)}_{\mu} X^{\mu\,(n,\sigma)} \right) \right.$$
$$\left. + \sum_{n>0} \left(\frac{1}{2} \chi_4 F^{\mu\nu} X^{(n,+\ldots+)}_{\mu\nu} \right) + \ldots \right]. \tag{3.11}$$

The $\vec{n} = 0$ mode has not been included in the above. Since it is massless, the mixing with the photon can be removed by a simple field redefinition and it has no observable effects on the model. Also not included above are the towers of scalar particles associated with the KK decomposition of the higher dimensional gauge field, which likewise decouple. The scalar sector comprises d massless scalars, and $d-1$ associated towers of massive (linear combinations of) scalar KK modes. The remaining stack of massive scalar KK modes are eaten by the corresponding modes in the massless vector KK stack. This essentially represents n copies of the Higgs mechanism, and generates a massive stack of KK vector modes with masses,

$$m^2_{\gamma'} = \frac{n^2}{R^2}(1 + \mathcal{O}(\chi^2)). \tag{3.12}$$

To maintain correct dimensionality in the action, the kinetic mixing parameter is suppressed by a volume factor. Notice that the mapping between the higher dimensional mixing parameter and the 4D mixing parameter is dependent upon the number of extra dimensions. One may expect that for higher numbers of extra dimensions, the constraint on χ_4 becomes stronger, since more modes contribute to any given process, and the volume factor increases.

Upon compactification, the coupling constants of higher dimensional fields are scaled by volume factors. In the present case, this manifests in a rescaling of the kinetic mixing parameter. The four dimensional kinetic mixing is matched to the D-dimensional mixing by,

$$\chi_4 = \frac{\chi_D}{(\pi R)^{d/2}} \prod_{i=1}^{d} \eta_{n_i}, \qquad \text{where} \qquad \eta_{n_i} = \begin{cases} 1/\sqrt{2} & n_i = 0 \\ 1 & n_i \neq 0 \end{cases}, \tag{3.13}$$

and η_{n_i} is a notational convenience to account for the different normalisation of the zero modes of the KK tower.

3.3 Gravity

Crucial to the notion of extra dimensions is the introduction of a fundamental scale, which is supposed to be much lower than the 4D scale. Recall that the two scales are related by,

$$M_\star^{2+d} = \frac{M_{\rm Pl}^2}{(2\pi R)^d}. \tag{3.14}$$

The interactions of gravity with the fields of a particular theory may be extracted from the Lagrangian,

$$\mathcal{L} = -\frac{1}{2M_{\rm Pl}} \sum_{\vec{k}} \left(G_{\mu\nu}^{(\vec{k})} T^{\mu\nu} + \sqrt{\frac{2}{3(d+2)}} \phi^{(\vec{k})} T_\mu^\mu \right), \tag{3.15}$$

where $T_{\mu\nu} = \frac{\partial \mathcal{L}}{\partial(\partial^\mu \phi)} \partial\phi - g_{\mu\nu}\mathcal{L}$ is the energy momentum tensor of the theory (simplified here to contain only a single scalar field) and $\phi^{(\vec{k})}$ is the scalar "dilaton" field.

Should we be concerned about gravity when calculating the phenomenology of our model? The interactions of gravitons (and the particles associated with the KK decomposition - "gravi-vectors" and "gravi-scalars") are all suppressed by a factor of the (4D) Planck scale. However, the stack of KK modes attached to the hidden photon also exists for the graviton, and the large number of modes could enhance the strength of the interactions substantially. Note that the graviton modes have the same mass spectrum as the HP modes, having been compactified on the same manifold. Thus the contribution to a process from gravity grows with the number of modes in the same way that the hidden photon contribution grows. As such, if the contribution of a single graviton mode is insignificant compared to the contribution of a single hidden photon mode in a given process, we can safely ignore gravitational interactions in that process. To estimate the relative size of the contributions, one can simply compare the effective "couplings" of gravitons and hidden photons respectively, namely the inverse of the (4D) Planck mass and the kinetic mixing parameter. Then, for a process occurring at energy scale Λ, gravitational interactions are important relative to hidden photon interactions only when $\chi_4 \lesssim \Lambda/M_{\rm Pl}$.

The above concerns only gravitational interactions with the Standard Model occurring independently to the hidden photon interactions. However, there are possible interactions of

the graviton with the hidden photon to consider. Let us split these interactions into those that may occur in the full bulk space, and those that may occur only on the brane.

Gravity in the bulk

In interactions involving only the hidden photon field and gravity, the presence of the 3-brane is unimportant – neither field is localised there, so neither "feels" the brane except via interactions with the SM fields. As such, both the graviton and HP fields exhibit translational invariance along the extra d dimensions, and momentum along these directions is conserved. Post compactification, extra dimensional momentum is represented by the KK mode number. Recall the mass of a mode is directly proportional to its mode number n, $m = |\vec{n}|/R$. If we then consider the decay of a hidden photon mode of mode number[2] n into a lighter mode (k) and a graviton mode (l), we have, by conservation of mode number $|\vec{n}| = |\vec{k}| + |\vec{l}|$. In terms of the particle masses, $m_n = m_k + m_l$, and the phase space for the decay vanishes precisely. Thus decays of the form $X^{(\vec{n})} \to X^{(\vec{k})} + G^{(\vec{l})}$ are kinematically forbidden. Note that the species of the particles involved are insignificant. Any initially massless particle that is compactified on the same manifold will generate a KK stack with precisely the same mass spectrum, and decays between these particles will have likewise vanishing phase space.

Note that the model does not include a brane localised hidden photon term. This would break the invariance discussed above, and permit decays forbidden in the present set up. As such the argument is not completely general, but rather a special feature of the symmetries that are preserved by this specific and simple model.

Gravity on the brane

When on-brane interactions are considered, the translational symmetry of the extra dimensions is broken, and momentum need no longer be conserved along those directions; consequently KK mode number is not conserved. Many of the observations that have been used to constrain the parameters of hidden photons rely upon the hidden photon having only a negligible probability of interacting once produced. It is thus important that we understand any mechanisms that could enhance the HP interaction with SM particles after

[2]Here we simplify the discussion – we are really referring to a vector of length d of mode numbers, one for each extra dimension.

production. The inclusion of gravity in the model presents a novel decay mode with the potential to do just that: $X \to G + \gamma$.

For a single graviton mode in the final state, one can bound the decay width by the case of a massless graviton,

$$\Gamma(X^{(k)} \to G^{(l)} + \gamma) < \Gamma(X^{(k)} \to G^{(0)} + \gamma) = \frac{\chi^2 m_X^3}{12\pi M_{\text{Pl.}}^2}. \tag{3.16}$$

One can see that such a decay is strongly suppressed by the both the (4D) Planck mass squared and the smallness of the kinetic mixing parameter. However, a given hidden photon mode can decay to a SM photon plus any of the kinematically accessible graviton modes, so we must perform a sum over available graviton modes. The result of this sum is to replace the suppression by the (4D) Planck mass $M_{\text{Pl.}}$ by the weaker suppression with the fundamental scale $M_\star$, by virtue of Eq. (3.5),

$$\begin{aligned}\Gamma(X^{(k)} \to G + \gamma)_{\text{total}} &< \Gamma(X^{(k)} \to G^{(0)} + \gamma) \times \int_0^{m_X/m_0} d^d l \\ &< \frac{1}{2^{d-1}\pi^{d/2} d\,\Gamma(d/2)} \frac{\chi^2 m_X^{d+3}}{12\pi M_\star^{2+d}}\end{aligned} \tag{3.17}$$

Since we would like to determine whether such decays are important for our phenomenology, we should consider the limiting cases where they are most likely to be so. With only a single extra dimension, the limit on the fundamental scale $M_\star^{(d=1)}$ is strong, and the decay is strongly suppressed. Moving up to $d = 2$, the limit on $M_\star^{(d=2)}$ decreases by 5 orders of magnitude, and the power of the fundamental scale suppression is still low. At the LHC, HP masses of order 1-3 TeV can be probed, so we can consider the very limiting case that $m_X \sim M_\star$, and hypothesise an extremely low mass splitting m_0. In this case, the decay rate reaches the same order as $\Gamma(X \to e^+e^-)$. Since the strongest constraints from the LHC come from a dilepton search, the constraints are not actually affected by this additional decay mode. It is possible that it could lead to some sort of novel signature, but at present this could access only a small fraction of the hidden photon parameter space and we do not investigate further.

In all of the non-LHC experiments, where $m_X < M_\star$, the decay is sufficiently suppressed as to be negligible.

3.4 Constraints

3.4.1 General features with KK modes

Before deriving specific constraints on the mass and kinetic mixing of hidden photons for the LED scenario, let us first outline some general considerations relevant to constructing bounds with contributions from a tower of Kaluza-Klein modes.

The salient feature of the extra dimensional scenario we investigate is the stack of massive KK modes associated with the hidden photon. Processes that otherwise would involve only a single hidden photon may now be accessible to a large range of hidden photon modes, though typically the dominant effect will come from a relatively small range of masses.

We can approximate the sum over all the KK modes in the stack by an integral, on the proviso that the mode spacing ($m_0 = 1/R$ for a single extra dimension) is small compared to the energy range of the dominant contribution to an observable. The approximation is,

$$\sum_{\vec{n}>0} \to \frac{1}{2^d} \int d^d k. \tag{3.18}$$

One can imagine some observable that receives a contribution from hidden photons, and that the contribution of a single hidden photon of mass m is $\chi^p \mathcal{P}(m)$. The total KK mode contribution to the process, for KK modes lying in the mass range M_1 to M_2 (and with the mode spacing sufficiently small, $m_0 \ll M_1$) is then,

$$\chi^p \frac{2\pi^{\frac{d}{2}}}{\Gamma(\frac{d}{2})} \frac{1}{2^d} \int_{M_1/m_0}^{M_2/m_0} dk k^{d-1} \mathcal{P}(k\, m_0) = \chi^p \frac{1}{m_0^d} \frac{2\pi^{\frac{d}{2}}}{\Gamma(\frac{d}{2})} \frac{1}{2^d} \int_{M_1}^{M_2} dM M^{d-1} \mathcal{P}(M). \tag{3.19}$$

Ignoring constant factors, one can see that the magnitude of the HP contribution, after summation over the KK stack scales as,

$$\sim \frac{\chi^p}{m_0^d} M^d. \tag{3.20}$$

where M is representing the energy scale of the experiment. Typically, the constraint on the HP parameter space arises by asserting that the HP contribution to a given process is bounded above, for example by the error on the measurement of an observable, or at the

extreme, by the value of the observable itself. From this we can deduce that we expect to see the constraint on χ increase as m_0 decreases, with power law,

$$\chi \sim \left(\frac{m_0}{M}\right)^{\frac{d}{p}}. \tag{3.21}$$

The power p depends upon the process under consideration, but we generically expect small mass splittings, m_0, to be very tightly constrained.

The existing constraints in 4 dimensions for a hidden photon with a Stueckelberg mass are shown in Fig. 3.1. The overlaid lines show the minimum mass of a KK mode in each of $d = 1, \ldots, 6$ dimensions. We will now investigate in turn those of the 4D constraints that are

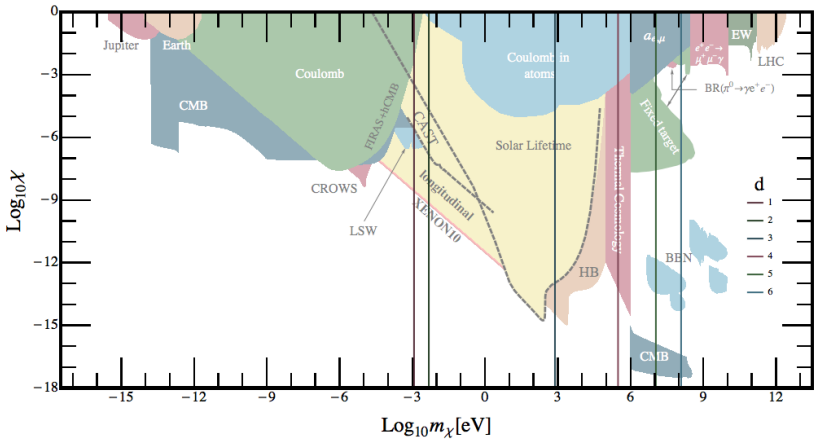

Fig. 3.1.: Limits on hidden photon parameter space in $D = 4$ dimensions with lines overlaid showing the lowest possible mass of a KK mode with $d = 1, \ldots, 6$ extra spatial dimensions.

relevant to the KK scenario. They arise from:

- Stellar evolution [109, 111, 112, 128].
- IDPB [135, 136].
- Electron fixed target experiments [58, 129–133]
- LHC [134].
- Atomic spectra [137–139].
- Anomalous magnetic moments [9, 139, 169–171].

In principle there exist several other bounds that could contribute.

SN1987a. The supernova SN1987a has been studied as a means of constraining light particles in several contexts (for examples, see [172]). Hidden photons have been constrained by energy loss arguments [58, 115], and more recently by considering the actual electromagnetic signal that would be generated by hidden photons decaying within the outer layers of the supernova [173]. Crucially, both of the existing treatments neglect some plasma effects we believe to be important, so we do not include a bound from SN1987a[3].

B Factories. In the absence of a hidden sector Higgs, the hidden photon searches at BABAR [174], DAΦNE [175] and similar facilities rely on a peak search in the dilepton invariant mass spectrum. The mass splittings of the KK modes in the $\mathcal{O}(0.01 - 10\,\mathrm{GeV})$ mass regime that these facilities can probe is smaller than the width of the modes, rendering a peak search ineffectual. Additionally, a proper analysis requires a simulation of the experimental detectors, which is not within the scope of this work. From the considerations in the preceding section, we expect constraints to become stronger for lower mass splittings m_0, and it is unlikely that the constraints from B factories will surpass those from the LHC, which are of comparable strength, but originate at a higher mass. When one considers a low mass splitting at the LHC, it is likely to give a stronger bound than the comparable mass splitting at a B factory, since the constraint will display the power law behaviour of Eq. (3.21).

BBN and CMB. The low mass constraints derived from the CMB are irrelevant to the KK scenario, since they are certainly eclipsed by higher mass constraints. The recent work [176] on higher mass constraints from the CMB and BBN could indeed yield constraints in the presence of a KK tower, and it would be interesting to include this bound in any related subsequent work.

3.4.2 Astrophysical constraints

Astrophysical environments offer several avenues of exploration when considering new, light species. Of particular interest in the present context are stellar interiors – effectively production factories for hidden photons – and the Intergalactic Diffuse Photon Background, which would receive contributions from decaying hidden photons.

[3] It was noted by my collaborator in his own doctoral thesis [145] that the existing treatments do not account for the electron plasma mass. In working further on the issue, we found it to be an extremely complex problem, worthy of a dedicated study in its own right, and as such do not include it in the KK scenario bounds. We note that in principle, treated correctly, SN1987a could contribute strong constraints.

Stellar lifetime

Stars, by their very nature, are photon factories. Introducing a mixing between hidden photons and SM photons opens up the potential for production of HPs in stellar interiors. Owing to its proximity, the best-studied star is the Sun, which appears to be reasonably well described by solar model BS05(OP) [128]. Among the features to consider when modelling a star is the rate of energy loss due to photon and neutrino emission. Hidden photons constitute a new channel for energy loss. If it is too great, such that the power emitted exceeds that emitted through SM photons, it becomes impossible to construct a model whereby the Sun survives until the present day.

The question then is can hidden photons be efficiently produced in the Sun. The answer is a resounding yes, with a range of masses capable of being resonantly produced at varying radial points in the Sun (since temperature varies radially). Once produced, it is unlikely that hidden photons will interact again within the Sun, since the low stellar energies ($\lesssim 0.1$MeV) mean that HPs massive enough to decay to electrons are not produced en masse. Nevertheless, it is possible that a hidden photon is reabsorbed by oscillating into a photon. However, this contributes to non-local energy transfer, for which solar models also cannot account, and the constraint on the kinetic mixing remains intact.

The above arguments apply also to horizontal branch (HB) stars, with minimal modifications: horizontal branch stars have a higher luminosity, $\sim 20\, L_\odot$ ($L_\odot$ is the luminosity of the Sun, $\sim 3.8 \times 10^{26}$ W). Additionally, there are two resonant regions in a HB star, corresponding to the hydrogen burning shell and helium burning core. This is place of the single resonant region in the Sun, where the hidden photon mass m_X is degenerate with the plasma frequency ω_p at some point in the stellar interior.

Field theory at finite temperature

Calculating many-body scattering amplitudes in quantum field theory quickly becomes an intractable problem. Ergodic systems (those in which, all else being equal, each microstate is equiprobable, so that the time the system spends in each microstate is proportional only to the phase space volume of the state) left to evolve over a sufficiently long period of time may thermalize, whereby the *average* properties of the system are calculable in terms of only a few observables, principally temperature T and chemical potentials μ_i, each of which associated with a conserved charge of the system. In moving to this thermal (or finite temperature) field theory description, we necessarily abandon some knowledge of the microphysics in exchange for the benefit of otherwise insoluble systems becoming tractable.
The expectation values of operators in regular quantum field theory are calculated as,

$$\langle \mathcal{O} \rangle = \langle \text{out} | \mathcal{O} | \text{in} \rangle. \tag{3.22}$$

In thermal field theory, the principal object is the partition function, $\mathcal{Z}(T) \equiv \text{Tr}[e^{-\mathcal{H}/T}]$, and the expectation values of operators are,

$$\langle \mathcal{O} \rangle = \frac{1}{\mathcal{Z}} \text{Tr}\Big[\mathcal{O} e^{-\beta(\mathcal{H} - \mu_i \mathcal{N}_i)}\Big], \tag{3.23}$$

where β is the inverse temperature $\beta = 1/T$ (and here $k_B = 1$), $\mathcal{H}$ is the system Hamiltonian, μ_i are the chemical potentials of species i. $\mathcal{N}_i$ are relevant conserved quantities, for example $\#(\text{particles})_i - \#(\text{antiparticles})_i$ in relatively low energy scatterings, or $B - L$ at the GUT scale.
While thermal field theory calculations are in general complex, for sufficiently complicated many-body QFT processes, moving to a thermal field theory description can dramatically simplify the system by masking the internal dynamics. This simplification is illustrated with cartoon diagrams in Fig. 3.2.

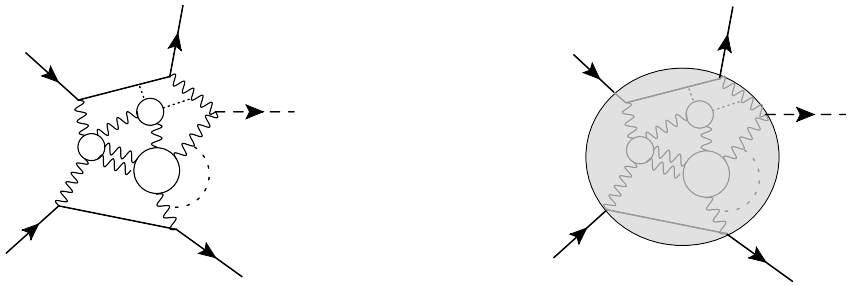

(a) A full, many-body QFT process. All the dynamics are resolved, but the problem rapidly becomes incomputable.

(b) The thermal field theory effective view of the same process. The dynamics inside the grey blob are not resolved, and only average properties known.

Fig. 3.2.: Cartoon illustration of the regular vs. thermal field theory pictures of a complex process.

When considering the production of hidden photons in stellar interiors, one must recognize the non-trivial effect of the thermal medium in which interactions are taking place. These

effects may be encoded in the self-energy for a particle in the medium; for example the rate at which a given particle species approaches its equilibrium distribution is related to the imaginary part of its in-medium self-energy,

$$\mathrm{Im}\,\Pi(\omega) = -\omega\,\Gamma(\omega). \tag{3.24}$$

The principle of detailed balance (to say, at equilibrium all processes are equilibriated to their respective reverse processes) relates the production and absorption rates by $\Gamma_{\mathrm{prod.}} = e^{-\omega/T}\,\Gamma_{\mathrm{abs.}}$, where the exponential is a factor arising due to the difference in Fermi and Bose statistics[4]. Thus, $\Gamma = \Gamma_{\mathrm{abs.}} - \Gamma_{\mathrm{prod.}} = (e^{\omega/T} - 1)\Gamma_{\mathrm{prod.}}$. In the calculation below, we follow the treatments of [109] and [111, 112].

To arrive at the differential production rates (per unit frequency and element volume), we can write a Boltzmann equation for SM photons,

$$\frac{dn_{\mathrm{T,L}}}{d\omega\,dt} = \frac{d\Gamma^{\mathrm{prod.}}_{\mathrm{T,L}}}{d\omega\,dV}\frac{1}{1-e^{-\omega/T}} - \frac{dn_{\mathrm{T,L}}}{d\omega}\Gamma^{\mathrm{abs.}}_{\mathrm{T,L}}, \tag{3.25}$$

and relate the hidden photon case to this. The production rate for hidden photons is simply,

$$\frac{d\Gamma^{\mathrm{prod.,X}}_{\mathrm{T,L}}}{d\omega\,dV} = \chi^2_{\mathrm{T,L}}\frac{d\Gamma^{\mathrm{prod.}}_{\mathrm{T,L}}}{d\omega\,dV} \tag{3.26}$$

The electron plasma frequency, in terms of the number density n_e and the electromagnetic fine structure constant α is,

$$\omega_p^2 = \frac{4\pi\alpha n_e}{m_e}. \tag{3.27}$$

The real parts of $\Pi_{\mathrm{T,L}}$, with the normalisation of the longitudinal mode used in [111][5], for non-relativistic, non-degenerate electrons appropriate to the Sun are [178],

$$\mathrm{Re}\,\Pi_{\mathrm{T}} = \omega_p^2, \quad \mathrm{Re}\,\Pi_{\mathrm{L}} = \omega_p^2\left(1 - \frac{|\vec{k}|^2}{\omega^2}\right) \tag{3.28}$$

For transverse photon modes, the dominant production mechanism is inverse bremsstrahlung (free-free absorption), with a smaller contribution from Compton scattering,

$$\Gamma_T = \frac{16\pi^2\alpha^3}{3m_e^2\omega^3}\sqrt{\frac{2\pi m_e}{3T}}n_e\sum_i Z_i^2 n_i \bar{g}_{ffi}(1-e^{-\frac{\omega}{T}}) + \frac{8\pi\alpha^2}{3m_e^2}n_e. \tag{3.29}$$

[4]This seemingly simple relation is subject to a surprisingly involved derivation [177].

[5]This differs from the normalisation of used in the standard reference [178] by a factor $\frac{|\vec{k}|^2}{\omega^2-|\vec{k}|^2}$.

The sum runs over the light ions i, in this case of elements hydrogen and helium, with Z_i the atomic number and n_i the corresponding number density. The Boltzmann averaged Gaunt factor $\bar{g}_{ffi}$ accounts for the deviation of the expression from Kramers' classical law for bremsstrahlung [179] [6]. The stellar interior is assumed to be fully ionised, and free-bound and bound-bound transitions are ignored as subdominant.

For longitudinal modes, bremsstrahlung is again dominant,

$$\Gamma_L = \frac{64\pi^2\alpha^3 n_e \sum_i Z_i n_i}{3\sqrt{2\pi T} m_e^{3/2}\omega^3} F\left(\frac{\omega}{T}\right) + \frac{8\pi\alpha^2}{3m_e^2} n_e \sqrt{1-\frac{\omega_p^2}{\omega^2}}. \tag{3.30}$$

Ignoring screening effects (a reasonable approximation – we are also ignoring Sommerfeld enhancement, Pauli blocking and $e^- e^-$ bremsstrahlung, together giving a correction $\lesssim 20\%$),

$$F(\omega) = K_0\left(\frac{\omega}{2}\right)\sinh\left(\frac{\omega}{2}\right) \tag{3.31}$$

In general, the power radiated into hidden photons is given by the sum of the transverse and longitudinal parts,

$$P = \int d\omega \int dV \left(\chi_{\rm T}^2 \omega \frac{d\Gamma_{\rm T}^{\rm prod.}}{d\omega\, dV} + \chi_{\rm L}^2 \omega \frac{d\Gamma_{\rm L}^{\rm prod.}}{d\omega\, dV}\right). \tag{3.32}$$

V is the finite size of the system. The effective (in-medium) kinetic mixing parameters, $\chi_{\rm T,L}$ are defined,

$$\chi_{\rm T,L}^2 = \frac{\chi^2 m_X^4}{(m_X^2 + {\rm Re}\,\Pi_{\rm T,L})^2 + ({\rm Im}\,\Pi_{\rm T,L})^2}. \tag{3.33}$$

Recalling from detailed balance the relationship between Γ and $\Gamma_{\rm prod.}$ given above, we have everything we need to calculate the power emitted in the hidden photon channel. It is interesting to note that due to the structure of the longitudinal effective mixing parameter,

$$\chi_L^2 = \frac{\chi^2}{\left(1-\frac{\omega_p^2}{\omega^2}\right)^2 + \left(\frac{{\rm Im}\,\Pi_L}{m_X^2}\right)}, \tag{3.34}$$

longitudinal modes can be resonantly produced (at $\omega = \omega_p$) for any $m_X < \omega_p$. Then, incredibly, the contribution to the luminosity is independent of the production mechanism,

$$\frac{P_L}{dV\, d\omega} \approx \frac{1}{4\pi}\frac{\chi^2 m_X^2 \omega_p^3}{e^{\omega_p/T}-1}\,\delta(\omega-\omega_p). \tag{3.35}$$

[6] We followed the procedure of [109] and references therein for the calculation of this factor.

Enforcing that the total power from BSM channels is not more that 10% of the solar or HB star luminosity results in an exclusion region on the (m_X, χ) plane.

The effect of KK modes on the bound is straightforward. Each mode constitutes a new channel for energy loss, and the sum over the losses via all modes, performed as en Eq. (3.19) must not be greater than 10% of the observed luminosity. This enhances the constraints greatly, as shown in the yellow and orange regions of 3.3, since even masses far below the Sun's usual reach have heavier modes that can be resonantly produced.

Longitudinal modes

The treatment of [109] was recently improved by the inclusion of the effects of previously ignored longitudinal modes of the hidden photons within stellar plasmas [111, 112]. Longitudinal modes in general are subdominant to transverse modes, however when the transverse modes die off in the low mass regime (with χ^4), the longitudinal modes die with only χ^2, enhancing the previous constraint.

The longitudinal modes had previously been thought unimportant due to a missing factor of m^2/ω_p^2. The plasma frequency in the Sun is small relative to the typical HP masses one considers, $\omega_p \sim 0.3\,\text{keV}$, which results in a large correction factor and significant strengthening of the previous constraints.

Naturally, the constraint from horizontal branch stars is also subject to the same longitudinal mode correction. As detailed above, we have included longitudinal modes in all our calculations.

Intergalactic diffuse photon background

Should hidden photons survive until modern times, their decays into photons would enhance the Intergalactic Diffuse Photon Background[7] (IDBP) [135, 136]. HPs with a mass above $2m_e$ decay dominantly to electrons, which do not contribute to the IDPB. In our KK scenario, this puts a natural upper limit on the mass of contributing modes at $m_X \sim 1\,\text{MeV}$, above

[7] Also sometimes the Isotropic Diffuse Photon Background.

which no constraint can be derived. Below this threshold, the dominant decay is the loop induced three-photon decay, with rate [99, 136],

$$\Gamma_{X\to\gamma\gamma\gamma} = \frac{17\alpha^4\chi^2}{1164000\pi^3}\frac{m_X^9}{m_e^8}. \tag{3.36}$$

As with the other bounds, there is no lower limit on the minimum HP mass m_0 except that imposed by the constraints on the size R of the extra dimensions. In the 4D case, the constraint only exists in the mass range $10^4 - 10^6$eV, reflecting the energy resolution of the COMPTEL [180], INTEGRAL [181] and EGRET [182, 183] satellites that have measured the IDPB. In the KK case, for m_0 lower than this, the higher mass modes of the KK stack will contribute decays in the observed range, so a constraint can still be devised.

The lower limit to the bound is formed, in the 4D case, by asserting that the photon flux from HP decays cannot exceed the total measured IDPB, a constraint which may be cast in the form [135],

$$\frac{m_X\tau(m_x,\chi)}{\text{GeV}\,\text{s}} \lesssim 10^{27}\left(\frac{\omega}{\text{GeV}}\right)^{1.3}\left(\frac{\Omega_{DM}(\chi^2)h^2}{0.1}\right). \tag{3.37}$$

The experimental analysis from which the original, 4D, constraint is calculated bins the energy spectrum of the IDPB into bins of constant logarithmic width 0.4 dex. We make the simplifying assumption of the photon energy being peaked at $m_X/3$ for the three photon decay, and sum the Kaluza-Klein contributions to each bin. For a given lowest mode mass m_0, the constraint plotted in Fig. 3.3 represents the bound from the tightest constrained bin.

Note that in Eq. (3.37), no assumption is made about the fraction of dark matter comprised of hidden photons, since the relic density in the final factor on the r.h.s is calculated in each case. This is in contrast to [135], where the dark matter relic density is assumed to be complete (i.e. $\Omega_{\rm DM}h^2 \sim 0.1$).

The upper limit on the constraint plotted (visible only in the $d = 1, 2$ cases) arises by asserting that the lifetime of the hidden photons, $\tau = \Gamma^{-1}_{X\to\gamma\gamma\gamma}$, must be sufficient that they survive until after the CMB decoupling time, $\sim 10^{12}$ s after the Big Bang.

3.4.3 Collider based constraints

While the experimental search for hidden photons has fostered some innovation in its use of many relatively small experiments, such as in the case of resonant microwave cavities and some light-through-walls setups, it can also make use of high energy experiments. For the purpose of the ensuing discussion, high energy particle colliders will be divided into two categories: fixed target experiments, whereby a particle (in the cases we consider in this chapter, an electron) is incident upon a stationary block of material, and particle-particle colliders (here, the LHC), where both particles in the collision are accelerated towards one another in the lab frame.

Fixed targets

In the first kind of collider experiment we discuss, a single high energy beam is incident upon a fixed target. Usually this is a block of metal, and the incident particle interacts with a proton or electron within the target. The application to hidden photons works off the light-shining-through-walls principle – that sufficiently weakly interacting particles can pass through the shielding unhindered – and a fraction of these will decay into e^+e^- pairs in the detector region.

We follow the analysis of [58] and employ the same three fixed target experiments, Fermilab E137 and E141 and SLAC E774. All three constraints arise from counting electron events at the detector, which makes them highly suited to the KK scenario under study. In the case of a search for peaks in the invariant mass distribution of detected particles, for example, the KK modes create a very wide peak, and a much more involved analysis would be necessary. (As in the case of B factories).

Hidden photons are produced via bremsstrahlung from the incoming electron beam. They pass without interaction through the target and shielding and decay to an electron-positron pair in the beam pipe, which may be detected. The requirement that the hidden photon decay within a given region introduces an additional factor of χ^2 into the total amplitude for the process. We observe in Fig. 3.3 that the slope of the fixed target region (green) obeys a different power law to that of, say, the stellar lifetime constraints (yellow and orange regions), since those constraints require only that the HP is produced. This is consistent with the earlier general analysis of Section 3.4.1. The upper limit on the constraint arises due

to hidden photons which mix too strongly with the photon, and decay to electrons rapidly, such that they are stopped in the shielding region.

The constraints obtained on the usual 4D hidden photon parameter space are easy to generalise to the case in the presence of a Kaluza-Klein stack. The KK modes simply increase the number of channels into which a bremsstrahlung photon may oscillate to circumvent the shielding region.

The constraints arising from this procedure are plotted in green (with shades denominating the different experiments [light: E137, mid: E141, dark: E774]) in Fig. 3.3.

LHC

The LHC provides at least two avenues of investigation for hidden photons, depending upon the HP lifetime. For long lived hidden photons, i.e. those with a very small kinetic mixing parameter to suppress the decay to lepton pairs, a missing transverse energy search may prove fruitful. Alternatively, in the opposite regime of short lived HPs, a dilepton search is more suited. Each of these possibilities is investigated in turn below.

Monojets

An on-shell hidden photon may be produced at the LHC though the s-channel interaction $qg \to q\gamma'$ or t-channel interaction $q\bar{q} \to g\gamma'$. If the hidden photon decay rate to SM particles (in practice, this is dominated by decays to fermion pairs),

$$\Gamma(X \to f\bar{f}) = \frac{\chi^2 Q_{e/m}^2 \alpha m_X}{3} \sqrt{1 - 4\frac{m_f^2}{m_X^2}} \left(1 + 2\frac{m_f^2}{m_X^2}\right), \tag{3.38}$$

is sufficiently small, owing to a small value of χ, then the hidden photon may escape the LHC beamline without interaction, creating a missing transverse energy (MET) signal.

For a single hidden photon with $m_X = 100\,\text{GeV}$, its total decay width to all open SM channels is $\Gamma_{\text{tot.}} \sim \chi^2 \times 1\,\text{GeV}$. In order to contribute to a MET signal, the hidden photon must survive long enough to escape the ~ 10 m ATLAS detector[8]. For the lifetime, $\tau = 1/\Gamma_{\text{tot.}}$, to be sufficient for a typical hidden photon to travel that distance before decaying, the kinetic

[8] Clearly, the same considerations apply to CMS, whose detector is slightly smaller.

mixing parameter is required to be $\chi \lesssim 5 \times 10^{-9}$. Such a small mixing greatly suppresses the production cross-section to $\sim 6 \times 10^{-14}$ pb. This is far too small to result in a detectable event rate at the LHC.

Due to the mixing-induced coupling to the electromagnetic current, the primary decay mode of hidden photons is to lepton-antilepton pairs. However, in reality the mixing is not between the photon and hidden photon, but between the hidden gauge field and hypercharge. As such, for sufficiently massive hidden photons, the mixing of the Z boson becomes important. In this instance, it facilitates the hidden photon decay to neutrinos. This is not insubstantial: for a HP with all decay modes open (i.e. $m_X > 2m_{top}$), the branching ratio to neutrinos is $\sim 8\%$. Any hidden photon that decays to neutrinos would certainly contribute to MET.

Considering only a single hidden photon (without the whole KK stack), and using the `CheckMATE` [184–189] software tool on a model generated with `Herwig++` [190], we find no constraint better than unity on the kinetic mixing parameter from monojet searches. Including the effect of the many KK modes in the stack, it is likely some bound would arise. However, since the effect of the KK modes is the same in the case of decay to neutrinos and dileptons, we can be assured that if a constraint arises for a single hidden photon from a dilepton search then the bound including the KK modes will also be stronger in that channel. We turn now to dilepton searches, where a constraint does indeed arise.

Dileptons

In a BSM context, dilepton analysis attempts to identify or exclude new particles by searching for a resonant peak in the invariant mass distribution of a lepton-antilepton pair ($e^{\pm}$ or $\mu^{\pm}$) signaling a new massive particle decaying into the pair. Using a model created in `FeynRules` [191] and generating cross sections with `MadGraph 5` [192] (via the `FeynRules` UFO output [193]), the results of the existing ATLAS Z' search [194] can be mapped directly to the model we consider. This is straightforward in the case of only a single hidden photon, but more involved when the stack of KK modes is considered.

It was just claimed that a new particle (with appropriate couplings) would decay into an l^+l^- pair. In fact the hidden photon mediating the s-channel interaction between quarks and the lepton pair need not be on-shell, and the effect of the KK modes should strictly be summed at the amplitude level, with each mode entering as a propagator in the calculation

of the S-matrix element for the scattering. This requires the introduction of a UV cutoff, or the summation (approximated as an integral due to the near-continuous mass spectrum of the KK stack) is divergent. Since in any case the signal is dependent on a peak in the invariant mass spectrum of the resulting dilepton pair, we make the simplifying assumption of an on-shell mediator, neglecting the effects of amplitude interference.

The KK modes are summed per energy bin used in the collaboration's experimental analysis, assuming an invariant mass spectrum strongly peaked around the mode mass. The limit placed on χ is the strongest limit arising from any bin for a given m_0.

This analysis is sufficient if the peaks from the decay of hidden photons into dileptons are well separated. In the high m_0 region ($\sim$ TeV), this is the case and the mode width is much smaller than the mode spacing, $\Delta m \gg \Gamma(m_X, \chi)$. As m_0 decreases, the mode spacing also does (for a single extra dimension, $m_0 = \Delta m$ *is* the mode spacing), and at some stage the spacing becomes comparable to the width. The blue bound representing the LHC dilepton constraint in Fig. 3.3 is shaded darker in the region where there is peak overlap (i.e. when $\Gamma(m_X, \chi) \gtrsim \Delta m$). In principal, a more detailed analysis is required here, and the cross-section should be calculated at the amplitude level. This analysis has not been performed, since it will be shown in Section 3.5 that for any of several reasonable cutoff schemes, the region bounded by dileptons has a non-perturbative $\chi_{\text{eff.}}$, which invalidates the whole analysis.

3.4.4 Laboratory constraints

At the opposite end of the energy spectrum to the LHC, constraints may be derived from low energy precision measurements. The constraints of this section are of a different nature to those from previous sections, in that they do not involve the production of real (on-shell) hidden photons. Instead, the hidden photon enters the process as a propagator insertion, in the same way as the virtual photon that mediates the process in the Standard Model case.

In the case of real HP production, there is an energy scale associated with the production environment which provides a natural cut-off to the mass of the heaviest KK mode that may be produced. When the mode is virtual, there is no such natural cut-off. In higher dimensional theories, the integral over KK mode number is divergent. In the absence of a well defined UV complete theory, we must impose an artificial cut off, Λ in order to tame the

divergent behaviour. In Section 3.5, consideration is given to some issues arising from the imposing of a cut-off energy scale.

Atomic spectra

Constraints on 4D hidden photons have been derived by considering the effect of the new particle on the spectra of atomic transitions. Several transitions were considered in [139]; it turns out the most stringent constraint for our scenario arises from the Lamb shift in the $2s_{1/2} - 2p_{1/2}$ transition in atomic hydrogen.

The constraint arises by relating the amplitude for the interaction of an electron with a heavy target to the Born approximation for the same process, from which one can read off the Coulomb potential. The hidden photon enters the amplitude as a new propagator, and in the KK case, we can here perform the sum over KK modes (in reality, we will integrate over the KK mode density later as in Eq. (3.19), which is precisely equivalent). The presence of a hidden photon results in a Yukawa-like modification to the Coulomb potential: $\delta V(r) = -(\chi^2 Z\alpha e^{-m_X r})/r$ for a single hidden photon.

When integrating the KK mode density to obtain the results plotted in dark red in Fig. 3.3, a finite UV cut-off was imposed. The integration was cut-off at the point where the effective kinetic mixing parameter $\chi_{\text{eff.}}$ becomes non-perturbatively large (in this case, we take $\chi_{\text{eff.}} > 1$ to signal non-perturbativity). Further discussion of perturbativity will be given in Section 3.5.

Electron and muon $g-2$

The anomalous magnetic moment of leptons arises due to quantum corrections to their interaction with an applied electromagnetic field. The leading order correction is that caused by a single additional photon in the vertex. The interaction of an electron with a vector potential can be parametrised by two form factors, $F_1(q^2)$ and $F_2(q^2)$. The magnetic moment may be expressed as,

$$\langle\vec{\mu}\rangle = \frac{e}{m}\left(F_1(0) + F_2(0)\right)\xi'^{\dagger}\frac{\sigma}{2}\xi, \tag{3.39}$$

(ξ is a two-component spinor). To leading order, $F_1 = 1$ and $F_2 = 0$. The additional photon in the vertex renders F_2 non-zero. Comparing to the classical expression for the magnetic moment,

$$\vec{\mu} = g\left(\frac{e}{2m}\right)\vec{S}, \tag{3.40}$$

we define the Landé g-factor by $g = 2\,(F_1(0) + F_2(0))$. As mentioned, to leading order, $F_1(0) = 1$, so it is useful to define an anomalous magnetic moment,

$$a_e = \frac{g-2}{2} \qquad (= F_2(0)) \tag{3.41}$$

Hidden photons modify this value in much the same way as for the atomic spectra, via a propagator insertion into the amplitude, causing an adjustment proportional to the square of the kinetic mixing parameter, χ^2. If there were only a single measurement of the anomalous magnetic moment, the modification would be undetectable, since it can be accounted for by simple renormalisation of the fine structure constant, $\alpha \to \alpha/(1-\chi^2)$. However, the measurement has been accurately performed for both electrons and muons, and by combining the measurements, we can arrive at a limit on the maximum experimentally allowed magnitude of any modification to the anomalous magnetic moment.

The treatment of [139] details this procedure, and also resolves a problem with the scaling of earlier constraints in the low mass region. We perform the integration over the KK spectrum similarly to the atomic spectra case.

The anomalous magnetic moment of the muon is truly anomalous - around 3σ deviated [9] from the SM expectation, accounting for higher order corrections that produce anomalous magnetic moments at all (at tree level, $\frac{g-2}{2} = 0$). There exists a narrow, unconstrained region of parameter space where the presence of a (4D) hidden photon can explain the discrepancy in the muon $g-2$ [169–171]. Further, the entire region can be probed by the upcoming DarkLight [195] and HPS [196] experiments, with the possibility of results as early as 2015.

3.4.5 Summary of constraints

Fig. 3.3 shows the combined constraints for each of $d = 1, \ldots, 6$ extra dimensions. In each case, the region of the 4D kinetic mixing parameter excluded by a given process is plotted against the mass of the lightest KK mode, m_0. The minimum value of m_0 probed increases with the number of extra dimensions, corresponding to the limits on the size of extra dimensions shown in Table 3.1.

The solid and dashed black lines on the plots illustrate the point above which the effective kinetic mixing parameter becomes non-perturbatively large (greater than one). The point

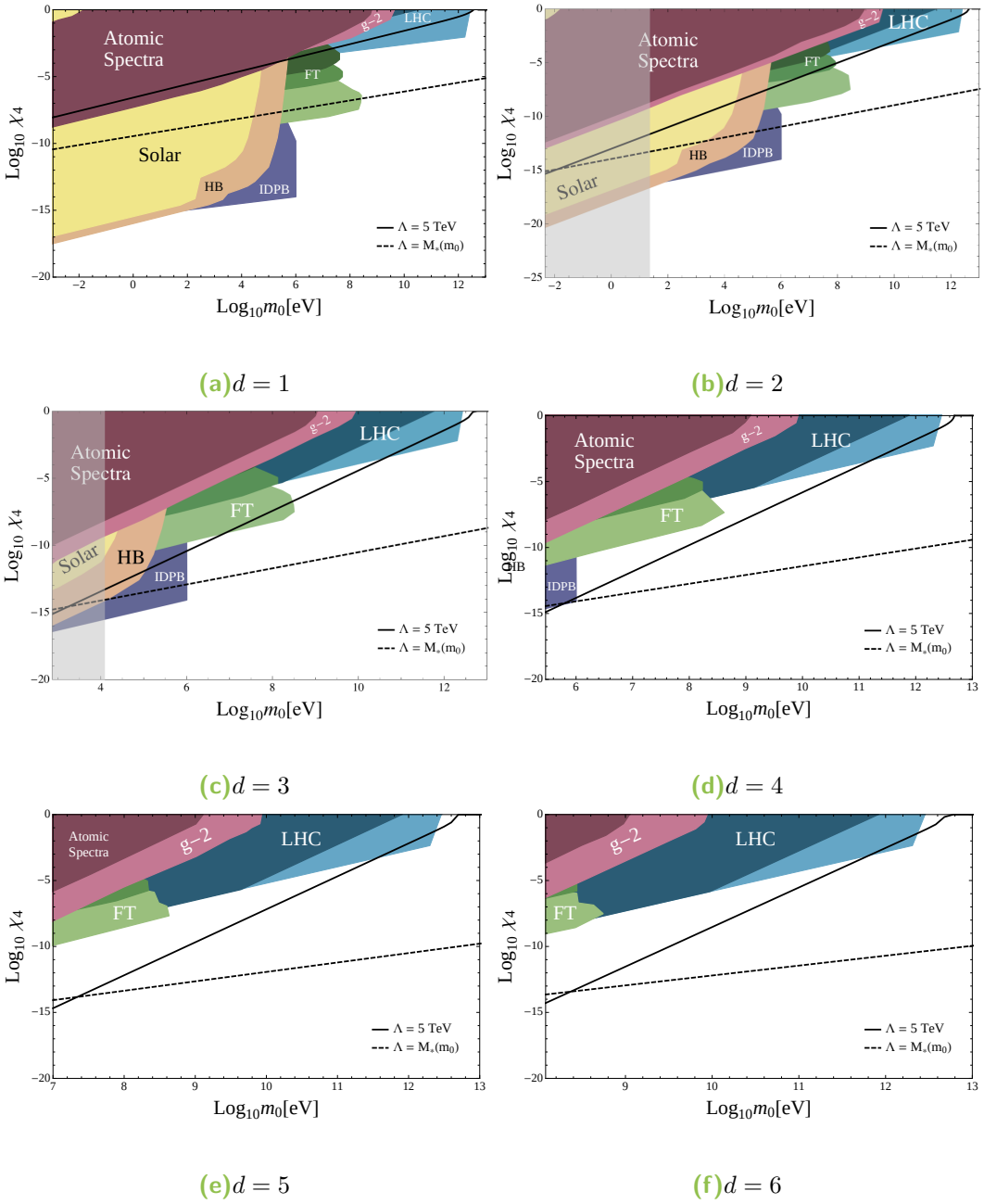

(a) $d = 1$ (b) $d = 2$

(c) $d = 3$ (d) $d = 4$

(e) $d = 5$ (f) $d = 6$

Fig. 3.3.: Limits on hidden photon parameter space for $d = 1, \ldots, 6$ extra dimensions. The mass constrained, m_X, represents the lowest KK mode mass, i.e. also the spacing between modes (for a single extra dimension). The lowest value of the mass axis is set by constraints on the maximum size, R, of the extra dimensions from graviton searches, see Table 3.1. The light grey shaded region for $d = 2$ and $d = 3$ indicates the region that is ruled out by neutron star processes, but not yet at the LHC. The solid and dashed black lines represent the boundary of the perturbative region if a finite cutoff scheme is applied at the corresponding scale. In the region above the lines, the effective kinetic miking parameter (summing for the effect of all modes) is greater than one. We see that this is very restrictive, rendering a perturbative description incorrect in most of the accessible parameter space. Refer to the text for further discussion.

depends upon the cutoff scheme employed. Alternatively stated, if we demand perturbativity of the effective mixing parameter up to $5\,\mathrm{TeV}$, the solid black line indicates the region of (m_χ,χ_4) parameter space that falls foul of this constraint (above the line). The dashed line indicates the same constraint, where perturbativity of the theory is demanded up to the fundamental scale $M_\star$ (note that this is a function of m_0). Further discussion of cut-off schemes and perturbativity is given in the next Section (3.5)).

3.5 Perturbativity

Reference has been made in preceding Sections to issues of cut-off dependence and perturbativity of the theory. To frame the discussion, we first define an effective kinetic mixing parameter, which accounts for the summation over many KK modes contributing to a process,

$$\chi^2_{\mathrm{eff.}} = \chi_4^2 \times \int_1^{\frac{\Lambda}{m_0}} d^d k = \chi_4^2 \times \int_1^{\frac{\Lambda}{m_0}} \frac{2\pi^{\frac{d}{2}}}{\Gamma(\frac{d}{2})} k^{d-1} dk. \tag{3.42}$$

The stack of KK modes are all mediating the same, extra dimensional, force, and as such we are interested in their combined behaviour, not that of individual modes. Hence, in discussions of perturbativity, this is the relevant parameter to consider. The region where a perturbative treatment is valid is defined by $\chi_{\mathrm{eff.}} \ll 1$.

In defining the effective mixing above, it is necessary to include a cut-off mass scale, Λ, at which the integral is terminated (since we are actually integrating over the *number* of available KK modes, we terminate the integral at Λ/m_0, the mode number of the highest accessible mode). Clearly, the higher the scale Λ, the more modes contribute to the effective mixing parameter.

In the case of real production of KK hidden photon modes, there is a natural value for Λ at the highest energy scale of the process, $\Lambda = E_{\mathrm{max.}}$ (for example, the beam energy in electron fixed target experiments). In the case of virtual production of the modes (rather of any process involving virtual modes), there is no such natural cut-off. The integral over loop momentum runs in principal to infinity. In the case that the amplitude for a process involving virtual modes decouples slowly from the loop momentum, in order to extract meaningful information one must assert a finite cut-off by hand. Such an arbitrary dependence is extremely undesirable in any theory of physics. However, it is already explicitly clear from our formulation that the model Langrangian represents an effective theory, supposed to be

a valid approximation only up to some finite energy scale, at which a more fundamental theory is resolved. By asserting a cut-off, we are admitting ignorance of physics beyond this point. Discussion will be given to three cut-off schemes.

The first is a finite cut-off at a fixed energy scale. As per Fig. 3.3, $\Lambda = 5\,\text{TeV}$ is chosen as a reasonable toy value, being higher than the current constraints on the minimum fundamental scale (Table 3.1) for $d > 2$. As shown by the solid black line in Fig. 3.3, it seems very little of the experimentally accessible parameter space results in $\chi_{\text{eff.}}$ remaining perturbative up to that scale.

However, it is not necessary to impose the same perturbativity requiremens on all constraints. For example, in order that the treatment given to fixed target experiments be valid, perturbativity is needed only up to a scale around a GeV. For the stellar lifetime constraints, the maximum energy of the process is of the order of $10\,\text{MeV}$, and perturbativity is not required any further than that for the treatment to be valid (we return to this momentarily).

In place of the somewhat arbitrarily chosen 5TeV cutoff, one could instead set the cut-off at the fundamental scale, $\Lambda = M_\star$. This introduces a dependence on the lowest KK mode mass, m_0,

$$M_\star = \left(\frac{M_{\text{Pl}}^2}{(2\pi)^d} m_0^d \right)^{\frac{1}{2+d}} . \tag{3.43}$$

which has been arrived at by use of the relationship $M_\star^{2+d} = M_{\text{Pl.}}^2/(2\pi R)^d$. This turns out to be an even more restrictive requirement than choosing $\Lambda = 5$TeV (since for much of the space, $M_\star > 5$TeV).

Note that the crossing point of the solid and dashed lines in Fig. 3.3 is the point in m_0 at which the fundamental scale is precisely 5TeV. Below this value of m_0, $M_\star$ is actually less than 5TeV, and it is perhaps unreasonable to expect perturbativity beyond $M_\star$, as by definition of our effective theory for the brane, we are ignorant of physics beyond that scale.

As previously mentioned, it is understood that the kinetic mixing phenomenon we are investigating is also an effective theory only. It can be that the scale at which the new physics represented by the effective theory becomes accessible is lower than the fundamental scale.

A second cut-off scheme is possible. One can first calculate the point at which the effective kinetic mixing χ_{eff} becomes larger than one, and cut-off the integration there. This is the scheme applied to the atomic spectra and anomalous magnetic moment constraints. It diverges from a finite cut-off (in this instance) only when $d = 1, 2$, leaving a small corner of parameter space unconstrained by these bounds.

Finally, we may consider applying cut-offs on a bound by bound basis, at the relevant energy scale of the experiment (this is reasonable only for constraints arising from the real production of hidden photon KK modes). The result of this is shown in Fig. 3.4, where regions that are not suitable for perturbative analysis have been whited out. For example, the E774 fixed target experiment used a $275\,\text{GeV}$ electron beam, so we cut-off the integration of KK modes at $\Lambda = 275\,\text{GeV}$. This is as before (in the results in Fig. 3.3), since clearly no modes can be produced with a mass higher than the available energy. Now we compute the effective kinetic mixing parameter $\chi_{\text{eff.}}$ with the same cut-off. Any combination of (m_0, χ_4) that results in $\chi_{\text{eff.}} > 1$ is not suitable for a perturbative treatment. We do not plot these regions, as we can make no statement about their validity, having used perturbative techniques throughout. The regions shown in 3.4 are thus ruled out with only the relatively modest assumption that the photon-hidden photon kinetic mixing interaction remains perturbative up to the energy of the experiment.

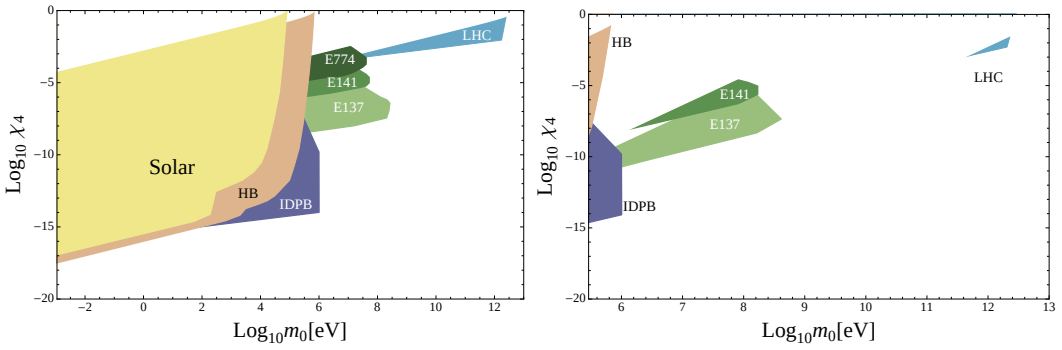

(a) $d = 1$ (b) $d = 4$

Fig. 3.4.: Limits on hidden photon parameter space for $d = 1, 4$ extra dimension. Perturbativity limits have been enforced on a bound-by-bound basis, with modes included up to the energy scale of each constraint. Regions where a perturbative treatment is invalid are not shown as constrained (see text for details).

3.6 Conclusion

We have investigated the phenomenological impact of hidden photons arising from a higher dimensional field. Upon compactification, this generates a massive stack of Kaluza-Klein modes, which negates the possibility of the hidden photon decoupling from the Standard Model by a field redefinition. In particular, since the KK mode tower is massive, it does not require an additional Higgs or Stueckelberg mechanism in order to generate observable effects.

The constraints on hidden photons from flat extra dimensions prove strong, with the enhancement from the KK modes becoming stronger as the lowest mode mass m_0 decreases, reflecting the greater number of modes contributing. This study illustrates that one must consider the mechanism of mass generation carefully, since it can drastically affect the experimental signatures.

4 Coy Dark Matter

> *. . . all along the formless coast bordered by dangerous surf, as if Nature herself had tried to ward off intruders . . .*
>
> **— Marlow**

4.1 Coy dark matter

The central thesis of [2] is that there exists a perfectly viable model of dark matter that explains the apparent excess of photons from the Galactic Centre and yet is unlikely to be give rise to detectable signals in either direct detection or at the LHC. This runs counter to the usual implicit assumption (based on the complementarity diagram in Fig. 1.1 in the Introduction) that dark matter would be discovered in multiple channels. It has since been highlighted in [197] that the same model (as [2]) can also account for the tension between the claimed annual modulation at DAMA [20] and the strong constraints from XENON100 [32] and LUX [18]. Further, the model can also be adapted to explain the anomalous magnetic moment of the muon [198].

Consider dark matter composed of a single species of Dirac fermion, ψ, which couples to the Standard Model only via interaction with a pseudoscalar a, as described by the Lagrangian,

$$\mathcal{L} \supset -i\frac{g_{\rm DM}}{\sqrt{2}} a\bar{\psi}\gamma^5\psi - i\sum_f \frac{g_f}{\sqrt{2}} a\bar{f}\gamma^5 f + \text{h.c.} \tag{4.1}$$

We could parametrize our ignorance of the pseudoscalar couplings in several ways, so taking motivation from minimal flavour violation, we choose that the couplings g_f are equal to the SM Yukawa values, $g_f = y_f \equiv m_f/174\text{GeV}$. The coupling $g_{\rm DM}$ of a to the hidden sector fermions is a free parameter, as are, a priori, the masses of the hidden sector fermions and the mediating pseudoscalar. We do not specify any further field content of the model, assuming it is sufficiently heavy to decouple from the relevant processes in astrophysics

and at the LHC, but note that similar scenarios arise in SUSY (though with much richer phenomenology) and other theories featuring multiple Higgs doublets.

The simple model in Eq. (4.1) results in the thermally averaged cross section (times velocity) for $\bar{\psi}\psi \to \bar{f}f$ annihilation,

$$\langle \sigma v \rangle_f = \frac{N_C}{8\pi} \frac{y_f^2 g_{\rm DM}^2 m_\psi^2}{(m_a^2 - 4m_\psi^2)^2 + m_a^2 \Gamma_a^2} \sqrt{1 - \frac{m_f^2}{m_\psi^2}}. \tag{4.2}$$

Notice that the r.h.s of the above cross-section is not dependent on the velocity distribution of dark matter. However, one finds that the same Lagrangian results in a velocity suppressed cross-section for interaction with a nucleus in a direct detection experiment. Let us examine the phenomenon of velocity suppression.

4.1.1 Spin dependent vs. spin independent interactions

Unlike in high energy, relativistic processes, at the low energies associated with the non-relativistic WIMPs in the galactic halo the difference between spin-dependent (SD) and spin-independent (SI) scattering is pronounced. To illustrate this, consider the Lagrangian (4.1), and the equivalent Lagrangian, with the pseudoscalar mediator replaced by a scalar ϕ,

$$\mathcal{L}_{\rm scalar} \supset -\frac{g'_{\rm DM}}{\sqrt{2}} \phi \bar{\psi}\psi - \sum_f \frac{g'_f}{\sqrt{2}} \phi \bar{f} f \tag{4.3}$$

One can compute the cross-section for annihilation of each of these cases explicitly (see Appendix C for the matrix element calculation), in which case the velocity suppression will be apparent, but there is a physical reasoning behind the result.

Consider the annihilation of two Dirac fermions into two SM fermions, mediated by a (pseudo)scalar. The total spin of the incoming fermion anti-fermion pair is 1, which allows the projection along a chosen axis to take values $-1, 0, 1$. Assuming CP conservation, the dark fermion Dirac bilinear must have the same CP properties as the resulting final state and the intermediate particle. For fermions,

$$C : (-1)^{L+S}, \qquad P : (-1)^{L+1}, \tag{4.4}$$

whereas for bosons,

$$C : (-1)^{L+S}, \qquad P : (-1)^{L}. \tag{4.5}$$

A combination of dark matter and SM bilinears can only result in a non-zero matrix element if they respectively annihilate and create a state with the same total angular momentum J. With a scalar interaction, the bilinear is $\bar{\psi}\psi$, which is CP even, having $L = S = 1$, with $J = 0$. The scalar mediating the interaction interacts in the same fashion with SM fermions, so the interaction is allowed. The restriction for like J values simply eliminates interactions where the Lorentz structure of the interaction is different for the DM and SM bilinears. This makes sense, since a mediating particle (which, in the case of effective operators, has been integrated out) must have definite spin, and cannot, for example, interact as a vector with some fermions and a scalar with others. Note though, that the interaction has $L = 1$, and as such the annihilation occurs in the p-wave, the $L = 1$ term in the partial wave expansion. Partial wave amplitudes scale with v^{2L}, where v is the relative velocity of the interacting particles, so in the low energy limit, such an interaction is "velocity suppressed" by the non-relativistic $v \sim 10^{-3}c$.

Conversely, if the interaction with both DM and SM is pseudoscalar (we will not consider the CP violating case that the interaction with one of DM and SM is scalar and the other pseudoscalar), the resulting CP odd bilinear has $L = S = 0$. Thus, it has an s-wave amplitude, and is not velocity suppressed.

Summarising the CP properties above:

	$\bar{\psi}\psi$	$i\bar{\psi}\gamma_5\psi$	$\bar{\psi}\gamma^\mu\psi$	$i\bar{\psi}\gamma^\mu\gamma_5\psi$
C	$+1$	$+1$	-1	$+1$
P	$+1$	-1	$(-1)^\mu$	$-(-1)^\mu$
CP	$+1$	-1	$(-1)^\mu$	$-(-1)^\mu$

(4.6)

Included also are the vector and axial vector bilinears, where, using the notation of [199], $(-1)^\mu = 1\,(-1)$ for $\mu = 0\,(1, 2, 3)$. From these CP properties, one can determine the lowest L state in which an interaction can occur, and thus whether or not the interaction is velocity suppressed. A complete analysis of the suppression of many operators for fermionic, scalar and vector dark matter for in both annihilation and scattering processes is given in [200], including cases where even the s-wave amplitudes are helicity suppressed.

In general, the thermally averaged cross-section may be expanded as [201],

$$\langle \sigma v \rangle = \langle a + b\,v^2 + c\,v^4 + \dots \rangle = a + \frac{3}{2} b\,x^{-1} + \dots \tag{4.7}$$

where with $x = m/T$, and m being the mass of a the incoming particles and T the temperature. Processes with an s-wave amplitude have non-zero coefficients a and b, whereas those with no s-wave have non-zero b only, corresponding to the p-wave. For the model we are considering in this Chapter, where DM annihilates through a pseudoscalar interaction, there is an s-wave amplitude, so the thermal averaging process does not change σv (ignoring the highly suppressed p-wave contribution).

4.2 Indirect detection with the Fermi satellite

It was reported in [49] that there is a significant gamma ray excess distributed around the galactic centre. Owing to the complex nature of the astrophysical environment, coupled with our relative ignorance of some aspects of astrophysics, it is not possible to rule out completely a Standard Model explanation of the excess. However, it has been found [202, 203] that neither millisecond pulsars nor cosmic ray interactions (two of the most promising SM candidates),can provide a suitable fit to the excess. It is known from simulations that the galactic centre contains a dense population of dark matter. If that dark matter has an annihilation chain to photons, it is not unreasonable to interpret the excess as a result of this. Speculating that this is the case, one can constrain the parameters of a given DM model in order that the excess is produced at the right level. Of course, there could be several contributing processes, but it can at least be inferred that dark matter annihilations cannot be responsible for an excess *greater* than that observed.

The prompt photon flux from DM annihilations (i.e. that which arises from direct annihilation into photons, rather than those produced in the subsequent interactions of SM particles) at Earth from a region of solid angle $\Delta\Omega$ of the galactic centre is, in terms of the per annihilation energy spectrum dN/dE,

$$\frac{d\Phi}{dE_\gamma} = \frac{1}{4}\frac{r_\odot}{4\pi}\left(\frac{\rho_\odot}{m_{\rm DM}}\right)^2 \langle J\rangle \Delta\Omega \sum_f \langle\sigma v\rangle_f \frac{dN_\gamma^f}{dE_\gamma}. \tag{4.8}$$

The local dark matter density is $\rho_\odot = 0.42\,\text{GeV}\,\text{cm}^{-3}$, at a distance $r_\odot = 8.25\,\text{kpc}$ from the galactic centre. The J factor, which contains the elements of the above formula for calculating the flux that are a function of the halo profile, is

$$\langle J\rangle = \frac{1}{\Delta\Omega}\int \cos b\, J(b,l)\, db\, dl, \tag{4.9}$$

with

$$J(b,l) = \int_{\text{l.o.s.}} \frac{ds}{r_\odot} \left(\frac{\rho(r)}{\rho_\odot}\right)^2 \Bigg|_{r=\sqrt{r_\odot^2+s^2-2r_\odot s\cos b\cos l}}. \tag{4.10}$$

The element of integration, ds, is to be performed along the line of sight, to say along a line connecting Earth and the Galactic centre. For the density function we choose a NFW profile with $\gamma = 1.2$, which gives a good fit to the gamma-ray excess [204],

$$\rho(r) = \rho_s \left(\frac{r}{r_s}\right)^{-\gamma} \left[1 + \left(\frac{r}{r_s}\right)\right]^{\gamma-3}. \tag{4.11}$$

The final factor in Eq. (4.8), the photon energy spectrum per annihilation, and the J factor are taken from precomputed tables [205] where the parton shower has been performed by `PYTHIA 8.135` [206]. Non-prompt photons, i.e. those produced by secondary processes and particle decay cascades, are ignored. The cross-section (which to leading order in $v \ll c$ is not affected by the thermal averaging process) is that in Eq. 4.2.

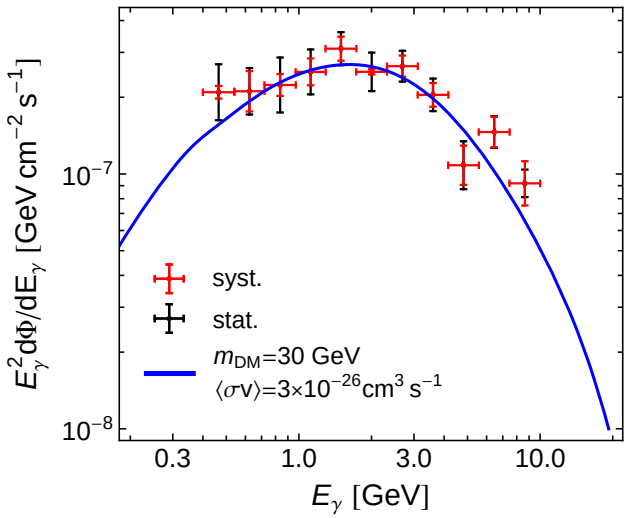

Fig. 4.1.: Data points and error bars for the photon excess in a $7^\circ \times 7^\circ$ region about the galactic centre. The blue line provides an example photon spectrum generated for $m_{\text{DM}} = 30\,\text{GeV}$, with a cross-section appropriate to allow the DM to be a cold thermal relic.

For $m_{\text{DM}} = 30\,\text{GeV}$, annihilating primarily to b quarks (as determined by the Yukawa hierarchy of the couplings), fitting to the observed galactic excess (minimising chi-squared [204]) results in a weak scale cross section compatible with the DM being a thermal relic. Fig. 4.1 shows the differential photon flux as a function of the photon energy for this set up with a cross-section $\langle\sigma v\rangle = 3 \times 10^{-26}\text{cm}^3\text{s}^{-1}$. This cross section gives an excellent fit to the observed data. Fig. 4.2 shows the best fit value of the cross-section as a function of the DM

mass, with contours for the first 3 standard deviations from the best fit. The fit assumes the branching ratio for decays to depend only on the Yukawa couplings.

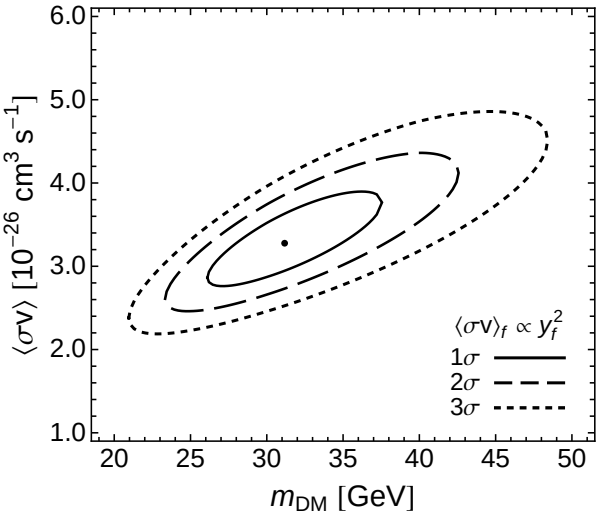

Fig. 4.2.: The point in the DM (mass, cross-section) plane that best fits the observed gamma ray excess for, assuming branching ratios with a SM Yukawa structure, along with standard deviation contours.

4.3 Direct detection

Having found the WIMP mass and cross-section that best fit the galactic centre excess, one can now consider other experimental means by which such a model may be detected. We will first discuss the prospects of discovery at direct detection experiments.

The dark matter galactic halo is constituted by primarily non-relativistic dark particles. The WIMPs are assumed to have a Maxwellian velocity distribution [17],

$$f(\vec{v}, \vec{v}_E) = e^{-\frac{(\vec{v}+\vec{v}_E)^2}{v_0^2}}, \tag{4.12}$$

where $\vec{v}$ is the velocity of the WIMP w.r.t the terrestrial target nucleus, $\vec{v}_E$ is the Earth's velocity relative to the DM halo and v_0 is the average WIMP velocity relative to Earth. The expected event rate per unit mass on the target is then,

$$dR = \frac{N_0}{A}\sigma v\, dn \tag{4.13}$$

The number density of WIMPs is $dn = (n_0/k) f(\vec{v}, \vec{v}_E) d^3\vec{v}$, with $n_0 = \rho_{\rm DM}/m_\psi$ is the average number density and k is a normalisation constant[1] such that $\int_0^{v_{\rm esc.}} dn = n_0$. N_0 is Avogadro's number, $6.02 \times 10^{26}\,{\rm kg}^{-1}$.

In general (by construction), the elastic scattering cross-section can be written as a sum of spin independent and spin-dependent terms [207],

$$\frac{d\sigma}{dE_R} = \frac{m_N}{2\mu_{\psi N}^2 v^2}(\sigma^{\rm SI} F^2(E_R) + \sigma^{\rm SD} S(E_R)), \tag{4.14}$$

where $F(E_R)$ and $S(E_R)$ are form factors accounting for nuclear effects (each of $\sigma^{\rm SI,SD}$ is a nuclear cross-section). $\mu_{\psi N}$ is the reduced mass of the DM with the nucleus. In terms of the DM-proton interaction $\sigma_p^{\rm SI}$, the nuclear cross- section for spin independent scattering is,

$$\sigma^{\rm SI} = \frac{(Z f_p + (A-Z) f_n)^2}{f_p^2} \frac{\mu_{\psi N}}{\mu_{\psi p}} \sigma_p^{\rm SI}. \tag{4.15}$$

The DM couplings to the proton and neutron are f_p and f_n respectively. Still following [207], the spin dependent cross-section is,

$$\sigma^{\rm SD} S(E_R) = \frac{4\pi\mu_{\psi S}^2}{3\mu_{\psi p}^2 a_p^2 (2J_N+1)}(a_0^2 S_{00}(q) + a_0 a_1 S_{01}(q) + a_1^2 S_{11}(q))\sigma_p^{\rm SD}. \tag{4.16}$$

The couplings $a_{0,1}$ are combinations of the proton (p) and neutron (n) couplings, $a_0 = a_p + a_n$ and $a_1 = a_p - a_n$. The $S_{00,01,11}$ functions are nuclear structure functions which depend on spin and the species of nucleus.

The low energy of the interactions means that even theories with a relatively light, GeV-scale particle mediating the interaction of dark mater with the standard model can be well described by an effective theory. The theory expressed by the Lagrangian (4.1) can be equivalently described in the low energy regime by,

$$\mathcal{L}_{\rm eff.} = \frac{y_f g_{\rm DM}}{2m_a^2} \bar{\psi}\gamma_5\psi \bar{f}\gamma_5 f \tag{4.17}$$

though in practice we are interested only in the interactions with quarks for direct detection. In fact, since the scattering occurs at such low energies (typical recoil energies for, e.g. LUX are in the $\mathcal{O}(10\,{\rm keV})$ range [18]) the relevant quantity is in fact the nucleon scattering

[1] Therefore, $k = \int_0^{2\pi} d\phi \int_-^+ d(\cos\theta) \int_0^{v_{\rm esc.}} f(\vec{v}, \vec{v}_E) v^2\, dv$, $v_{\rm esc.} = \sqrt{2GM_{\rm halo}/r_{\rm halo}}$.

cross-section. The nucleon-level matrix element can be related to the quark level matrix element as (in the non-relativistic limit),

$$\frac{y_q g_{\rm DM}}{2m_a^2}\langle\psi_f|\bar{\psi}\gamma_5\psi|\psi_i\rangle\langle n_f|\bar{q}\gamma_5 q|n_i\rangle \to \frac{g_{nna} g_{\rm DM}}{2m_a^2}\langle\psi_f|\bar{\psi}\gamma_5\psi|\psi_i\rangle\langle n_f|\bar{n}\gamma_5 n|n_i\rangle \tag{4.18}$$

where n is a nucleon and the nucleon coupling is

$$g_{nna} = m_n\left(\sum_{q=u,d,s}\frac{y_q\Delta q}{m_q} - \bar{m}\left(\sum_{q=u,d,s}\frac{\Delta q}{m_q}\right)\sum_{q=u,\ldots,t}\frac{y_q}{m_q}\right). \tag{4.19}$$

The Δq values are form factors, calculated based on nuclear measurements and lattice simulations, and $\bar{m} = (1/m_u + 1/m_d + 1/m_s)^{-1}$. We take the values [208],

$$\Delta u = -0.44, \quad \Delta d = 0.84, \quad \Delta s = -0.03, \tag{4.20}$$

which represent a neutron. $g_{nna} \simeq 2.8\times10^{-3}$ for a neutron which interacts with DM via Yukawa couplings, $y_q = m_q/174$GeV. Though the current most sensitive limits on spin-dependent WIMPs arise from the fluorine based SIMPLE [34], PICASSO [44] and COUPP [35] (with the latter providing the most stringent constraint for $m_{\rm DM}\sim 30$GeV), the forthcoming LZ experiment is likely to surpass all present sensitivities [30, 209] and is xenon-based. In principle, the proton content of a nucleus should also be accounted for, in this case though, it is not necessary, since neutrons carry most of the spin in a xenon nucleus.

The non-relativistic limit of the nucleon level matrix element (4.18) leads to a nuclear level cross-section [210] for a nucleus of spin $J_{\rm N}$,

$$\frac{d\sigma}{dE_R} = \frac{q^4}{m_{\rm DM}^2 m_{\rm N}^2}\frac{3g_{naa}^2 g_{\rm DM}^2 m_{\rm N}}{8m_a^4 v^2}\frac{1}{2J_{\rm N}+1}S_A(q). \tag{4.21}$$

$S_A(q)$ a the spin structure function, which is dependent on the momentum transfer $q^2 = 2m_{\rm N}E_R$, where E_R is the recoil energy ($\mathcal{O}(10$keV$)$) and $m_{\rm N}$ the mass of the nucleus. The first factor in (4.21) is of order $\mathcal{O}(10^{-12})$, suppressing the cross-section substantially. Here is the crucial observation central to "coy" dark matter. We earlier observed that the annihilation cross-section was unsuppressed, and the model can account for the Galactic Centre excess. However, the differential cross-section above is velocity suppressed (by $v^2 \sim q^4/v^2$), making detection difficult.

The number of expected events with between 2 and 30 photo-electrons in the LZ detector, assuming the efficiencies of LZ to be the same as LUX, for $m_{\rm DM} = 30$GeV is [17, 211],

$$N_{\rm exp.} = \left(\frac{g_{\rm DM}}{1}\right)^2 \left(\frac{250\,\text{MeV}}{m_a}\right)^4 \left(\frac{\text{Exposure}}{10^7\,\text{kg days}}\right) \text{events}. \tag{4.22}$$

One can also map the cross-section to the form constrained by the experiments to allow direct comparison with experimental limits,

$$\begin{aligned}\tilde{\sigma}_n^{\rm SD} &= \frac{9}{16\pi}\frac{q^4}{m_{\rm DM}^2}\frac{g_{nna}^2 g_{\rm DM}^2 \mu_n^2}{m_a^4} \\ &\simeq 8\times 10^{-43}\text{cm}^2 \left(\frac{g_{\rm DM}}{1}\right)^2 \left(\frac{250\,\text{MeV}}{m_a}\right)^4 .\end{aligned} \tag{4.23}$$

The above form assumes fixed momentum transfer $q = 100\,$MeV, compatible with $E_R \sim 10\,$keV and $m_{\rm DM} = 30\,$GeV. μ_n is the DM-nucleon reduced mass.

The projected limit from LZ is $\tilde{\sigma}_s^{\rm SD} \leq 7\times 10^{-43}\,\text{cm}^2$ for a 30 GeV WIMP [30], on the order of the estimate above for very low pseudoscalar masses. Clearly, for pseudoscalar masses $\gtrsim 1\,$GeV considered in [2], the cross-section is highly suppressed, and no events are expected.

The forthcoming PICO250 experiment uses fluorine in place of xenon, which results in greater sensitivity to the WIMP-proton cross-section. The collaboration estimate that PICO250 will be sensitive to cross-sections lower than $8\times 10^{-43}\text{cm}^2$ (again, for $m_{\rm DM} = 30\,$GeV) [30]. Modifying the above to account for the proton coupling, $g_{ppa} \simeq -1.1\times 10^{-2}$ and the lower mass of a fluorine nucleus, resulting in $q = 50\,$MeV for $10\,$keV recoil energy, the cross-section in Eq. (4.23) grows approximately 45 times larger,

$$\tilde{\sigma}_p^{\rm SD} \simeq 8\times 10^{-43}\text{cm}^2 \left(\frac{g_{\rm DM}}{1}\right)^2 \left(\frac{250\,\text{MeV}}{m_a}\right)^4 . \tag{4.24}$$

As such, PICO250 will nominally set a stronger constraint than LZ, but is nonetheless insufficiently sensitive to detect scattering via a $\sim 10\,$GeV mediator, even for couplings of order unity.

While for many spin-dependent operators, the first signal could actually come from loop-induced spin-independent interactions, it is calculated in [212] that this is not the case for light pseudoscalar mediators. Thus direct detection can provide no constraints on the scenario discussed.

4.4 LHC Signatures

Since direct detection suffers from velocity suppression for pseudoscalar mediated fermionic WIMPs, perhaps creating the particles at relativistic energies, so the interaction rates are not suppressed (since $v \sim c$) could be more successful.

One could expect that the Yukawa coupling structure of the pesudoscalar makes a search involving the $t\bar{t}a$ coupling viable. For example, the ATLAS $t\bar{t}+\mathrm{MET}$ search [213]. In fact, the $pp \to t\bar{t}a$ cross-section is very small, $\sim 40\,\mathrm{fb}$, and this analysis results in no constraint. This and other analyses (jets plus MET [214], jets plus one isolated lepton plus MET [215] and three leptons plus MET [216]) were tested with `CheckMATE` [184], yielding no constraints.

The most relevant operator for a collider search is in fact the top-loop induced dimension five $a\,G_{\mu\nu}\tilde{G}^{\mu\nu}$. The most sensitive search for this operator then turns out to be the CMS monojet search with 19.5 fb^{-1} of data collected with $8\,\mathrm{TeV}$ centre-of-mass energy [65]. Cross sections for the model are calculated with `MadGraph 5` [192], using the UFO output [193] of `FeynRules` [191]. The resulting exclusion limit (at 90% C.L.), as a function of the pseudoscalar mass m_a is plotted in Fig. 4.3 as the solid blue line – the region above the line is excluded by the search. Notice the extremely large couplings that are still viable: the current LHC data is inadequate to constrain this model. In fact, for such large g_{DM}, the pseudoscalar decay width is larger than its mass, making even interpreting the mediator as a particle suspicious. Note also that use of the effective operator for the top loop is likely to overestimate the cross-section for monojet production, so the bounds presented are optimistic [217].

Making a projection of the potential of the full $14\,\mathrm{TeV}$ search to constrain the same process, we see that it is possible that monojet searches will yet rule out some of the higher mass region that can fit the galactic excess. The estimate assumes 40 fb^{-1} of data, where the monojet signal over background has remained constant (though of course each individually will have increased). The increase in the gluon PDF for the higher energy scatterings at $14\,\mathrm{TeV}$ increases the cross-section for pseudoscalar plus monojet production. If the pseudoscalar has a mass that facilitates decay to two WIMPs, $m_a > 2m_{\mathrm{DM}}$, the cross-section for a monojet plus missing transverse energy is approximately $\sigma(pp \to a + \mathrm{jet}) \times \mathrm{BR}(a \to \bar{\psi}\psi)$. So long as the pseudoscalar-dark matter coupling g_{DM} is larger than the bottom Yukawa y_b (and provided that the pseudoscalar is not so heavy that it can decay to top quarks), the branching ratio to

WIMPs is high, $\sim 100\%$. This explains the step like potential exclusion region (dashed blue in Fig. 4.3) – the exclusion is much weaker when decay to dark matter is not possible, but beyond that threshold, the pseudoscalar mass is does not much change the cross-section.

Even then, there remains a large range of pseudoscalar masses that can couple to $30\,\text{GeV}$ dark fermions with a Yukawa hierarchy and explain the galactic excess, while leaving no trace at the LHC or in direct detection experiments.

The solid blue line in Fig. 4.3 represents the only current constraint on the model. The dashed red line represents the best fit to the Fermi excess, with the shaded area covering the 3 standard deviation region of parameter values giving a good fit. In both cases the WIMP mass has been fixed to $m_{\text{DM}} = 30\,\text{GeV}$.

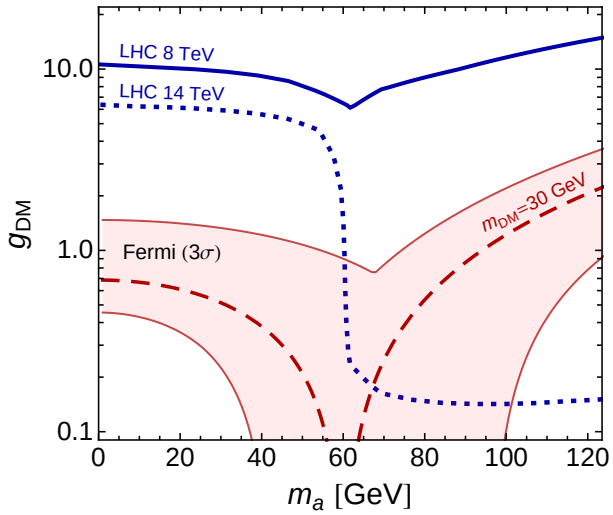

Fig. 4.3.: The monojet exclusion limits plotted with the 3σ region that best fits the Fermi gamma ray excess from the Galactic Centre. A WIMP mass $m_{\text{DM}} = 30\text{GeV}$ is assumed.

It is very difficult to constrain the model we have constructed with colliders, and should dark matter truly be composed as such, it is possible that our only non-gravitational observation of it will be the galactic centre excess.

4.5 Conclusion

We have underlined the known importance of the nature of the scattering in dark matter searches. Understanding which interactions in a DM model will be suppressed by the non-relativistic velocity of the halo allows one to construct models to fit the available potential

signals, or inversely, tells one where to look for signals given a model. In particular, we found a simple model with Dirac fermion WIMPs and a pseudoscalar mediated interaction that can fit the Galactic Centre gamma ray excess while potentially leaving no signal in terrestrial experiments.

The existence of this scenario highlights the importance of understanding astrophysical backgrounds, particularly in regions of likely DM annihilation signals, since it may be the only non-gravitational window on dark matter we can access.

5 Deep, Dark Scattering

> *The horror! The horror!*
>
> **— Kurtz**

In this Chapter we focus our attention on a particular search technique for dark matter - that of fixed target, or beam dump, experiments. There is a fundamental distinction between the operating principles of high energy pp colliders (such as the LHC) and pA colliders (where A is the atomic number of the atom in the target material). The former focus on expanding the energy frontier, giving access to particles with high masses. The latter are more limited in their mass range, but are ideal for investigating lower mass particles with very small couplings due to their high luminosity.

5.1 Beam dumps for new physics

In Section 3.4.3 of Chapter 3, constraints on the hidden photon parameter space were derived from collider experiments. Among them were electron fixed target experiments, in which a beam of electrons is fired (or *dumped*) into a solid metal target. It was shown in [58] that they make an effective testing ground for hidden photons. Since then there has been a renewed interest in studying new physics at beam dump experiments (which have long been employed in, for example, SUSY searches).

In particular, proton beam dumps make a suitable testing ground for light particle dark matter candidates. The combination of reasonably high energy, circa tens to hundreds of GeV, and high luminosity makes them ideally matched to a MeV – GeV mass particle with a low interaction cross section with the Standard Model [4, 61, 62, 101, 102]. The centre of momentum (CoM) energy provides the upper limit on the mass of particles that can be produced in a collision. For a pp collider the CoM energy is simply the sum of the two beam energies $E_{\text{beam}\,1} + E_{\text{beam}\,2}$, whereas fixed targets suffer from the substantially worse scaling, $\sqrt{2E_{\text{beam}}m_p}$. This restricts the mass range that can be probed, but the

high luminosity combined with the ability to shield from charged particles presents novel detection opportunities for light particles not available at the LHC.

In light of strong constraints on the interactions of single new particles species with SM particles (at least when no mechanism to suppress the coupling is present, such as kinetic mixing), particular interest has arisen in "portal" models [80]. In such models, at least two new BSM species are postulated, typically one is stable, to act as a dark matter candidate, and one mediates the interaction between BSM and SM fields. As discussed in Chapter 1, this gives rise to the possibility of whole hidden sectors of physics that couple to the SM only weakly through mediator particles. There are then two regimes, defined by the mass of the mediating particle. Either *(i)* the particle is heavy with respect to the mass of the dark matter candidate and the energy scale of a process under consideration, in which case an effective theory with a four point DM-DM-SM-SM interaction may be constructed or *(ii)* the mediator particle is light, and the interaction may be resolved. The former case has generated much interest from the LHC community; both CMS and ATLAS quote their monojet results in terms of the effective operators presented in [64]. Here we specify to the latter case, where the interaction may be resolved.

We find that with a light mediator we are in a somewhat unique scattering situation at proton beam dumps. We have the deep inelastic scattering of neutral particles, precisely as in the case of neutral current (NC) neutrino scattering, but without a heavy electroweak gauge boson to mediate the process. The cross section for deep inelastic scattering scales as $\sigma \propto 1/(Q^2 + m_v^2)^2$, where Q^2 is the four-momentum squared (alternatively, the *virtuality* of the process) and m_v is the mediator mass. Clearly, if m_v is very low, in the MeV range say, then a large part of the cross section arises in the region where Q^2 is low. In constrast, with a heavy Z boson mediating the neutrino case, the low-Q^2 region is relatively unimportant. quantum chromodynamics is non-perturbative for values of Q^2 less than a GeV, with the evolution equations becoming non-linear owing to the self interactions of gluons. Thus in this Chapter we employ a combination of theory and modelling to devise a reasonable description of the low-Q^2 scattering of dark particles, enabling us to fully exploit the phase space, rather than cutting off the important contributions from low virtuality mediator exchanges.

5.2 Dark particles at beam dumps

First let us set up a toy model. We do not want it to interfere much with the successful phenomenology of the SM, so we will work through a vector portal in a secluded scenario. We add to the model a dark Dirac fermion ψ and dark vector boson V_μ which mediates the fermion interaction with quarks via the effective Lagrangian,

$$\mathcal{L}_I = V_\mu \left(g_{q\bar{q}v} \sum_q \bar{q}\gamma^\mu q + g_{\psi\bar{\psi}v}\, \bar{\psi}\gamma^\mu \psi \right) . \tag{5.1}$$

This model may be considered leptophobic, including no direct couplings to SM leptons and instead coupling only to the quarks. It is extremely similar, however, to a hidden photon model, where the coupling is initially to hypercharge (which facilitates interactions with leptons). We will consider both of these cases separately when placing constraints, but the formalism follows purely from the Lagrangian (5.1). The dark particles will be pair-produced at beam dumps in a Drell-Yan process

$$pp \to \bar{\psi}\psi \ + X, \tag{5.2}$$

where here X represents the additional QCD matter produced by the proton constituents that do not annihilate into $\psi\bar{\psi}$. There are additional production mechanisms from the decays of mesons produced in the reaction (part of th "X" above). For low enough dark particle masses ($\mathcal{O}(100\text{MeV})$), production from mesons in fact dominates [62]. However, since the mission of this study is to investigate the scattering of dark particles, we do not concern ourselves with these additional production mechanisms. Drell-Yan production has the advantage of being computationally simpler and is implemented in several widely available software tools – the production cross-sections employed in this section are generated with `Madgraph 5` [192] (from a `FeynRules` [191] model with UFO output [193]). The number of fermions produced, as a function of protons on target (POT), is,

$$\frac{dN}{dE\, d\theta} = A\, \frac{d\sigma(pp \to \psi\bar{\psi})}{dE\, d\theta}\, L_T\, n_T\, \text{POT} . \tag{5.3}$$

where appropriate kinematic and geometric cuts must be applied to properly simulate detection and. In particular, the opening angle of the dark fermions is bounded, in the lab frame, by

$$\theta_{\text{max}} = \frac{0.75\ \text{m}}{55.8\ \text{m}} = 0.0134 , \tag{5.4}$$

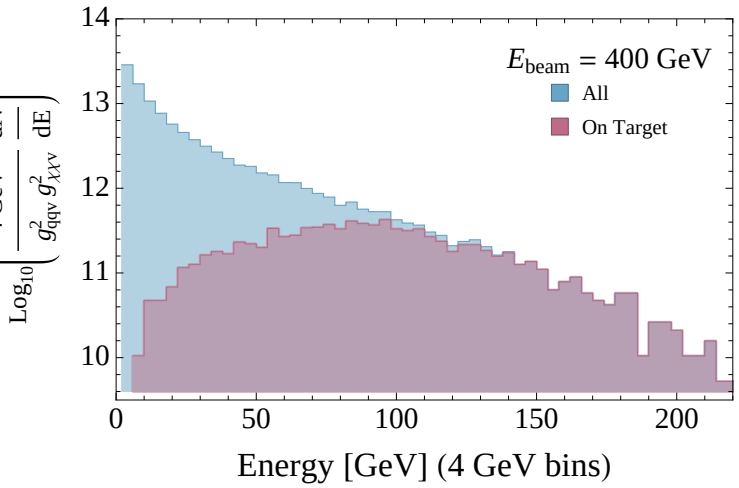

Fig. 5.1.: Binned energy distribution of ψ and $\bar{\psi}$ particles, $(g_{q\bar{q}v}^{-2} g_{\psi\bar{\psi}v}^{-2}) dN/dE$, simulated with `Madgraph 5`. The light blue region represents all produced particles, the purple region only the subset that are on target for the detector at production, i.e. those with opening angle $\theta < \theta_{\text{max}}$.

such that we expect,

$$\frac{dN}{dE} = \int_0^{\theta_{\text{max}}} d\theta \, \frac{dN}{dE \, d\theta} \,, \tag{5.5}$$

dark particles produced on-target. Except for very large couplings, there is practically no rescattering in the shielding and rock between the target and detector, so that essentially all dark particles produced on target will reach the detector.

The energy distribution of dark particles, indicating those that are on target with the purple shaded region is plotted in Fig. 5.1.

With production in hand, we may now turn our attention to the scattering of dark particles.

The essence of dark particles scattering from stationary (in the lab frame) hadrons – in the present case nuclei – is captured by the formalism of deep inelastic scattering (DIS). DIS has been a vital component in the development of the quark parton model, QCD and continues to provide some exciting experimental frontiers (e.g. [218]). From [219], the cross section for a charged lepton scattering from a hadron is given by,

$$\frac{d^2\sigma}{dx\,dy} = \frac{8\pi\alpha^2 ME}{Q^4}\left[\left(\frac{1+(1-y)^2}{2}\right)2xF_1 + (1-y)(F_2 - 2xF_1) - \frac{M}{2E}xyF_2\right]. \tag{5.6}$$

We use the kinematic variables (slightly modified from the convention in [219]),

$$\begin{aligned} M^2 &= P^2 \\ \nu &= P \cdot q / M = (E - E') \\ x &= \frac{Q^2}{2M\nu} \\ y &= \frac{\nu}{E} \end{aligned} \tag{5.7}$$

In particular, we have defined ν as the energy exchange from the incoming lepton to the struck quark. x is often referred to as "Bjorken-x", due to it's importance in the phenomenon of Bjorken scaling, whereby the at extremely high values of the four-momentum transfer squared (Q^2), the structure functions of deep inelastic scattering lose their dependence on Q^2 and scale only with x. This phenomenon provided the critical evidence for nucleons being composed of point-like constituents (which at high Q^2 are displaying asymptotic freedom), rather than protons and neutrons themselves being fundamental.

Such scaling does not persist to arbitrarily low values of Bjorken-x, however. A definite departure from scaling (called "scaling violation") was observed with the HERA collider [220]. The reason for this lies in the essential non-linearity of the evolution equations in such a kinematic regime, coming from full QCD, rather than a pure quark–parton model.

5.3 Two models of scattering

In the small-x or small-Q^2 regime, nuclear interactions become decidedly non-perturbative. Since the small-Q^2 regime is of particular interest in this kind of scattering (due to the unregulated $1/Q^4$ divergence of the cross section), it pays to give close attention to it. Below the QCD scale, $\Lambda_{\mathrm{QCD}} \sim 200\,\mathrm{MeV}$, the strong coupling constant grows non-perturbatively large. To deal with non-perturbative physics, new machinery is needed. We will employ a very simple analogy to optical transmission to model the scattering of particles of a nucleus with non-perturbative interactions.

As the scale Q^2 decreases, and x decreases in tandem (for a scattering event occurring at some fixed energy transfer, ν), the gluon content of the nucleons rises steeply. At some point, the nucleon (indeed, nucleus) becomes completely saturated by gluons, with almost no sea quark content. Because gluons interact with themselves, the evolution equations describing the content of the nucleus become non-linear, departing from the linear DGLAP equations.

Though there is little experimental data, it is widely believed that the gluon content of the nucleus *saturates* for sufficiently low values of x.

In such a regime, we can not rely on deep inelastic scattering for two reasons.

i. Our mediator particle interacts only with quarks, not gluons, so the gluon-saturated nucleus would be transparent to the mediator and no interaction would occur.

ii. The physics is non-perturbative, and the parton distribution functions (themselves non-perturbative objects) are not known below $Q^2 = 1\,\text{GeV}$.

Because it provides a reasonable and well theoretically motivated solution, we model the scattering of the dark particle from the nucleus in the saturation regime with a dipole model [221–224]. First, let us establish the kinematic framework.

5.4 Kinematics

Here we present the kinematics of neutral current scattering with a light mediator. We will calculate the cross section for a Dirac fermion scattering from a hadron of mass M, in this case a nucleus. The Bjorken scaling variable is defined

$$x_{\text{Bj}} = \frac{Q^2}{2M\nu}\,. \tag{5.8}$$

This definition corresponds to scattering from a nucleus. In cases where the nucleon level Bjorken-x is required, Eq. (5.8) must be multiplied by a factor of the nuclear mass number, A (resulting the standard definition: $x = Q^2/(2m_p\nu)$, where the nuclear mass $M \sim A\,m_p$ is replaced by the proton mass).

There is a standard differential form for the deep inelastic scattering cross section in first order perturbation theory that we will employ,

$$d\sigma = \frac{1}{4M[E^2 - m_\psi^2]^{1/2}}\,(2\pi)^{-3} d^4p'_\psi\;\delta({p'_\psi}^2 - m_\psi^2)\,\frac{g^2_{\psi\bar{\psi}v} L^{\mu\nu}\; 4\pi g^2_{q\bar{q}v} W_{\mu\nu}}{(q^2 - m_v^2)^2}\,. \tag{5.9}$$

The leptonic and hadronic tensors respectively are,

$$L^{\mu\nu} = 4p^\mu_\psi p^\nu_\psi - 2(p^\mu_\psi q^\nu + q^\mu p^\nu_\psi) + q^2 g^{\mu\nu}, \tag{5.10}$$

and,

$$W_{\mu\nu} = \frac{1}{4\pi}\sum_X \langle P|J_\mu(0)|X\rangle\langle X|J_\nu(0)|P\rangle(2\pi)^4\delta(P+q-p_X)\ . \tag{5.11}$$

The vector particle couples to the quark currents in the hadronic matrix element above with strength $g^2_{q\bar{q}v}$, which we factor out. We can simplify Eq. (5.9) by changing integration variables with the Jacobian,

$$d^4p'_\psi\ \delta({p'_\psi}^2 - m^2_\psi) = \frac{k'^2dk'}{2E'}\,d\cos\theta\,d\phi = \frac{\pi}{2\sqrt{E^2-m^2_\psi}}\,d\nu\,dQ^2\ \ . \tag{5.12}$$

The differential cross section becomes,

$$d\sigma = \frac{g^2_{\psi\bar{\psi}v}\,g^2_{q\bar{q}v}}{16\pi M}\,\frac{d\nu\,dQ^2}{E^2-m^2_\psi}\,\frac{L^{\mu\nu}W_{\mu\nu}}{(Q^2+m^2_v)^2}\ . \tag{5.13}$$

Here ν is the energy exchange defined in Eq. (5.7) and Q^2 is the square four-momentum transfer. We can impose kinematic constraints on the integral. In the lab frame, where the nucleus is at rest, we can write the initial momenta of the nucleus and incoming dark particle,

$$\begin{aligned} P &= (M,0,0,0)\ , \\ p_\psi &= (E,0,0,k)\ , \end{aligned} \tag{5.14}$$

with $k=\sqrt{E^2-m^2_\psi}$. The ψ particle imparts energy ν to the nucleus, so that its final state energy is

$$k' = \sqrt{(E-\nu)^2-m^2_\psi}\ , \tag{5.15}$$

and the corresponding final state four-momentum of the scattered ψ particle is,

$$p'_\psi = (E-\nu, k'\sin\theta\cos\phi, k'\sin\theta\sin\phi, k'\cos\theta)\ . \tag{5.16}$$

We note that the ψ particle momentum cannot be measured directly, and, due to the inelastic nature of the scatter, cannot practically be reconstructed by momentum conservation. Eq. (5.12) shows that integration over ν and Q^2 is equivalent to integration over the momenta of the unobserved ψ particle. The four-momentum transferred in the scatter is,

$$q = p_\psi - p'_\psi \tag{5.17}$$

which can be related to the energy transfer by Eq. (5.7), $q \cdot P = M\nu$, and also provides a simple definition of Q^2,

$$Q^2 = -q^2, \tag{5.18}$$

which is manifestly Lorentz invariant. Explicitly,

$$Q^2 = 2E(E-\nu) - 2kk'\cos\theta - 2m_\psi^2 \, . \tag{5.19}$$

The final state momentum k' of the ψ particle is unknown, so we define a function $\mu(\nu)$, purely for convenience, by,

$$kk' = E(E-\nu) - \mu^2(\nu) - m_\psi^2 \ \ , \tag{5.20}$$

so that the explicit form of $\mu(\nu)$ is,

$$\mu^2(\nu) = \frac{m_\psi^2\nu^2}{[E(E-\nu) - m_\psi^2] + \sqrt{[E(E-\nu)-m_\psi^2]^2 - m_\psi^2\nu^2}} \, . \tag{5.21}$$

Then, in terms of the function $\mu(\nu)$, Q^2 takes the simple form,

$$Q^2 = 2[E(E-\nu) - m_\psi^2][1-\cos\theta] + 2\mu^2(\nu)\cos\theta \ \ . \tag{5.22}$$

The kinematic limits on Q^2 are now clear, corresponding to the limiting values of $\cos\theta$, or equivalently forward and backward scattering. The lower boundary of the Q^2 integral is for $\cos\theta = 1$ (forward scattering):

$$Q^2 = 2\mu^2(\nu) \ \ , \tag{5.23}$$

and for the upper boundary, $\cos\theta = -1$,

$$Q^2 = 4[E(E-\nu) - m_\psi^2] - 2\mu^2(\nu) \ \ . \tag{5.24}$$

Taken together, we have the kinematic constraints on Q^2,

$$2\mu^2(\nu) < Q^2 < 4[E(E-\nu) - m_\psi^2] - 2\mu^2(\nu) \ \ . \tag{5.25}$$

Additionally, noting that the Bjorken scattering variable defined in Eq. (5.8) cannot, by definition, exceed unity,

$$Q^2 < 2M\nu. \tag{5.26}$$

We now turn to the bounds on integration over ν. Experimentally, a certain fixed amount of energy, $E_{\rm cut}$, is required to be deposited in the detector in order for a jet to be registered. Therefore, at least this much energy must be delivered to the hadron by the scattering dark particle, so,

$$\nu > E_{\rm cut} \tag{5.27}$$

The upper limit on the energy transfer follows from Eq. (5.15). Using the fact that $k'^2 > 0$, but taking the limit where $k' = 0$, we get $\nu < E - m_\psi$. Combined, the integration limits for ν are,

$$E_{\rm cut} < \nu < E - m_\psi. \tag{5.28}$$

Having addressed the integration variables in the differential cross section, we return to Eq. (5.9). We can split the hadronic tensor into structure functions representing transverse and longitudinal states of the exchanged vector boson,

$$W^{\mu\nu} = C_{\rm T}^{\mu\nu} F_{\rm T}(x_{\rm Bj}, Q^2) + C_{\rm L}^{\mu\nu} F_{\rm L}(x_{\rm Bj}, Q^2) \,, \tag{5.29}$$

where the coefficient tensors are,

$$\begin{aligned} C_{\rm T}^{\mu\nu} &= -g^{\mu\nu} + \frac{q^\mu q^\nu}{q^2} + \frac{2x_{\rm Bj}}{P\cdot q + 2x_{\rm Bj}M^2}\left(P^\mu - \frac{P\cdot q}{q^2}\,q^\mu\right)\left(P^\nu - \frac{P\cdot q}{q^2}\,q^\nu\right) \,, \\ C_{\rm L}^{\mu\nu} &= \frac{1}{P\cdot q + 2x_{\rm Bj}M^2}\left(P^\mu - \frac{P\cdot q}{q^2}\,q^\mu\right)\left(P^\nu - \frac{P\cdot q}{q^2}\,q^\nu\right) \,. \end{aligned} \tag{5.30}$$

With these forms of the coefficient tensors, we can easily check that $C_{\rm T}^{\mu\nu} v_\nu = 0$ for any vector v that lies in the plane of P and q and similarly $C_{\rm L}^{\mu\nu} v_\nu = 0$ for any vector orthogonal to both P and q, justifying our labelling the structure functions "transverse" and "longitudinal" respectively. In deep inelastic scattering, the structure functions are often referred to as F_1 and F_2, which obey the Callan-Gross relationship $F_2 = 2x_{\rm Bj}F_1$ and relate to the structure functions defined here by $F_{\rm T} = F_1$ and $F_{\rm L} = (1 + 2x_{\rm Bj}M^2/P\cdot q)F_2 - 2x_{\rm Bj}F_1$.

We can now recast the cross section as,

$$d\sigma = \frac{g_{\psi\psi v}^2\, g_{qqv}^2}{16\pi M}\,\frac{d\nu\, dQ^2}{E^2 - m_\psi^2}\,\frac{1}{(Q^2 + m_v^2)^2}\left[C_{\rm T}^{\mu\nu} L_{\mu\nu}\, F_{\rm T}(x_{\rm Bj}, Q^2) + C_{\rm L}^{\mu\nu} L_{\mu\nu}\, F_{\rm L}(x_{\rm Bj}, Q^2)\right] \,, \tag{5.31}$$

where the contractions of the coefficient tensors with the leptonic tensors are

$$\begin{aligned} C_{\mathrm{T}}^{\mu\nu} L_{\mu\nu} &= \frac{Q^2(2E-\nu)^2}{\nu^2+Q^2} + Q^2 - 4m_\psi^2 \,, \\ C_{\mathrm{L}}^{\mu\nu} L_{\mu\nu} &= M\nu \, \frac{4E(E-\nu)-Q^2}{\nu^2+Q^2} \,. \end{aligned} \tag{5.32}$$

Finally, we arrive at the differential cross section written in terms of the integration variables $d\nu$, dQ^2 (whose limits we have defined), couplings and masses to be defined by the theory, and structure functions, all as a function of the scattering energy, E,

$$\begin{aligned} d\sigma = \frac{g_{\psi\psi v}^2 \, g_{qqv}^2}{16\pi} \, \frac{d\nu \, dQ^2}{E^2 - m_\psi^2} \, \frac{\nu}{(Q^2+m_v^2)^2} \Bigg\{ \left[\frac{(2E-\nu)^2}{\nu^2+Q^2} + \frac{Q^2-4m_\psi^2}{Q^2} \right] 2x_{\mathrm{Bj}} F_{\mathrm{T}}(x_{\mathrm{Bj}}, Q^2) \\ + \frac{4E(E-\nu)-Q^2}{\nu^2+Q^2} \, F_{\mathrm{L}}(x_{\mathrm{Bj}}, Q^2) \Bigg\} \,. \end{aligned} \tag{5.33}$$

The scattering is now parametrised in terms of F_{T} and F_{L}, which are addressed in the following sections.

5.5 Structure functions for scattering

Eq. (5.33) describes the cross section for the inelastic scattering of a dark fermion ψ from a target hadron, in this case a nucleus, in terms of two structure functions, F_{L} and F_{T}. In the following sections, the full forms of these structure functions are derived.

5.5.1 Large Q^2: deep inelastic scattering

As a first approach, we can consider the scattering in a traditional, perturbative QCD framework. The deep inelastic scattering process, sketched in Fig. 5.2, consists of the incoming dark particle exchanging a virtual dark vector boson with a quark from the nucleus.

The structure functions for deep inelastic scattering are simply parton distribution functions (into which initial state radiation may be factored) convoluted with the partonic structure functions, denoted $\hat{F}_{\mathrm{T}}$ and $\hat{F}_{\mathrm{L}}$. To lowest order in perturbation theory, $\hat{F}_{\mathrm{L}} = 0$ for both quarks and gluons, owing to the Callan-Gross relationship, $F_2 = 2x_{\mathrm{Bj}}F_1$. The transverse partonic structure function $\hat{F}_{\mathrm{T}}$ also vanishes for gluons, and for quarks is a delta function

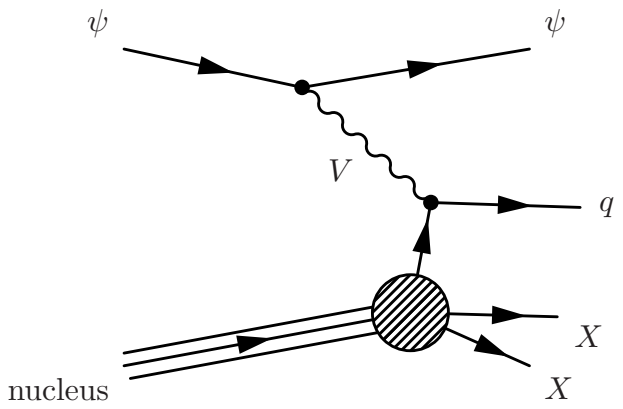

Fig. 5.2.: Deep inelastic scattering of a dark ψ particle from a nucleus by the exchange of a dark vector boson, V. The lines labelled X represent additional QCD matter from the disintegrating proton.

ensuring the momentum fraction of the quarks is $x_{\rm Bj}$. In the quark-parton model for a nucleus then,

$$F_{\rm T} = \frac{1}{2x_{\rm Bj}} \sum_q x_{\rm Bj} f_{q/A}(x_{\rm Bj}, Q^2)$$
$$F_{\rm L} = 0, \tag{5.34}$$

where the sum in $F_{\rm T}$ runs over light quark and anti-quark flavours, $q = \{u, \bar{u}, d, \bar{d}, s, \bar{s}\}$. The dark particle couplings are not included in the structure functions, since we take the dark vector boson to couple flavour-universally to quarks and the couplings have already been factored out of the hadronic matrix element in Eq. (5.9).

The parton distribution function used here is that for the whole nucleus. In terms of nucleon level distribution functions $f_{{\rm u}/p}$ and $f_{{\rm d}/p}$, one can approximate the nucleus (with Z protons and $A - Z$ neutrons) as simply a sum of its constituent nucleons,

$$f_{{\rm u}/A}(x_{\rm Bj}, Q^2) dx_{\rm Bj} \approx [Z f_{{\rm u}/p}(A x_{\rm Bj}, Q^2) + (A - Z) f_{{\rm d}/p}(A x_{\rm Bj}, Q^2)] d(A x_{\rm Bj}) \tag{5.35}$$

so that the complete nuclear distribution function for a u quark (for example) is approximated by,

$$f_{{\rm u}/A}(x_{\rm Bj}, Q^2) \approx AZ f_{{\rm u}/p}(A x_{\rm Bj}, Q^2) + A(A - Z) f_{{\rm d}/p}(A x_{\rm Bj}, Q^2)\,. \tag{5.36}$$

Notice that the first argument of the distribution functions has been scaled by A, since $x_{\rm Bj}$ is here defined with respect to the nucleus. In the following calculations, the leading order Hirai-Kumano-Nagai (HKNlo) nuclear parton distribution functions for lead [225] are used.

Nuclear parton distribution functions average over nuclear effects, so that in practice the relationship is simply $f_{\mathrm{u}/A}(x_{\mathrm{Bj}}, Q^2) = A\, f_{\mathrm{u}/p}(A x_{\mathrm{Bj}}, Q^2)$.

Inserting the structure functions from Eq. (5.34) into Eq. (5.33), the total parton model cross section is,

$$d\sigma = \frac{g^2_{\psi\psi v}\, g^2_{qqv}}{16\pi} \frac{d\nu\, dQ^2}{E^2 - m^2_\psi} \frac{\nu}{(Q^2 + m^2_v)^2} \left[\frac{(2E-\nu)^2}{\nu^2 + Q^2} + \frac{Q^2 - 4m^2_\psi}{Q^2} \right] \sum_q x_{\mathrm{Bj}} f_{q/A}(x_{\mathrm{Bj}}, Q^2)\ . \tag{5.37}$$

5.5.2 Small Q^2: saturation model

Inspecting Eq. (5.33) reveals that the cross section scales with $1/(Q^2 + m_v^2)^2$. This essentially describes a $1/Q^4$ divergence, regulated by the mass of the particle mediating the interaction. In the Standard Model, neutral current deep inelastic scattering occurs only with neutrinos, and as such must be mediated by a Z boson. Since $m_Z \sim 90\,\mathrm{GeV}$, the scattering can never enter a region where small Q^2 is very important; even at very low Q^2, the divergence is still regulated.

In the present scenario, where the dark particle scattering is mediated by a new, light, gauge boson, the cross section is not suppressed at small Q^2. In fact, for the very light mediators that we investigate ($m_v \sim \mathcal{O}(\mathrm{MeV})$), the low Q^2 region is extremely important, contributing heavily to the cross section.

For very low Q^2, below a few GeV, the deep inelastic description of scattering is no longer appropriate. The strong coupling constant $\alpha_S(Q^2)$ becomes non-perturbatively large and the parton distribution functions themselves are not measured. Additionally, with low Q^2 and the relatively high typical scattering energies shown in Fig. 5.1, Bjorken-x can be extremely small. Parton distribution functions are subject to large uncertainties at small x_{Bj}, but it is certain that the gluon distribution rises very steeply in this regime. We will model the scattering here with a *saturation* model. The name derives from the expected behaviour of gluons as the density rises: the gluons self-interact and the gluon content of a nucleon or nucleus "saturates" at a high value.

Such models have been studied in a wide literature [226–236]. The model of Nikolaev and Zakharov, Golec-Biernat and Wüsthof and Mueller is suitable to this situation and features an intuitive physical interpretation as colour dipole scattering. We closely follow

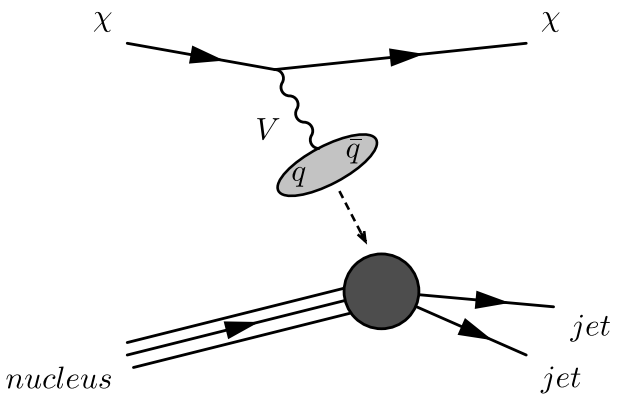

Fig. 5.3.: Sketch of the colour dipole picture of scattering from a gluon saturated nucleus.

the analysis of Hautmann and Soper, with some features of Bartels, Golec-Biernat and Kowalski. The longitudinal structure function is investigated in detail in the saturation model in [237], but for our purpose a simple analysis is suitable. The region of small Q^2 where we will employ the dipole model is, by definition of Q a region where the virtuality of the exchanged vector boson is small – it is the transition region between DIS and vector production (in pure QED and QCD, photoproduction). On-shell massive vector bosons have no longitudinal polarisation, so F_{L} is insignificant compared to $2x_{\mathrm{Bj}}F_{\mathrm{T}}$ and we make the reasonable approximation that $F_{\mathrm{L}} = 0$, as in the parton model.

The result for the transverse structure function is quoted from [235],

$$2x_{\mathrm{Bj}}F_{\mathrm{T}} = \frac{1}{4\pi}\sum_f \frac{24Q^2}{(2\pi)^3}\int d\boldsymbol{b}\int d\boldsymbol{\Delta}\,\frac{G(\sqrt{Q^2+\Lambda_\rho^2}\,\Delta)}{\Delta^2}\,\Xi(\boldsymbol{b},\boldsymbol{\Delta})\,. \tag{5.38}$$

The sum runs over quark flavours, $f = \{u, d, s\}$, not anti-flavours, which are accounted for in the dipole picture, where each dipole is composed of a q-$\bar{q}$ pair.

Let us examine this expression. The two dimensional integration vectors $\boldsymbol{b}$ and $\boldsymbol{\Delta}$ represent the impact parameter and dipole separation respectively. More precisely, the centre of the two quarks in the dipole has its closest approach to the nucleus at transverse position $\boldsymbol{b}$, and each (anti-)quark in the dipole resides $\boldsymbol{\Delta}/2$ away from the dipole centre of mass in its rest frame. The squared wavefunction for the for the dipole is represented by the function $G(\sqrt{Q^2+\Lambda_\rho^2}\Delta)/\Delta^2$, where,

$$G(z) = \int_0^1 d\alpha\,[1-2\alpha(1-\alpha)]\left[\sqrt{\alpha(1-\alpha)}\,z\,K_1(\sqrt{\alpha(1-\alpha)}z)\right]^2\,. \tag{5.39}$$

The integration over α corresponds to integrating over the longitudinal momentum fraction of the dipole carried by the quark (so the anti-quark carries fraction $1-\alpha$). $K_1(z)$ is the first order modified Bessel function. The whole function $G(z)$ may be approximated to within $\sim 15\%$ everywhere by,

$$G(z) \approx \frac{2}{3[1+z^2/4]} \,. \tag{5.40}$$

The argument of G describes the spatial extent of the wavefunction multiplied by Q, which is approximately $\Delta \sim 1/Q$ in a perturbative calculation. However, for small Q, a perturbative calculation cannot be trusted. The additional scale Λ_ρ is the inverse size of a ρ meson, $\sim 200\,\text{MeV}$, which is formed by gluon exchange in the dipole and included as a first approximation to account for non-perturbative effects.

The second function under the integral in Eq. (5.38), $\Xi(\boldsymbol{b}, \boldsymbol{\Delta})$ is simply the probability of a scatter occuring. It has the simple form,

$$\Xi(\boldsymbol{b}, \boldsymbol{\Delta}) = 1 - e^{-\Delta^2 Q_s^2(b)/4} \,, \tag{5.41}$$

which can be arrived at by a direct analogy with classical optics. Let us define a transmission function T by $\Xi(\boldsymbol{b}, \boldsymbol{\Delta}) = 1 - T(\boldsymbol{b}, \boldsymbol{\Delta})$. The function $T(\boldsymbol{b}, \boldsymbol{\Delta})$ represents the probability for the colour dipole to pass through the nucleus without interacting, and conversely, Ξ is the probability of an interaction. We arrive at the explicit form of $T(\boldsymbol{b}, \boldsymbol{\Delta})$ in Eq. (5.41) by considering the necessary limiting behaviours of the function [235], and making a reasonable ansatz.

- The dipole can miss the nucleus entirely, when $|\boldsymbol{b}| > R_A + \Delta/2$. Clearly in this case it cannot rescatter, so $\Xi(\boldsymbol{b}, \boldsymbol{\Delta}) = 0$ and $T(\boldsymbol{b}, \boldsymbol{\Delta}) = 1$.

- In the opposite case, a dipole with large separation between the quarks (large Δ) that hits the nucleus with small $|\boldsymbol{b}| < R_A$ is extremely unlikely to pass through the nucleus without interaction, $T(\boldsymbol{b}, \boldsymbol{\Delta}) \approx 0$.

- When $\Delta \to 0$, the quark-antiquark pair form a colour singlet object that cannot interact with the nucleus, so $T(\boldsymbol{b}, \boldsymbol{\Delta}) = 1$.

- When Δ is small the we expect that the probability of interaction is proportional to the square colour dipole moment, Δ^2. This reflects the two gluons that must be exchanged in the cut Feynman diagram for the interaction.

- The coefficient of Δ^2 can be calculated in perturbative QCD for small Δ.

The saturation scale depends upon on the nuclear gluon density,

$$Q_{\mathrm{s}}^2(b) = \frac{2\pi^2 \alpha_{\mathrm{s}}(\mu^2)}{3}\, xG(x,\mu^2)\, \phi(b)\ . \tag{5.42}$$

The function $\phi(b)$ parametrizes the transverse distribution of gluons from the centre of the nucleus (thus it is a function only of the impact parameter $b = |\vec{b}|$). It is normalized such that $\int d\vec{b}\, \phi(b) = 1$,

$$\phi(b) = \frac{3}{2\pi R_A^3}\, \sqrt{R_A^2 - b^2}\, \Theta(b^2 < R_A^2)\ . \tag{5.43}$$

The gluon distribution, $G(x,\mu^2)$, used is the HKNlo distribution for lead. Nuclear parton distributions are usually normalized per nucleon number (to allow comparison between different species of nuclei), as is the case here, so that the total nuclear gluon content $G(x,\mu^2)$ in Eq. (5.42) is given by $A \times G_{\mathrm{HKN}}(x,\mu^2)$. We have thus far followed the formalism of [235] precisely; now we will include some refinements from a later work [236]. The scale μ^2 is defined,

$$\mu^2 = \frac{C}{\Delta^2} + \mu_0^2\ , \tag{5.44}$$

with a regulator μ_0 which prevents it from becoming arbitrarily small. Above μ_0^2 though, μ^2 is still (approximately) proportional to the inverse size of the dipole squared, which seems a reasonable scale for the perturbative regime (where Δ^2 is small). The value of the constants C and μ_0^2 is to be obtained from fitting to the measured gluon PDF data. This is computationally expensive, but a reasonable fit may be found by inspection, with $C = 6.0$ and $\mu_0^2 = 2.0\,\mathrm{GeV}^2$, where we have prioritized maintaining a reasonably low IR regulator, μ_0.

Similarly, we include a regulator term in the parton momentum fraction x as it appears in the gluon distribution (we do not apply the same regulation to appearances of x elsewhere). Following [238], we take

$$x = \frac{Q^2 + 4m_{\mathrm{q}}^2}{2M\nu}\ , \tag{5.45}$$

which ensures x does not become arbitrarily small at low Q^2, but $x \sim x_{\mathrm{Bj.}}$ when Q^2 is not too low.

Returning to the probability Ξ for a $q-\bar{q}$ dipole to scatter from a hadron, we have applied both theory and modelling. How severe is the dependence on modelling? The function$\Xi(\vec{b},\vec{\Delta})$ is plotted in Fig. 5.4. Notice that for the large majority of the parameter space, corresponding

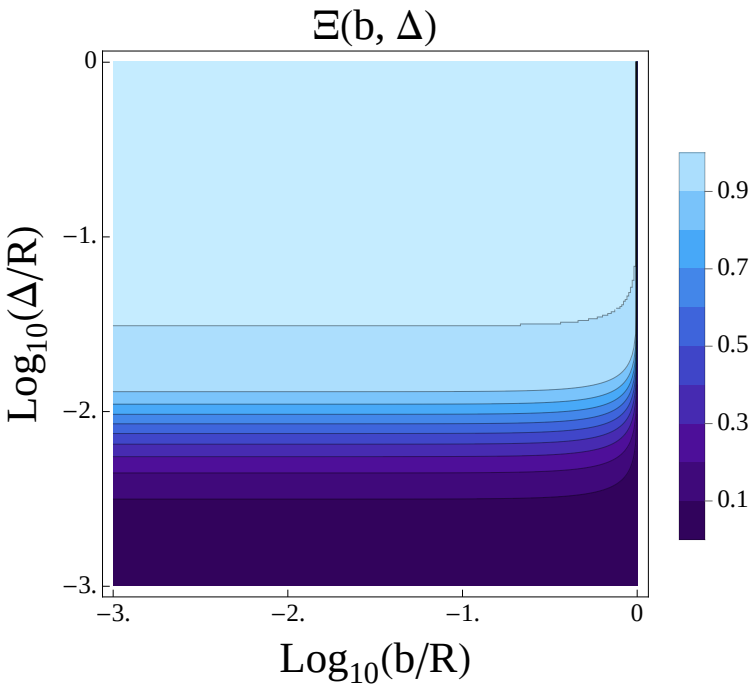

Fig. 5.4.: $\Xi(\boldsymbol{b}, \boldsymbol{\Delta})$ for $x = 10^{-4}$ and $Q^2 = 1\text{GeV}^2$.

to a wide range of impact parameters and dipole separations (both taken in ration to the atomic radius), the scattering probability is one, so the modelling dependence is not too severe.

5.6 Connecting the saturation model to the parton model

Having derived a seemingly suitable model for the low-Q^2 scattering regime, it behooves us to compare the model to perturbative QCD. We'll first qualitatively compare the DIS and saturation models, considering the physical picture represented by each. Before making the comparison in detail, we first introduce a more appropriate reference frame for the saturation model.

A lightning introduction to lightcone coordinates

For computational ease, we can redefine the coordinate system in which we calculate the kinematics. Define, in terms of a four-vector $x^\mu = (x^0, x^1, x^2, x^3)$,

$$\begin{aligned} x^+ &= \frac{1}{\sqrt{2}}(x^0 + x^3), \\ x^- &= \frac{1}{\sqrt{2}}(x^0 - x^3), \\ x^{\mathbf{T}} &= (x^1, x^2), \end{aligned} \tag{5.46}$$

so that the new four-vector reads $x^\mu = (x^+, x^-, x^{\mathbf{T}})$. These coordinates coordinates are referred to as "lightcone" coordinates, reflecting the fact that x^+ and x^- are both null coordinates, though the components of $x^{\mathbf{T}}$ remain space-like. To maintain Lorentz invariance of the scalar product, it is defined,

$$a \cdot b = a^+ b^- + a^- b^+ - a^{\mathbf{T}} b^{\mathbf{T}}. \tag{5.47}$$

Note that the metric tensor (the lightcone equivalent to the Minkowski metric) is non-diagonal,

$$g_{\mu\nu} = g^{\mu\nu} = \begin{pmatrix} 0 & 1 & 0 & 0 \\ 1 & 0 & 0 & 0 \\ 0 & 0 & -1 & 0 \\ 0 & 0 & 0 & -1 \end{pmatrix}, \tag{5.48}$$

and the integration measure is written $d^4x = dx^+ dx^- dx^{\mathbf{T}}$.

Consider the saturation picture in the rest frame of the nucleus, and define the negative z-axis to be aligned with the momentum $\vec{q}$ of the mediating dark vector boson V_μ. We write q in lightcone coordinates, so that, after some algebra, $q^- \approx \sqrt{2}\nu$ (which is large for large ν and small Q^2, our region of interest) and $q^+ \approx -2^{-3/2} Q^2/\nu$ (which is small in the same situation). As depicted in Fig. 5.5, the vector boson splits into a $q - \bar{q}$ colour dipole, i.e. it couples to two quarks. Label the momentum of one quark propagator p_q. Then we can take p_q^- large and p_q^+ small, as an estimate, following from the momentum of the exchanged vector boson. Now consider the position space description of this process. There is a finite separation Δx between the coupling of the quark to the vector boson and its interaction with a gluon from the nucleus. In lightcone coordinateso the scalar product of this distance with the quark momentum is $p_q \cdot \Delta x = p_q^+ \Delta x^- + p_q^- \Delta x^+ - p_q^\perp \Delta x^\perp$. Thus, there is an inverse relationship in the magnitude of the $(+)$ and $(-)$ coordinates between the elements of the position and momentum vectors that multiply one another. To say, for p_q^- large, Δx^+ is small and vice versa (this is clearly not rigorous, but we may talk in broad strokes to come up with an average description of a typical dipole interaction). So in the situation we have described Δx^- is large, since p_q^+ is small. Estimating $p_q^+ \approx 2^{-3/2} Q^2/\nu$, the typical range

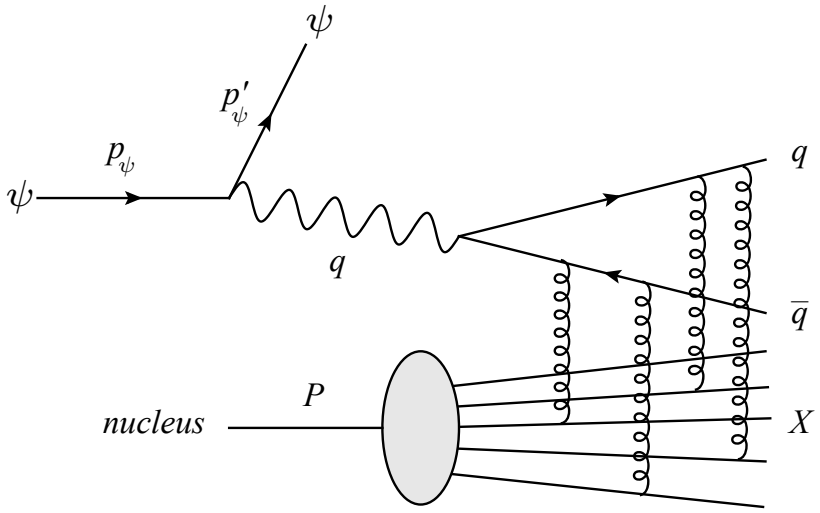

Fig. 5.5.: The dipole scattering with occurs via gluon exchange between the dipole and quarks in the nucleus.

of the quark, in the minus z direction is $\Delta x^- \approx 2^{5/2}\pi\nu/Q^2$ (where a factor 2π has been brought in from the Heisenberg uncertainty relation). If the quark gluon interaction occurs within the nuclear radius, this implies the interaction with the dark vector boson is located far outside the nucleus.

This may seem quite different to the picture of deep inelastic scattering, where the interaction of the vector boson with a quark takes place entirely within the nucleus. The views could be somewhat reconciled by choice of reference frame, but recall that the saturation model is, after all, describing scattering in a non-perturbative regime of QCD, and we should not be surprised that the physics described is different. Nonetheless, there is a regime at large ν and large Q^2 where both physical pictures should agree - we will now investigate this.

To compare the perturbative QCD (i.e. DIS) and saturation models quantitatively, we should consider the latter in the limit of large Q^2. To do this, we can consider the transverse structure function for the saturation model, Eq. (5.38), and take the large Q^2 limit under the integral over $\mathbf{\Delta}$. This results in the argument of $G(z)$ collapsing to simply $Q\Delta$, and $G(Q\Delta) \sim 8/(3Q^2\Delta^2)$. To enforce the largeness of Q^2 (and thus $Q\Delta$), we include a crude cut $\Theta(\Delta > a/Q)$, for constant a. The resulting large Q^2 approximation of the structure function is,

$$2x_{\mathrm{Bj}}F_{\mathrm{T}} \approx \sum_f \frac{2}{\pi^4}\int d\boldsymbol{b}\int d\mathbf{\Delta}\,\frac{\Theta(\Delta > a/Q)}{\Delta^4}\,\Xi(\boldsymbol{b},\mathbf{\Delta})\,. \tag{5.49}$$

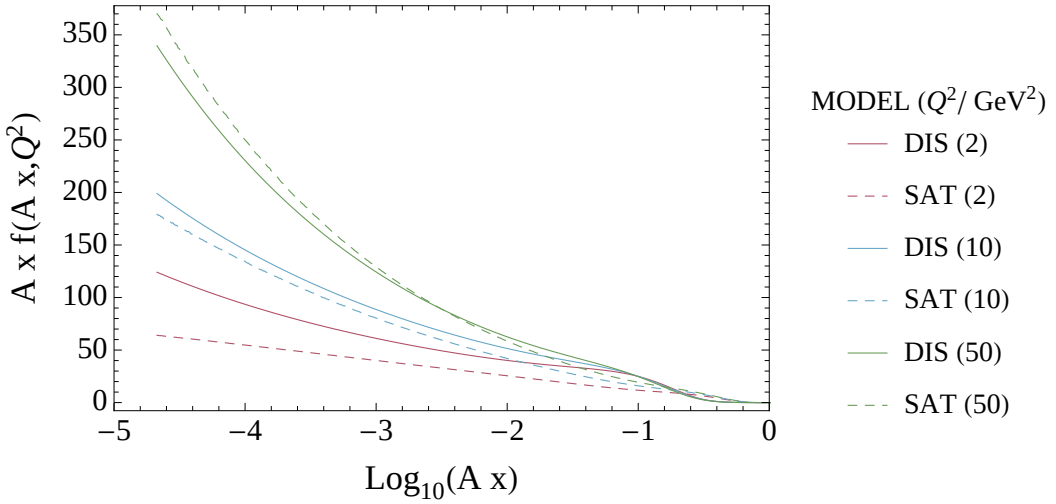

Fig. 5.6.: The parton distribution function $f_{q/A}(x, Q^2)$ for $\bar{\text{u}}$ quarks in a lead nucleus according to the HKNlo parton distributions [225] used in this work compared to the same distribution in the saturation model, Eq. ((5.50)). We plot $Axf_{q/A}(Ax, Q^2)$ versus $\log_{10}(Ax)$ for $Q^2 = 2\text{GeV}^2$, 10GeV^2, and 50GeV^2.

This is similar in structure to the corresponding DIS structure function in Eq. (5.34), and can be made to match with the identification,

$$x\, f_{q/A}(x, Q^2) = \frac{1}{\pi^4} \int d\boldsymbol{b} \int d\boldsymbol{\Delta}\, \frac{\Theta(\Delta > a/Q)}{\Delta^4}\, \Xi(\boldsymbol{b}, \boldsymbol{\Delta})\ . \tag{5.50}$$

Notice the careful accounting for a factor of two, arising from the sum over quark flavours in Eq. (5.49) compared to the sum over both flavours and anti-flavours in the DIS case, Eq. (5.34). The saturation version is flavour agnostic - the x dependence comes from the gluon PDF in the exponent contained in $\Xi(\boldsymbol{b}, \boldsymbol{\Delta})$. The inclusion of the cut on Δ in Eqns. (5.49) and (5.50) also serves to regulate the divergence from small Δ in the integral. Choosing $a = 2e^{1/6-\gamma_{\text{E}}} \approx 1.32657$ makes this cut equivalent to a $\overline{\text{MS}}$ renormalisation scheme (at one loop order).

Fig. 5.6 shows a comparison between the saturation and DIS models of the parton distribution functions. The approximation of Eq. (5.50) works well for Q^2 around $10\,\text{GeV}^2$ and reasonably for $Q^2 = 2\,\text{GeV}^2$. As Q^2 increases though, one expects the saturation model approximation to fail, as it does not include the effects of DGLAP evolution for the partons.

5.7 Application at E613

Having developed the formalism for a detailed treatment of dark particles scattering from nuclei in the toy model, constraints may now be placed upon the parameters of the model. The experiment under consideration throughout has been the Fermilab E613 beam dump. This was chosen as an example of a beam dump experiment with high beam energy (rivalled only by CHARM [239]). The detector of E613 was configured to count charged and neutral current neutrino events. The toy model introduced here produces scattering events that replicate neutrino neutral current events very closely. The collaboration estimated that the muonless neutral current events that the dark particles replicate appear with a maximum rate (at 90%C.L.) of 100 events per 10^{17} protons on target (POT) [240–242]. E613 featured 1.8×10^{17} POT, resulting in a maximum experimentally allowed number of dark particle events of $N_\psi = 180$ (to obtain 90%C.L. limits).

The mean free path of a dark particle passing through a material with nucleon number A is

$$\lambda = \frac{1}{\rho_A \sigma(\psi N \to \psi N)}. \tag{5.51}$$

ρ_A is the number density of nuclei, so all of the physics is contained within the nuclear scattering cross section, $\sigma(\psi N \to \psi N)$, the calculation of which is detailed above. From the mean free path, the probability of scattering in a length L of the material is straightforward to calculate,

$$P = \int_0^L dx \, \frac{1}{\lambda} e^{-\frac{x}{\lambda}} = 1 - e^{-\frac{L}{\lambda}} \tag{5.52}$$

Applying this to the geometry of E613 – a shielding region followed by a detector region – the predicted number of events in the detector is,

$$N_{det.} = \int dE \, (1 - P_{\text{shielding}}(E)) \times P_{\text{detector}}(E) \times \frac{dN}{dE}. \tag{5.53}$$

dN/dE is the differential production rate for dark particles at the dump, and includes geometric factors accounting for the shape and angular acceptance of the detector. The shielding region is approximately 15m long and composed of iron, being designed to stop or deflect charged particles with a magnetic field. A $1\,\text{GeV}$ infrared cut on the energy transfer required to constitute a scattering event in the shielding was imposed to cut-off the divergence of deep inelastic scattering. In the detector region, the corresponding cut is $20\,\text{GeV}$, but this has a physical origin – it is the trigger energy required to detect a jet

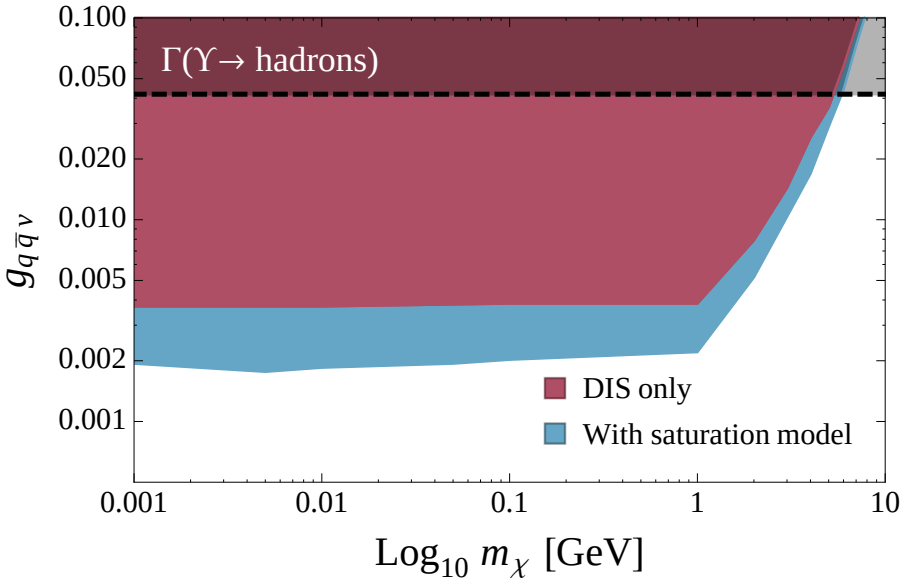

Fig. 5.7.: Exclusion regions for the leptophobic (toy) model with $m_V = 1\,\text{MeV}$. An additional constraint from Υ decays is also plotted [243]. See text for caveats to this plot.

in the scintillator. For the small couplings of interest, the scattering cross section in the shielding region is so small that practically no events are expected, and it could be accurately approximated that no scattering occurs there. Events are expected in the detector by virtue of the large proton flux at the beam dump; any given dark particle produced is unlikely to scatter in the apparatus at all. The calculation performed is complete, but degradation of the dark particle flux along the beam line is completely negligible, so the probability of a scatter can be approximated very simply as $P \sim L/\lambda$. To be conservative, we apply that any of the few particles that may scatter in the shielding region cannot continue to detection but are lost upon scattering.

We will apply our description of scattering to two similar BSM models, beginning with the toy Lagrangian in Eq. (5.1). In the first instance, we take the Lagrangian precisely as is, and derive constraints on the toy scenario, which is leptophobic. Next, we plot similar constraints for a minicharged particle scenario, where the mediator mass is taken to be zero, but the model is hidden photon inspired – the vector mediator can interact with leptons also. In practice, this does not affect our results, but does introduce many new constraints to the parameter space. The results for the leptophobic case are plotted in Fig. 5.7, where the mediator-dark particle coupling $g_{\psi\bar{\psi}v}$ is set at unity and the mediator mass is chosen to be $1\,\text{MeV}$. The two exclusion regions plotted in red and blue correspond to the DIS model alone (Section 5.5.1) and with the additional saturation model treatment (Section 5.5.2)

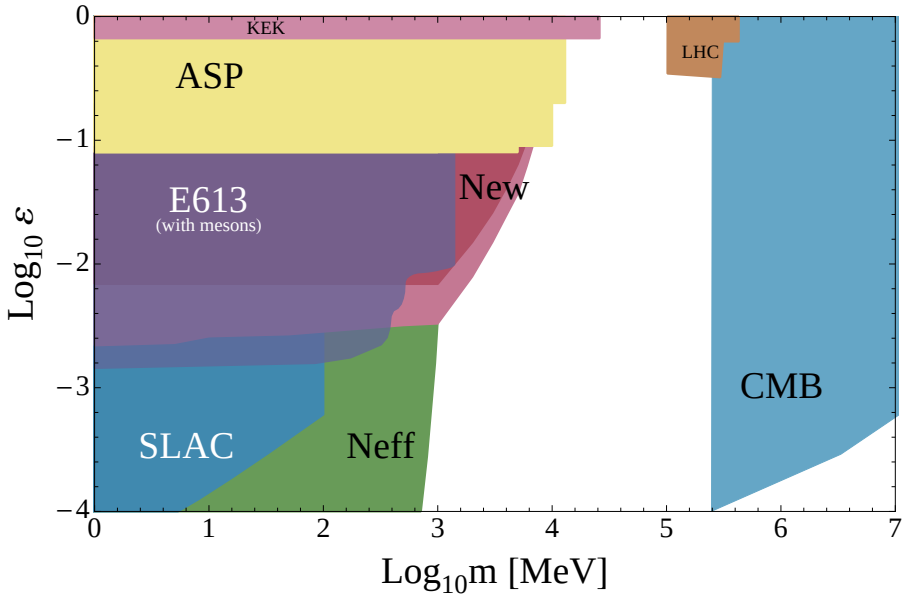

Fig. 5.8.: New limits on minicharged particles from E613 based on DIS only (dark red) and with saturation effects included (light red). Other constraints are shown, arising from colliders [247], a SLAC beam dump [248], the LHC [134], CMB [249, 250] and recent work on the number of light species, N_{eff} [251].

respectively. For the DIS only region, a hard cut on the four-momentum transfer squared was made to prevent the cross section diverging, $Q^2 > 1\text{GeV}^2$. We see that permitting this region (by using the dipole scattering picture) improves the constraint noticeably.

There are additional constraints that apply to this model [243–245]. The region labelled "$\Gamma(\Upsilon \to \text{hadrons})$" is a mapping of the constraint on a U(1) gauge boson which couples only to baryons to the model, and is derived from the upper limit on the new boson's contribution to the Upsilon decay width to hadrons. In fact, an extremely strong limit exists on a leptophobic vector boson mediator, arising from measurements of low-energy n-Pb scattering [246]. However, the strength of this constraint arises from a resonance structure around 1 MeV, and it rapidly dies off as the mass of the mediator changes from this value. Since we chose the value $m_v = 1\,\text{MeV}$ arbitrarily to stand in for a generically light, MeV-scale mediator, we can simply set the value to around $20\,\text{MeV}$ in order for the constraints in Fig. 5.7 to become novel again, without noticeably affecting the constraints plotted. The region excluded by Upsilon decay is relatively independent of the mediator mass up until GeV scales, at which point the importance of the low-Q^2 region diminishes in any case.

It seems natural, when considering such a light mediator mass, to ask what happens in the case that the limit is taken and the mass set strictly to zero. Doing so, in combination with allowing leptonic interactions of the vector mediator particle realizes a model of minicharge

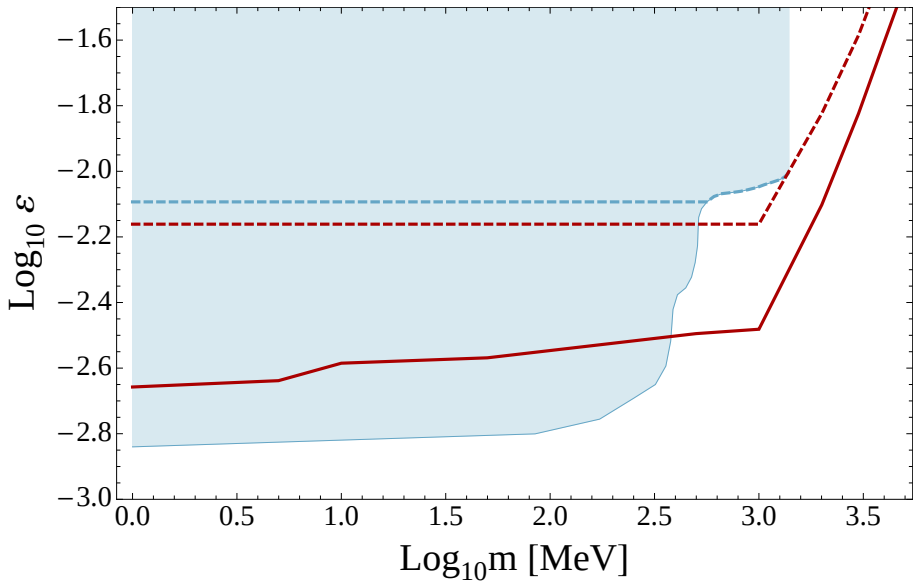

Fig. 5.9.: E613 constraints only. The blue shaded area shows a previously existing constraint [242]. The red lines represent the DIS only (dashed) and DIS plus saturation (solid) exclusion regions. The dashed blue line estimates the previous constraint without production from meson decays.

particles [85], introduced in Section 1.3.3. Recall that in such a scenario, the hidden sector fermion picks up an effective "mini" electric charge, $\epsilon = \chi g_h/e$, where χ is the kinetic mixing between the photon and the vector mediator and e is the unit electric charge. Since the production mechanism is Drell-Yan, i.e. quark annihilation, and the scattering is also from quarks, so the quark charges must also be accounted for in the cross section. The constraints arising from E613 on this model are plotted in Fig. 5.8. The dark red region corresponds to the DIS only treatment, with the same Q^2 cut as above, whereas the lighter red region also includes the saturation regime. In contrast to the previous plot, only a small novel area is ruled out by considering E613. There are several important considerations regarding this area. The first is that the competing constraint originating from the effective number of relativistic particle species N_{eff} is strong, but dependent on astrophysical measurements, which carry an intrinsic degree of uncertainty. While astrophysical limits are of course important, it is always beneficial to try to verify any limits in several complementary experiments. Either the limits agree and we gain confidence in our understanding, or they do not, and we learn something about one or more of the experimental environments. There are additional constraints from direct detection experiments if one asserts that minicharged particles constitute a given fraction of the dark matter relic density [252], which we do not.

In Fig. 5.9, we show constraints on minicharged particles derived only from the E613 experiment. The dashed and solid red lines correspond to the DIS and saturation enhanced constraints respectively. The light blue region shows the limits previously derived from the same experiment in [242]. The earlier constraint is significantly weaker than the saturation model limit for minicharged particle masses $m_\psi \gtrsim 500\,\text{MeV}$, but actually stronger for lower masses. The explanation is simple: since the focus of this work is an analysis of the scattering of dark particles, only Drell-Yan production was included, being simple to implement. For a more fully realistic simulation of the whole experiment in the context of a dark particle search (in either the leptophobic or minicharged scenario), production from meson decay must be included. This is by far the dominant production mechanism for sufficiently light $\mathcal{O}(100\text{MeV})$ dark particles from pp collisions, as reflected by the stronger constraints in Fig. 5.9. A rough estimate for the previous constraint without production via is shown as the dashed blue line. Clearly the saturation picture is a marked improvement over this, and it is to be expected that the full treatment would exceed the lower limit if all production mechanisms were included. The DIS-only result of the present work is consistent with the estimated earlier bound without meson decay, given the accuracy of approximations used in each analysis.

5.8 Conclusion

Motivated by dark matter searches at past and present beam dumps, we have investigated scattering in a context where DIS in no longer appropriate. We find that one can improve the experimental reach of beam dump experiments in the search for light dark matter by including non-perturbative scattering effects. This formalism should be applicable to a range of different dark matter and BSM models, with the importance of including the effect growing as the mediator mass decreases and the low-Q^2 region contributes more heavily to the cross-section.

6 Conclusion

> *"And this also," said Marlow suddenly, "has been one of the dark places of the earth."*
>
> **— Unnamed narrator**

This thesis has explored some aspects of the phenomenology of one or more species of light, weakly coupled particles, or WISPs, that provide a resolution to several of the outstanding theoretical (eg. strong CP problem) and observational (dark matter, a_μ anomaly) problems of particle physics. Let us briefly recap the common themes of the thesis.

6.1 The case for effective theories

Throughout the work, we have relied upon the framework of effective field theories in order to explore the potential of several models for new physics. Doing so acknowledges our ignorance of physics at energy scales to which we do not, and in the case of the highest scales likely never will, have access. However, we were nonetheless able to extract novel and informative results regarding hidden photons in a Kaluza-Klein scenario and the potential coupling of dark matter to Standard Model fermions through a pseudoscalar mediator.

Motivated by the principles of photon regeneration, or light-shining-through-walls, experiments, a test of one hereto unexplored aspect of effective field theories – the effective non-locality in the propagation of particles in an effective theory – was proposed. Our analysis suggests that while an experimental realisation of tunnelling of the third kind may be difficult in a quantum optical system, it is not beyond the realms of possibility, if a suitably narrow potential wall can be constructed, or if one considers transitions where the intermediate state is of lower energy than the initial state.

It is interesting that considerations that are principally concerned with a search for beyond the Standard Model physics led to an investigation of somewhat foundational ideas in quantum mechanics.

We nonetheless caution that effective field theories have a limited region of validity, and that there is a strong case for employing simple models in place of effective 4-point operators when quoting results at, for example, the LHC.

6.2 The case for WISPs

The search for dark matter has previously been focused largely on the WIMP paradigm, whereby the DM candidate is a thermal relic with a mass typically greater than $10\,\text{GeV}$. There is by now a strong case for the further exploration of the alternative, WISP, paradigm, whereby dark matter is composed of much lighter particles that have remained undetected by virtue of their extremely weak interactions. As we have seen, these particles can either form part or all of the relic density themselves, or mediate interactions to hidden sectors of particles, each perhaps having its own rich structure.

A single new species of light particle is not viable as a thermal relic, typically freezing out early and remaining too relativistic to allow for structure formation. Fortunately thermal production is not the only mechanism, and light dark matter is completely possible if produced by a misalignment mechanism. Alternatively, light dark matter may be thermally produced, if it interacts with the SM via a mediator particle whose couplings allow the correct cross- section to be obtained. Light, weakly coupled particles are in general less constrained than WIMPs – in particular traditional direct detection techniques are not suitable (though there is promising work in that direction). As such, there remain large areas of parameter space that can represent light dark matter, and it is encouraging to see increased experimental effort in these areas.

While the case for WISPs is strong, in Chapter 4, we constructed a simple model to illustrate that even WIMP dark matter could have thus far evaded all terrestrial detection efforts. This emphasises the requirement that we understand particle scattering at a coarse level. This point was developed in a much subtler way in Chapter 5, where we illustrated that low-Q^2 QCD effects can enhance exclusion constraints (equivalently discovery prospects) by understanding scattering at a much deeper level.

6.3 The case for the low energy frontier

Among the virtues of new light particle species is their accessibility via existing technology. In Chapters 3 and 5 it was demonstrated that relatively low energy apparatus can provide novel constraints on low mass particles. In the case of the hidden photon, higher energy facilities, such as the LHC, actually perform rather poorly by comparison. There is a clear case for high intensity experiments, and the work presented in Chapter 5 goes some way to exploring the potential of beam dump facilities by enhancing the existing formalism for dark particle scattering.

It is encouraging that intensity frontier experiments are receiving the attention warranted by their utility, and that dedicated runs are now in progress to search for light dark matter.

While any existing WISP has thus far evaded detection, a large and motivated community are invested in a continuing search. The field remains a promising avenue of research, to which this thesis represents a small, but hopefully significant, addition.

A

The origin of kinetic mixing

Here we'll present a worked example derivation of the origin of kinetic mixing. From an initially SU(2)×U(1) theory with two fermions, we break the SU(2) symmetry with an adjoint representation of a Higgs field. The remnant U(1) symmetry of the broken SU(2) then mixes kinetically with the original U(1) gauge group by the combination of the two fermion loop diagrams. This is not a unique origin or derivation, but does contain all the features necessary to result in an effective Lagrangian for kinetic mixing.

The Lagrangian of the SU(2)×U(1) field theory we begin with is [253, 254],

$$\mathcal{L} = -\frac{1}{4}G^{a,\mu\nu}G^{a}_{\mu\nu} - \frac{1}{2}D^{\mu}\varphi^{a}D_{\mu}\varphi^{a} - V\left((\varphi^{a})^{2}\right) - \frac{1}{4}F^{\mu\nu}F_{\mu\nu} - \frac{1}{2M}\varphi^{a}G^{a,\mu\nu}F_{\mu\nu}. \tag{A.1}$$

It is the final term that will lead to kinetic mixing after the spontaneous breaking of SU(2)→U(1). The fermions in the theory obey,

$$\mathcal{L}_{\Psi} = i\bar{\Psi}_{i}\gamma_{\mu}D^{\mu}_{ij}\Psi_{j} - m_{0}\bar{\Psi}\Psi - h\varphi^{a}\bar{\Psi}_{i}t^{a}_{ij}\Psi_{j}. \tag{A.2}$$

where the covariant derivative is $D^{\mu}_{ij} = (\partial^{\mu}\mathbf{1}_{ij} + ig_{1}A^{\mu}\mathbf{1}_{ij} + ig_{2}W^{a,\mu}t^{a}_{ij})$, with g_1 and g_2 the couplings to the original U(1) and the SU(2) respectively. The final term is a Yukawa coupling of the Higgs field to the fermions, with coupling constant h. $t^{a} = \sigma^{a}/2$ are the generators of SU(2), where the Pauli matrices are,

$$\sigma_{1} = \begin{pmatrix} 0 & 1 \\ 1 & 0 \end{pmatrix}, \quad \sigma_{2} = \begin{pmatrix} 0 & -i \\ i & 0 \end{pmatrix}, \quad \sigma_{3} = \begin{pmatrix} 1 & 0 \\ 0 & -1 \end{pmatrix}. \tag{A.3}$$

If the adjoint Higgs acquires a vacuum expectation value $\langle\varphi^{a}\rangle = (0, 0, v)$, by virtue of a suitable potential, $V \sim (\varphi^{a}\varphi^{a} - v^{2})^{2}$, then the fermion masses are determined by the matrix equation,

$$m_{0}\begin{pmatrix} 1 & 0 \\ 0 & 1 \end{pmatrix} + \frac{hv}{2}\begin{pmatrix} 1 & 0 \\ 0 & -1 \end{pmatrix}. \tag{A.4}$$

The spontaneous breaking of the SU(2) symmetry also gives rise to masses for the $W_\mu^{1,2}$ gauge fields. There is a remaining unbroken U(1) symmetry associated with the W_μ^3 field under which both fermions are charged. The first fermion has charge $+1$ and the second -1. However, both fermions are equally charged under the U(1) symmetry associated with A_μ, and so they realise precisely the requirements for kinetic mixing. The final term in Eq. (A.1) is the result of a loop calculation involving the two fermions $\Psi_{1,2}$. From that calculation, one finds [253],

$$\frac{1}{M} = \frac{g_1 g_2}{6\pi^2} \log\left(\frac{m_0 + hv/2}{m_0 - hv/2}\right) \approx \frac{ef}{6\pi^2}\frac{h}{m_0}, \tag{A.5}$$

where in the last equality we have expanded to leading order in $hv \ll m_0$.

B

Deriving the tunnelling probability in T3K

Here we present a schematic of the prescription for calculating the energy gap $\delta E = \Pi_{AA} - \Pi_{SS}$ in second order perturbation theory. We change from our left/right basis to a symmetric/anti-symmetric basis: $|1\rangle \equiv |\mathrm{sym}, 0\gamma\rangle$, $|2\rangle \equiv |\mathrm{anti}, 0\gamma\rangle$, $|3\rangle \equiv |b, 1\gamma\rangle$, $|4\rangle \equiv |b, 0\gamma\rangle$, $|5\rangle \equiv |\mathrm{sym}, 1\gamma\rangle$, $|6\rangle \equiv |\mathrm{anti}, 1\gamma\rangle$. The symmetric/antisymmetric basis is defined $|\mathrm{sym}, 0\gamma\rangle = \frac{1}{\sqrt{2}}(|a, L, 0\rangle + |a, R, 0\rangle)$ and $|\mathrm{anti}, 0\gamma\rangle = \frac{1}{\sqrt{2}}(|a, L, 0\rangle - |a, R, 0\rangle)$. We can rewrite the tunnelling probability in terms of the new basis (dropping the numeric prefactor for notational elegance – we will reinsert it later), in the notation of Section 2.2.2,

$$\begin{aligned} P_{T3K} &= |\langle a, R, 0\,|e^{-i\mathcal{H}t}|a, L, 0\rangle|^2 \\ &= |\langle \mathrm{sym}, 0\gamma|e^{-i\mathcal{H}t}|\mathrm{sym}, 0\gamma\rangle - \langle \mathrm{anti}, 0\gamma|e^{-i\mathcal{H}t}|\mathrm{anti}, 0\gamma\rangle|^2 \\ &= |\langle 1^{(0)}|e^{-i\mathcal{H}t}|1^{(0)}\rangle - \langle 2^{(0)}|e^{-i\mathcal{H}t}|2^{(0)}\rangle|^2 \end{aligned} \tag{B.1}$$

The mode number j indexing the energy levels of the infinite potential well has been inserted as a superscript. The zero mode states are not eigenstates of $\mathcal{H}$, so some trickery is in order. We may perturbatively expand the eigenstates to second order in the parameter λ:

$$\begin{aligned} |1\rangle &= |1^{(0)}\rangle + \lambda\left(\frac{V_{31}}{E_{13}}|3^{(0)}\rangle\right) - \lambda^2\left(\frac{V_{13}V_{31}}{2(E_{13})^2}|1^{(0)}\rangle\right) \\ |2\rangle &= |2^{(0)}\rangle + \lambda\left(\frac{V_{32}}{E_{23}}|3^{(0)}\rangle\right) - \lambda^2\left(\frac{V_{23}V_{32}}{2(E_{23})^2}|2^{(0)}\rangle\right) \\ |3\rangle &= |3^{(0)}\rangle + \lambda\left(\frac{V_{13}}{E_{31}}|1^{(0)}\rangle + \frac{V_{23}}{E_{32}}|2^{(0)}\rangle\right) - \lambda^2\left(\frac{V_{31}V_{13}}{2(E_{31})^2} + \frac{V_{32}V_{23}}{2(E_{32})^2}\right)|3^{(0)}\rangle \end{aligned}$$

where $V_{nm} \equiv \langle n^{(0)}|V|m^{(0)}\rangle$ is the interacting (off diagonal) part of the Hamiltonian and $E_{nm} \equiv E_n^{(0)} - E_m^{(0)}$. We can iteratively rearrange the above expressions for the zeroth order perturbation states (r.h.s.) in terms of the exact eigenstates of the Hamiltonian (l.h.s.). The

eigenvalues of $\mathcal{H}$ are the perturbatively corrected (to second order) energies for the states $|1,2,3\rangle$:

$$\mathcal{E}_1/\hbar = \omega_a + \frac{\tilde{g}^2_{\mathrm{sym},0\gamma}}{2(\omega_a - (\omega_b + \omega_c))} \tag{B.2}$$

$$\mathcal{E}_2/\hbar = \omega_a + \frac{\tilde{g}^2_{\mathrm{anti},0\gamma}}{2(\omega_a - (\omega_b + \omega_c))} \tag{B.3}$$

$$\mathcal{E}_3/\hbar = \omega_b + \omega_c - \frac{\tilde{g}^2_{\mathrm{sym},0\gamma}}{2(\omega_a - (\omega_b + \omega_c))} - \frac{\tilde{g}^2_{\mathrm{anti},0\gamma}}{2(\omega_a - (\omega_b + \omega_c))}. \tag{B.4}$$

Reinserting the expansions of the eigenvectors of $\mathcal{H}$ in terms of the zeroth order states makes performing the contractions trivial. We define $\Delta = \omega_b + \omega_c - \omega_a$ for simplicity. Then with some rearrangement (and inserting a factor of 1/4 for the change to the symmetric-antisymmetric basis which has so far been ignored), to lowest order in $\delta\omega^2$:

$$P_{T3K} = \frac{1}{4}\left|\left(1 + \frac{\tilde{g}^2_{\mathrm{sym}}}{2\Delta^2}\right) e^{i\frac{\tilde{g}^2_{\mathrm{sym}} - \tilde{g}^2_{\mathrm{anti}}}{2\Delta}t} - \left(1 + \frac{\tilde{g}^2_{\mathrm{anti}}}{2\Delta^2}\right) + \frac{(\tilde{g}^2_{\mathrm{sym}} - \tilde{g}^2_{\mathrm{anti}})}{2\Delta^2} e^{-i\Delta t} e^{i\frac{\tilde{g}^2_{\mathrm{sym}}}{2\Delta}t}\right|^2 \tag{B.5}$$

Importantly this agrees with the earlier naive estimate Eq. (2.18), to leading order in $\tilde{g}^2$. The dominating factor in the tunnelling probability is the argument of the first exponent, precisely $E_{\mathrm{anti}} - E_{\mathrm{sym}} = \Pi_{AA} - \Pi_{SS}$. We have the form of the overlap integrals $\tilde{g}_{\mathrm{sym/anti}}$ in Eq. (2.15). Recall that the width of each of the coupled wells is ℓ and that the solutions to the Schödinger equation for such a setup are of the form $\varphi_n(x) = \sqrt{\frac{2}{\ell}}\sin\left(\frac{n\pi x}{\ell}\right)$. Here n is the mode number which for the intermediate state of our system (ie. $\ell \to 2\ell + d$) must be summed over. The overlap integral is

$$\tilde{g} = \frac{1}{\sqrt{2}}\sqrt{\frac{2}{2\ell + d}}\sqrt{\frac{2}{\ell}}\left(\int_{-\ell-\frac{d}{2}}^{-\frac{d}{2}} dx \cos\left(\frac{n\pi x}{2\ell + d}\right)\sin\left(\frac{\pi\left(x + \ell + \frac{d}{2}\right)}{\ell}\right)\right.$$
$$\left. - \cos(n\pi)\int_{\frac{d}{2}}^{\ell+\frac{d}{2}} dx \cos\left(\frac{n\pi x}{2\ell + d}\right)\sin\left(\frac{\pi\left(x - \frac{d}{2}\right)}{\ell}\right)\right) \tag{B.6}$$

It turns out that the symmetric and antisymmetric parts may be consolidated into a single sum over all n as the even and odd cavity modes alternately pick up only the antisymmetric and symmetric parts respectively (this is how the integral is presented above). This sum can be performed by multiplying the resulting function (from the overlap integral) by $\pi\mathrm{cosec}(n\pi)$ and applying residue theorem. The poles arise from the zeroes of Δ.

This procedure results in the expression (2.21).

C

Annihilation amplitudes

Scalar

For a scalar mediated interaction, the amplitude for pair annihilation, $\bar{\psi}\psi \to f^+f^-$, with initial state momenta p_1, p_2 and final state momenta k_1, k_2 is,

$$i\mathcal{M} = \bar{u}(k_1)v(k_2)(-ig'_{\rm DM})\frac{i}{q^2 - m_\phi^2}(-ig'_f)u(p_1)\bar{v}(p_2), \tag{C.1}$$

so that,

$$|\mathcal{M}|^2 = \frac{g'^2_{\rm DM}g'^2_f}{(q^2 - m_\phi^2)^2}(\bar{u}(p_1)u(p_1))(\bar{v}(p_2)v(p_2))(\bar{u}(k_1)u(k_1))(\bar{v}(k_2)v(k_2)). \tag{C.2}$$

Taking the spin sum and average, we get,

$$\begin{aligned}\frac{1}{4}\sum_{\rm spins}|\mathcal{M}|^2 &= \frac{g'^2_{\rm DM}g'^2_f}{4(q^2 - m_\phi^2)^2}{\rm Tr}[(\not{p}_1 + m_\psi)(\not{p}_2 - m_f)]{\rm Tr}[(\not{k}_1 + m_\psi)(\not{k}_2 - m_f)] \\ &= \frac{4g'^2_{\rm DM}g'^2_f}{(q^2 - m_\phi^2)^2}(p_1\cdot p_2 - m_{\rm DM}^2)(k_1\cdot k_2 - m_f^2).\end{aligned} \tag{C.3}$$

Formally, one can calculate the amplitude by using non-relativistic spinors. However one can see the velocity suppression by simply expanding the scalar product of the incoming DM particle momenta and taking the non-relativistic limit. In the c.o.m. frame of the annihilating dark matter (i.e. $\cos(\theta) = -1$),

$$p_1\cdot p_2 = E_1E_2 + |\vec{p}_1||\vec{p}_2| \tag{C.4}$$

In the non-relativistic limit, we can use the Newtonian expression for momentum $|\vec{p}_{1,2}| = p \to m_{\rm DM}v$, $E_{1,2} = E \to m_{\rm DM}^2 + p^2 = m_{\rm DM}^2(1+v^2)$, with v the WIMP velocity in the c.o.m. frame. Reinserting this to the amplitude, we see the velocity suppression already at the amplitude level,

$$\frac{1}{4}\sum_{\rm spins}|\mathcal{M}|^2 = \frac{4v^2g'^2_{\rm DM}g'^2_f}{(q^2 - m_\phi^2)^2}(k_1\cdot k_2 - m_f^2). \tag{C.5}$$

Pseudoscalar

Now in the pseudoscalar mediated case the calculation proceeds precisely as for scalars, but there are additional factors of γ_5, which enter the trace in the squared matrix element as,

$$\begin{aligned}\frac{1}{4}\sum_{\text{spins}}|\mathcal{M}|^2 &= \frac{g_{\rm DM}^2 g_f^2}{4(q^2-m_a^2)^2}\text{Tr}[(\not{p}_1+m_\psi)\gamma_5(\not{p}_2-m_f)\gamma_5]\text{Tr}[(\not{k}_1+m_\psi)\gamma_5(\not{k}_2-m_f)\gamma_5] \\ &= \frac{4g_{\rm DM}^2 g_f^2}{(q^2-m_a^2)^2}(-p_1\cdot p_2-m_a^2)(-k_1\cdot k_2-m_f^2). \end{aligned} \tag{C.6}$$

The commutation relations of Dirac matrices mean that additional prefactors of minus one are picked up before the scalar products of the momenta. In the scalar case, the non-relativistic limit resulted in $(p_1\cdot p_2 - m_{\rm DM}^2)\to v^2$. With the additional negative however there remain terms that are not velocity suppressed, $-(p_1\cdot p_2+m_{\rm DM}^2)\to -m_{\rm DM}(2+v^2)$, leading to,

$$\frac{1}{4}\sum_{\text{spins}}|\mathcal{M}|^2 = \frac{4v^2 g_{\rm DM}'^2 g_f'^2}{(q^2-m_\phi^2)^2}(k_1\cdot k_2+m_f^2)+\frac{8m_{\rm DM}^2 g_{\rm DM}'^2 g_f'^2}{(q^2-m_\phi^2)^2}(k_1\cdot k_2+m_f^2). \tag{C.7}$$

Even in the limit $v\sim 10^{-3}$, there is a contribution from the v-independent second term, so annihilation of Dirac fermions through a pseudoscalar channel is not velocity suppressed[1].

From the above amplitudes, the annihilation cross section can be obtained via the formula (e.g. [199]),

$$d\sigma = \frac{1}{2E_1 2E_2|v_1-v_2|}\left(\prod_f \frac{d^3k_f}{(2\pi)^3}\frac{1}{2E_f}\right)\times|\mathcal{M}(p_1,p_2\to\{k_f\})|^2(2\pi)^4\delta^{(4)}(p_1+p_2-\sum k_f). \tag{C.8}$$

The phase space factor takes on a simple form in the case that the final state is two body, as is the case for pair annihilation of dark matter into two SM fermions here,

$$\left(\prod_f\int\frac{d^3k_f}{(2\pi)^3}\right)(2\pi)^4\delta^{(4)}(p_1+p_2-\sum k_f) = \int\frac{d\Sigma_{\rm cm}}{4\pi}\frac{1}{8\pi}\left(\frac{2|\vec{p}|}{E_{\rm cm}}\right). \tag{C.9}$$

[1] Aside: notice that neither the scalar nor pseudoscalar amplitude contains cross-terms in the incoming and outgoing momenta - (pseudo)scalar mediated scattering is isotropic! By contrast, vector mediated scattering is not. (For an explicit example, see, e.g., Bhabha scattering in Ch. 5 of [199]).

Bibliography

[1] Simon A. Gardiner, Holger Gies, Joerg Jaeckel, and Chris J. Wallace. *Europhys.Lett.* 101 (2013), p. 61001. arXiv: 1204.4802 [quant-ph].

[2] Céline Boehm, Matthew J. Dolan, Christopher McCabe, Michael Spannowsky, and Chris J. Wallace. *JCAP* 1405 (2014), p. 009. arXiv: 1401.6458 [hep-ph].

[3] Joerg Jaeckel, Sabyasachi Roy, and Chris J. Wallace (2014). arXiv: 1408.0019 [hep-ph].

[4] Davison E. Soper, Michael Spannowsky, Chris J. Wallace, and Tim M. P. Tait. *Phys.Rev.* D90 (2014), p. 115005. arXiv: 1407.2623 [hep-ph].

[5] Georges Aad et al. *Phys.Lett.* B716 (2012), pp. 1–29. arXiv: 1207.7214 [hep-ex].

[6] Serguei Chatrchyan et al. *Phys.Lett.* B716 (2012), pp. 30–61. arXiv: 1207.7235 [hep-ex].

[7] K.A. Olive et al. *Chin.Phys.* C38 (2014), p. 090001.

[8] P.A.R. Ade et al. *Astron.Astrophys.* (2014). arXiv: 1303.5076 [astro-ph.CO].

[9] G.W. Bennett et al. *Phys.Rev.* D73 (2006), p. 072003. arXiv: hep-ex/0602035 [hep-ex].

[10] Gerard Jungman, Marc Kamionkowski, and Kim Griest. *Phys.Rept.* 267 (1996), pp. 195–373. arXiv: hep-ph/9506380 [hep-ph].

[11] Kim Griest and David Seckel. *Phys. Rev. D* 43 (10 May 1991), pp. 3191–3203.

[12] P. J. McMillan and J. J. Binney. *MNRAS* 402 (Feb. 2010), pp. 934–940. arXiv: 0907.4685 [astro-ph.GA].

[13] Katherine Freese, Mariangela Lisanti, and Christopher Savage. *Rev.Mod.Phys.* 85 (2013), pp. 1561–1581. arXiv: 1209.3339 [astro-ph.CO].

[14] P. Salucci, F. Nesti, G. Gentile, and C. Frigerio Martins. *Astronomy & Astrophysics* 523 (Nov. 2010), A83.

[15] Fabio Iocco, Miguel Pato, Gianfranco Bertone, and Philippe Jetzer. *Journal of Cosmology and Astroparticle Physics* 2011.11 (Nov. 2011), pp. 029–029.

[16] Gianfranco Bertone, Dan Hooper, and Joseph Silk. *Physics Reports* 405.5-6 (Jan. 2005), pp. 279–390.

[17] J.D. Lewin and P.F. Smith. *Astroparticle Physics* 6.1 (Dec. 1996), pp. 87–112.

[18] Akerib D. S., H. M. Araújo, X. Bai, et al. *Physical Review Letters* 112.9 (Mar. 2014), p. 091303.

[19]C.E. Aalseth et al. (2014). arXiv: 1401.3295 [astro-ph.CO].

[20]R. Bernabei, P. Belli, F. Cappella, V. Caracciolo, S. Castellano, et al. *Eur.Phys.J.* C73 (2013), p. 2648. arXiv: 1308.5109 [astro-ph.GA].

[21]Z. Ahmed et al. *FERMILAB-PUB-12-102-AE* (2012). arXiv: 1203.1309 [astro-ph.CO].

[22]G. Angloher, M. Bauer, I. Bavykina, et al. *The European Physical Journal C* 72.4 (Apr. 2012), p. 1971.

[23]Josef Pradler, Balraj Singh, and Itay Yavin. *Phys.Lett.* B720 (2013), pp. 399–404. arXiv: 1210.5501 [hep-ph].

[24]Jonathan H. Davis. *Phys.Rev.Lett.* 113 (2014), p. 081302. arXiv: 1407.1052 [hep-ph].

[25]R. Bernabei, P. Belli, F. Cappella, V. Caracciolo, R. Cerulli, et al. (2012). arXiv: 1210.6199 [hep-ph].

[26]Josef Pradler and Itay Yavin. *Phys.Lett.* B723 (2013), pp. 168–171. arXiv: 1210.7548 [hep-ph].

[27]R. Bernabei, P. Belli, F. Cappella, V. Caracciolo, R. Cerulli, et al. (2012). arXiv: 1211.6346 [hep-ph].

[28]R. Bernabei, P. Belli, F. Cappella, V. Caracciolo, R. Cerulli, et al. (2014). arXiv: 1409.3516 [hep-ph].

[29]Rouven Essig, Aaron Manalaysay, Jeremy Mardon, Peter Sorensen, and Tomer Volansky. *Physical Review Letters* 109.2 (July 2012), p. 021301.

[30]P. Cushman, C. Galbiati, D.N. McKinsey, H. Robertson, T.M.P. Tait, et al. (2013). arXiv: 1310.8327 [hep-ex].

[31]J. Angle et al. *Phys.Rev.Lett.* 107 (2011), p. 051301. arXiv: 1104.3088 [astro-ph.CO].

[32]E. Aprile, M. Alfonsi, K. Arisaka, et al. *Physical Review Letters* 109.18 (Nov. 2012), p. 181301.

[33]E. Aprile et al. *Phys.Rev.Lett.* 107 (2011), p. 131302. arXiv: 1104.2549 [astro-ph.CO].

[34]M. Felizardo, T. Morlat, A.C. Fernandes, T.A. Girard, J.G. Marques, et al. *Phys.Rev.Lett.* 105 (2010), p. 211301. arXiv: 1003.2987 [astro-ph.CO].

[35]E. Behnke et al. *Phys.Rev.* D86 (2012), p. 052001. arXiv: 1204.3094 [astro-ph.CO].

[36]C.E. Aalseth et al. *Phys.Rev.* D88.1 (2013), p. 012002. arXiv: 1208.5737 [astro-ph.CO].

[37]R. Bernabei, P. Belli, F. Cappella, et al. *The European Physical Journal C* 67.1-2 (Mar. 2010), pp. 39–49.

[38]R. Agnese, Z. Ahmed, A. Anderson, et al. *Physical Review Letters* 111.25 (Dec. 2013), p. 251301.

[39]R. Agnese et al. *Phys.Rev.* D88 (2013), p. 031104. arXiv: 1304.3706 [astro-ph.CO].

[40]Z. Ahmed et al. *Science* 327 (2010), pp. 1619–1621. arXiv: 0912.3592 [astro-ph.CO].

[41]Z. Ahmed et al. *Phys.Rev.Lett.* 106 (2011), p. 131302. arXiv: 1011.2482 [astro-ph.CO].

[42]R. Agnese et al. *Phys.Rev.Lett.* 112.24 (2014), p. 241302. arXiv: 1402.7137 [hep-ex].

[43]E. Aprile et al. *Phys.Rev.Lett.* 111.2 (2013), p. 021301. arXiv: 1301.6620 [astro-ph.CO].

[44]S. Archambault et al. *Phys.Lett.* B711 (2012), pp. 153–161. arXiv: 1202.1240 [hep-ex].

[45]D.S. Akerib et al. *Phys.Rev.* D73 (2006), p. 011102. arXiv: astro-ph/0509269 [astro-ph].

[46]M.G. Aartsen et al. *Phys.Rev.Lett.* 110.13 (2013), p. 131302. arXiv: 1212.4097 [astro-ph.HE].

[47]Esra Bulbul, Maxim Markevitch, Adam Foster, Randall K. Smith, Michael Loewenstein, et al. *Astrophys.J.* 789 (2014), p. 13. arXiv: 1402.2301 [astro-ph.CO].

[48]Celine Boehm, Dan Hooper, Joseph Silk, Michel Casse, and Jacques Paul. *Phys.Rev.Lett.* 92 (2004), p. 101301. arXiv: astro-ph/0309686 [astro-ph].

[49]Lisa Goodenough and Dan Hooper. *FERMILAB-PUB-09-494-A* (2009). arXiv: 0910.2998 [hep-ph].

[50]Christoph Weniger. *JCAP* 1208 (2012), p. 007. arXiv: 1204.2797 [hep-ph].

[51]Oscar Adriani et al. *Nature* 458 (2009), pp. 607–609. arXiv: 0810.4995 [astro-ph].

[52]G.W. Fraser, A.M. Read, S. Sembay, J.A. Carter, and E. Schyns. *MNRAS 445, 2146-2168* (2014).

[53]V. Barger, K. Hagiwara, J. Woodside, and W. Y. Keung. *Phys. Rev. Lett.* 53 (7 Aug. 1984), pp. 641–643.

[54]E.W.N. Glover, A.D. Martin, and M.R. Pennington. *Physics Letters B* 153.45 (1985), pp. 330 –334.

[55]Lawrence J. Hall and Ann.E. Nelson. *Physics Letters B* 153.6 (1985), pp. 430 –432.

[56]Georges Aad et al. *CERN-PH-EP-2014-245* (2014). arXiv: 1411.1559 [hep-ex].

[57]Vardan Khachatryan et al. *CMS-EXO-12-047, CERN-PH-EP-2014-253* (2014). arXiv: 1410.8812 [hep-ex].

[58]JD Bjorken, Rouven Essig, Philip Schuster, and Natalia Toro. *Physical Review D* 1.1 (2009). arXiv: arXiv:0906.0580v1.

[59]Brian Batell, Maxim Pospelov, and Adam Ritz. *Physical Review D* March 2009 (2009). arXiv: arXiv:0903.0363v1.

[60]Sarah Andreas. *Frascati Phys.Ser.* 56 (2012), pp. 23–32. arXiv: 1212.4520 [hep-ph].

[61]Patrick DeNiverville, Maxim Pospelov, and Adam Ritz. *Physical Review D* 84.7 (Oct. 2011), p. 075020.

[62]Patrick DeNiverville, David McKeen, and Adam Ritz. *Physical Review D* 86.3 (Aug. 2012), p. 035022.

[63]J.L. Hewett, H. Weerts, K.S. Babu, et al. *Snowmass Report* (2013).

[64]Jessica Goodman, Masahiro Ibe, Arvind Rajaraman, et al. *Physical Review D* 82.11 (Dec. 2010), p. 116010.

[65]CMS Collaboration. *CMS-EXO-12-048, CERN-PH-EP-2014-164* (2014). arXiv: 1408.3583 [hep-ex].

[66]ATLAS Collaboration. *ATLAS-CONF-2012-147, ATLAS-COM-CONF-2012-190* (2012).

[67]O. Buchmueller, Matthew J. Dolan, and Christopher McCabe. *Journal of High Energy Physics* 2014.1 (Jan. 2014), p. 25.

[68] Sarah Malik, Christopher McCabe, Henrique Araujo, A. Belyaev, Celine Boehm, et al. *KCL-PH-TH-2014-37, LCTS-2014-36, CERN-PH-TH-2014-180* (2014). arXiv: 1409.4075 [hep-ex].

[69] Philip Harris, Valentin V. Khoze, Michael Spannowsky, and Ciaran Williams (2014). arXiv: 1411.0535 [hep-ph].

[70] Matthew R. Buckley, David Feld, and Dorival Goncalves (2014). arXiv: 1410.6497 [hep-ph].

[71] K Dienes. *Nuclear Physics B* 492.1-2 (May 1997), pp. 104–118.

[72] Steve A Abel and B W Schofield. *Nuclear Physics B* 685 (2004), pp. 150–170.

[73] S.A. Abel, M.D. Goodsell, J. Jaeckel, V.V. Khoze, and A. Ringwald. *JHEP* 0807 (2008), p. 124. arXiv: 0803.1449 [hep-ph].

[74] Mark Goodsell, Joerg Jaeckel, Javier Redondo, and Andreas Ringwald. *JHEP* 0911 (2009), p. 027. arXiv: 0909.0515 [hep-ph].

[75] Mark Goodsell. *DESY-09-228* (2009), pp. 165–168. arXiv: 0912.4206 [hep-th].

[76] Mathew Bullimore, Joseph P. Conlon, and Lukas T. Witkowski. *JHEP* 1011 (2010), p. 142. arXiv: 1009.2380 [hep-th].

[77] Mark Goodsell and Andreas Ringwald. *Fortsch.Phys.* 58 (2010), pp. 716–720. arXiv: 1002.1840 [hep-th].

[78] Mark Goodsell, Saul Ramos-Sanchez, and Andreas Ringwald. *JHEP* 1201 (2012), p. 021. arXiv: 1110.6901 [hep-th].

[79] Michele Cicoli, Mark Goodsell, Joerg Jaeckel, and Andreas Ringwald. *JHEP* 1107 (2011), p. 114. arXiv: 1103.3705 [hep-th].

[80] R. Essig, J. A. Jaros, W. Wester, et al. *Snowmass Report, arXiv:1311.0029 [astro-ph, physics:hep-ex, physics:hep-ph]* (2013). arXiv: 1311.0029.

[81] R. D. Peccei and Helen R. Quinn. *Phys. Rev. Lett.* 38 (25 June 1977), pp. 1440–1443.

[82] R. D. Peccei and Helen R. Quinn. *Phys. Rev. D* 16 (6 Sept. 1977), pp. 1791–1797.

[83] L.B. Okun. *Sov.Phys.JETP* 56 (1982), p. 502.

[84] Peter Galison and Aneesh Manohar. *Physics Letters B* 136.4 (Mar. 1984), pp. 279–283.

[85] Bob Holdom. *Physics Letters B* 166.2 (Jan. 1986), pp. 196–198.

[86] Andre Lukas and K.S. Stelle. *JHEP* 0001 (2000), p. 010. arXiv: hep-th/9911156 [hep-th].

[87] Ralph Blumenhagen, Gabriele Honecker, and Timo Weigand. *JHEP* 0506 (2005), p. 020. arXiv: hep-th/0504232 [hep-th].

[88] Steven A. Abel, Joerg Jaeckel, Valentin V. Khoze, and Andreas Ringwald. *Phys.Lett.* B666 (2008), pp. 66–70. arXiv: hep-ph/0608248 [hep-ph].

[89] Steve A Abel, Joerg Jaeckel, Valya V Khoze, and Andreas Ringwald. *Physics Letters B* 666.1 (2008), pp. 66–70.

[90] Jonathan J. Heckman and Cumrun Vafa. *Phys.Rev.* D83 (2011), p. 026006. arXiv: 1006.5459 [hep-th].

[91]Michele Cicoli, Mark Goodsell, Joerg Jaeckel, and Andreas Ringwald. *JHEP* 1107 (2011), p. 114. arXiv: 1103.3705 [hep-th].

[92]Markus Ahlers, Joerg Jaeckel, Javier Redondo, and Andreas Ringwald. *Phys.Rev.* D78 (2008), p. 075005. arXiv: 0807.4143 [hep-ph].

[93]Markus Ahlers, Joerg Jaeckel, Javier Redondo, and Andreas Ringwald. *Phys.Rev.* D78 (2008), p. 075005. arXiv: 0807.4143 [hep-ph].

[94]Alessandro Melchiorri, Antonello Polosa, and Alessandro Strumia. *Phys.Lett.* B650 (2007), pp. 416–420. arXiv: hep-ph/0703144 [hep-ph].

[95]Brian Patt and Frank Wilczek (2006). arXiv: hep-ph/0605188 [hep-ph].

[96]Sarah Andreas, Thomas Hambye, and Michel H.G. Tytgat. *JCAP* 0810 (2008), p. 034. arXiv: 0808.0255 [hep-ph].

[97]Christoph Englert, Tilman Plehn, Dirk Zerwas, and Peter M. Zerwas. *Phys.Lett.* B703 (2011), pp. 298–305. arXiv: 1106.3097 [hep-ph].

[98]Henri Ruegg and Martí Ruiz-Albata (2003). arXiv: 0304245v2 [arXiv:hep-th].

[99]Maxim Pospelov, Adam Ritz, and Mikhail B. Voloshin. *Physics Letters B* 662 (Nov. 2008), pp. 53–61. arXiv: 0711.4866.

[100]Celine Bœhm and Pierre Fayet. *Nuclear Physics B* 683 (May 2004), pp. 219–263. arXiv: 0305261 [hep-ph].

[101]Brian Batell, Maxim Pospelov, and Adam Ritz. *Physical Review D* 80.9 (Nov. 2009), p. 095024.

[102]Brian Batell, Patrick deNiverville, David McKeen, Maxim Pospelov, and Adam Ritz (2014). arXiv: 1405.7049 [hep-ph].

[103]B. W. Lee and S. Weinberg. *Physical Review Letters* 39 (July 1977), pp. 165–168.

[104]Alexey Golovnev, Viatcheslav Mukhanov, and Vitaly Vanchurin. *JCAP* 0806 (2008), p. 009. arXiv: 0802.2068 [astro-ph].

[105]Alexey Golovnev. *Class.Quant.Grav.* 28 (2011), p. 245018. arXiv: 1109.4838 [gr-qc].

[106]Paola Arias, Davide Cadamuro, Mark Goodsell, et al. *Journal of Cosmology and Astroparticle Physics* (2012). arXiv: arXiv:1201.5902v1.

[107]Joerg Jaeckel. *Frascati Phys.Ser.* 56 (2012), pp. 172–192. arXiv: 1303.1821 [hep-ph].

[108]B Lakić, M Arik, S Aune, et al. *Journal of Physics: Conference Series* 375.2 (July 2012), p. 022001.

[109]Javier Redondo. *JCAP* 0807 (2008), p. 008. arXiv: 0801.1527 [hep-ph].

[110]Sergei N. Gninenko and Javier Redondo. *Physics Letters B* 664.3 (June 2008), pp. 180–184.

[111]Haipeng An, Maxim Pospelov, and Josef Pradler. *Physics Letters B* (2013). arXiv: arXiv:1302.3884v2.

[112]Javier Redondo and Georg Raffelt. *JCAP* 1308 (2013), p. 034. arXiv: 1305.2920 [hep-ph].

[113]Joerg Jaeckel, Javier Redondo, and Andreas Ringwald. *Physical Review Letters* 101.13 (Sept. 2008), p. 131801.

[114]Javier Redondo (2010). arXiv: 1002.0447 [hep-ph].

[115]James B. Dent, Francesco Ferrer, and Lawrence M. Krauss (2012). arXiv: 1201.2683 [astro-ph.CO].

[116]Pieter van Dokkum, Marijn Franx, Mariska Kriek, Bradford Holden, Garth Illingworth, et al. *Astrophys.J.* 677 (2008), pp. L5–L8. arXiv: 0802.4094 [astro-ph].

[117]Ann E Nelson and Jakub Scholtz. *Physical Review D* 84 (May 2011), p. 16. arXiv: 1105.2812.

[118]Alfred Scharff Goldhaber and Michael Martin Nieto. *Reviews of Modern Physics* 82.1 (Mar. 2010), pp. 939–979.

[119]Javier Redondo and Andreas Ringwald. *Contemporary Physics* 52.3 (May 2011), pp. 211–236.

[120]M. Betz, F. Caspers, M. Gasior, and M. Thumm (2012), pp. 76–81. arXiv: 1204.4370 [physics.ins-det].

[121]Babette Döbrich (2013). arXiv: 1309.3965 [physics.ins-det].

[122]Babette Dobrich, Holger Gies, Norman Neitz, and Felix Karbstein. *Phys.Rev.* D87 (2013), p. 025022. arXiv: 1203.4986 [hep-ph].

[123]Joerg Jaeckel and Andreas Ringwald. *Physics Letters B* 659.3 (Jan. 2008), pp. 509–514.

[124]Stephen R. Parker, John G. Hartnett, Rhys G. Povey, and Michael E. Tobar. *Phys.Rev.* D88 (2013), p. 112004. arXiv: 1410.5244 [hep-ex].

[125]M. Betz, F. Caspers, M. Gasior, M. Thumm, and S.W. Rieger. *Phys.Rev.* D88.7 (2013), p. 075014. arXiv: 1310.8098 [physics.ins-det].

[126]Peter W. Graham, Jeremy Mardon, Surjeet Rajendran, and Yue Zhao. *Phys.Rev.* D90.7 (2014), p. 075017. arXiv: 1407.4806 [hep-ph].

[127]E. Armengaud, F.T. Avignone, M. Betz, P. Brax, P. Brun, et al. *JINST* 9 (2014), T05002. arXiv: 1401.3233 [physics.ins-det].

[128]John N. Bahcall, Aldo M. Serenelli, and Sarbani Basu. *The Astrophysical Journal* 621.1 (Mar. 2005), pp. L85–L88.

[129]Sarah Andreas, Carsten Niebuhr, and Andreas Ringwald. *Phys.Rev.* D86 (2012), p. 095019. arXiv: 1209.6083 [hep-ph].

[130]Matthew Reece and Lian-Tao Wang. *JHEP* 0907 (2009), p. 051. arXiv: 0904.1743 [hep-ph].

[131]Rouven Essig, Philip Schuster, Natalia Toro, and Bogdan Wojtsekhowski. *JHEP* 1102 (2011), p. 009. arXiv: 1001.2557 [hep-ph].

[132]S. Abrahamyan et al. *Phys.Rev.Lett.* 107 (2011), p. 191804. arXiv: 1108.2750 [hep-ex].

[133]H. Merkel et al. *Phys.Rev.Lett.* 106 (2011), p. 251802. arXiv: 1101.4091 [nucl-ex].

[134]Joerg Jaeckel, Martin Jankowiak, and Michael Spannowsky. *Physics of the Dark Universe* 2.3 (Sept. 2013), pp. 111–117.

[135]H Yüksel and MD Kistler. *Physical Review D* (2008), pp. 1–6. arXiv: arXiv:0711.2906v2.

[136]Javier Redondo and Marieke Postma. *Journal of Cosmology and Astroparticle Physics* (2009), pp. 1–25. arXiv: arXiv:0811.0326v1.

[137]S. G. Karshenboim. *Physical Review Letters* 104.22 (June 2010), p. 220406.

[138]S. G. Karshenboim. *Physical Review D* 82.7 (Oct. 2010), p. 073003.

[139]Joerg Jaeckel and Sabyasachi Roy. *Physical Review D* 82.12 (Dec. 2010), p. 125020.

[140]E.R. Williams, J.E. Faller, and H.A. Hill. *Phys.Rev.Lett.* 26 (1971), pp. 721–724.

[141]D.F. Bartlett and S. Loegl. *Phys.Rev.Lett.* 61 (1988), pp. 2285–2287.

[142]Vsevolod Popov. *Turk. J. Phys* 23 (1999), pp. 943–950.

[143]R. Dharmapalan et al. *FERMILAB-PROPOSAL-1032* (2012). arXiv: 1211.2258 [hep-ex].

[144]Kronfeld, Andreas S. and Tschirhart, Robert S. and Al-Binni, Usama and Altmannshofer, Wolfgang and Ankenbrandt, Charles and others (2013). Ed. by Andreas S. Kronfeld. arXiv: 1306.5009 [hep-ex].

[145]Sabyasachi Roy. PhD thesis. Durham University, 2013.

[146]H. Georgi. *Ann.Rev.Nucl.Part.Sci.* 43 (1993), pp. 209–252.

[147]Markus Ahlers, Joerg Jaeckel, and Andreas Ringwald. *Phys.Rev.* D79 (2009), p. 075017. arXiv: 0812.3150 [hep-ph].

[148]Babette Döbrich, Holger Gies, Norman Neitz, and Felix Karbstein. *Physical Review Letters* 109.13 (Sept. 2012), p. 131802.

[149]Holger Gies and Joerg Jaeckel. *arXiv.org* hep-ph (2009).

[150]E. K. Irish. *Physical Review Letters* 99.17, 173601 (Oct. 2007), p. 173601. arXiv: 0706.2087 [quant-ph].

[151]A. Kurcz, A. Capolupo, A. Beige, E. Del Giudice, and G. Vitiello. *Physical Review A* 81.6, 063821 (June 2010), p. 063821. arXiv: 0909.5337 [cond-mat.other].

[152]J. M. Raimond, C. Sayrin, S. Gleyzes, et al. *Physical Review Letters* 105.21, 213601 (Nov. 2010), p. 213601. arXiv: 1007.4942 [quant-ph].

[153]Theodor Kaluza. *Sitzungsber.Preuss.Akad.Wiss.Berlin (Math.Phys.)* 1921 (1921), pp. 966–972.

[154]Oskar Klein. *Z.Phys.* 37 (1926), pp. 895–906.

[155]Nima Arkani-Hamed, Savas Dimopoulos, and G.R. Dvali. *Phys.Rev.* D59 (1999), p. 086004. arXiv: hep-ph/9807344 [hep-ph].

[156]Nima Arkani-Hamed, Savas Dimopoulos, and G.R. Dvali. *Phys.Lett.* B429 (1998), pp. 263–272. arXiv: hep-ph/9803315 [hep-ph].

[157]Ignatios Antoniadis, Nima Arkani-Hamed, Savas Dimopoulos, and G.R. Dvali. *Phys.Lett.* B436 (1998), pp. 257–263. arXiv: hep-ph/9804398 [hep-ph].

[158]Lisa Randall and Raman Sundrum. *Phys.Rev.Lett.* 83 (1999), pp. 4690–4693. arXiv: hep-th/9906064 [hep-th].

[159]Lisa Randall and Raman Sundrum. *Phys.Rev.Lett.* 83 (1999), pp. 3370–3373. arXiv: hep-ph/9905221 [hep-ph].

[160]Lisa Randall and Raman Sundrum. *Nucl.Phys.* B557 (1999), pp. 79–118. arXiv: hep-th/9810155 [hep-th].

[161]Kristian L. McDonald and David E. Morrissey. *JHEP* 1102 (2011), p. 087. arXiv: 1010.5999 [hep-ph].

[162]Kristian L. McDonald and David E. Morrissey. *JHEP* 1005 (2010), p. 056. arXiv: 1002.3361 [hep-ph].

[163]V.H. Satheeshkumar and P.K. Suresh. *Adv.Astron.* 2011 (2011), p. 189379. arXiv: hep-th/0606194 [hep-th].

[164]Fermi-LAT Collaboration, Baldini L. Ajello M., and et. al. Barbiellini G. *JCAP* 2, 012 (Feb. 2012), p. 12. arXiv: 1201.2460 [astro-ph.HE].

[165]E.G. Adelberger, Blayne R. Heckel, and A.E. Nelson. *Ann.Rev.Nucl.Part.Sci.* 53 (2003), pp. 77–121. arXiv: hep-ph/0307284 [hep-ph].

[166]C.D. Hoyle, D.J. Kapner, Blayne R. Heckel, E.G. Adelberger, J.H. Gundlach, et al. *Phys.Rev.* D70 (2004), p. 042004. arXiv: hep-ph/0405262 [hep-ph].

[167]ATLAS Collaboration. *Journal of High Energy Physics* 2013.4 (Apr. 2013), p. 75.

[168]CMS Collaboration. *Journal of High Energy Physics* 2012.9 (Sept. 2012), p. 94.

[169]Maxim Pospelov. *Phys.Rev.* D80 (2009), p. 095002. arXiv: 0811.1030 [hep-ph].

[170]Hooman Davoudiasl, Hye-Sung Lee, and William J. Marciano. *Phys.Rev.* D86 (2012), p. 095009. arXiv: 1208.2973 [hep-ph].

[171]Motoi Endo, Koichi Hamaguchi, and Go Mishima. *Phys.Rev.* D86 (2012), p. 095029. arXiv: 1209.2558 [hep-ph].

[172]G.G. Raffelt. 1996.

[173]Demos Kazanas, Rabindra N. Mohapatra, Shmuel Nussinov, Vigdor L. Teplitz, and Yongchao Zhang. *Nucl.Phys.* B890 (2015), p. 17. arXiv: 1410.0221 [hep-ph].

[174]J.P. Lees et al. *Phys.Rev.Lett.* 113.20 (2014), p. 201801. arXiv: 1406.2980 [hep-ex].

[175]D. Babusci, D. Badoni, I. Balwierz-Pytko, et al. *Physics Letters B* 720.1-3 (Mar. 2013), pp. 111–115.

[176]Anthony Fradette, Maxim Pospelov, Josef Pradler, and Adam Ritz. *Physical Review D* 90.3 (Aug. 2014), p. 035022.

[177]H. Weldon. *Phys. Rev. D* 28 (8 Oct. 1983), pp. 2007–2015.

[178]Eric Braaten and Daniel Segel. *Physical Review D* January (1993). arXiv: 9302213v1 [arXiv:hep-ph].

[179]Hendrik A. Kramers. *Phil. Mag.* 46 (1923), p. 836.

[180]G. Weidenspointner, M. Varendorff, U. Oberlack, D. Morris, S. Plueschke, et al. *AIP Conf.Proc.* 510 (2004), pp. 581–585. arXiv: astro-ph/0012332 [astro-ph].

[181]E. Churazov, R. Sunyaev, M. Revnivtsev, S. Sazonov, S. Molkov, et al. *Astron.Astrophys.* 467 (2007), p. 529. arXiv: astro-ph/0608250 [astro-ph].

[182]P. Sreekumar et al. *Astrophys.J.* 494 (1998), pp. 523–534. arXiv: astro-ph/9709257 [astro-ph].

[183]A.W. Strong, I.V. Moskalenko, and O. Reimer. *Astrophys.J.* 613 (2004), pp. 956–961. arXiv: astro-ph/0405441 [astro-ph].

[184]Manuel Drees, Herbi Dreiner, Daniel Schmeier, Jamie Tattersall, and Jong Soo Kim (2013). arXiv: 1312.2591 [hep-ph].

[185]A L Read. *Journal of Physics G: Nuclear and Particle Physics* 28.10 (Oct. 2002), pp. 2693–2704.

[186]Matteo Cacciari, Gavin P Salam, and Gregory Soyez. *Journal of High Energy Physics* 2008.04 (Apr. 2008), pp. 063–063.

[187]Matteo Cacciari and Gavin P. Salam. *Physics Letters B* 641.1 (Sept. 2006), pp. 57–61.

[188]Matteo Cacciari, Gavin P. Salam, and Gregory Soyez. *The European Physical Journal C* 72.3 (Mar. 2012), p. 1896.

[189]J. de Favereau, C. Delaere, P. Demin, et al. *Journal of High Energy Physics* 2014.2 (Feb. 2014), p. 57.

[190]Manuel Bähr, Stefan Gieseke, Martyn A. Gigg, et al. *The European Physical Journal C* 58.4 (Nov. 2008), pp. 639–707.

[191]Adam Alloul, Neil D. Christensen, Céline Degrande, Claude Duhr, and Benjamin Fuks. *Computer Physics Communications* 185.8 (Aug. 2014), pp. 2250–2300.

[192]Johan Alwall, Michel Herquet, Fabio Maltoni, Olivier Mattelaer, and Tim Stelzer. *Journal of High Energy Physics* 2011.6 (June 2011), p. 128.

[193]Céline Degrande, Claude Duhr, Benjamin Fuks, et al. *Computer Physics Communications* 183.6 (June 2012), pp. 1201–1214.

[194]ATLAS Collaboration. *ATLAS-CONF-2013-017, ATLAS-COM-CONF-2013-010* (2013).

[195]J. Balewski, J. Bernauer, W. Bertozzi, J. Bessuille, B. Buck, et al. (2013). arXiv: 1307.4432.

[196]Andrea for the HPS Collaboration Celentano. *J.Phys.Conf.Ser.* 556.1 (2014), p. 012064.

[197]Chiara Arina, Eugenio Del Nobile, and Paolo Panci (2014). arXiv: 1406.5542 [hep-ph].

[198]Andi Hektor and Luca Marzola. *Phys.Rev.* D90 (2014), p. 053007. arXiv: 1403.3401 [hep-ph].

[199]Michael Edward Peskin and Daniel V Schroeder. Westview Press, 1995, p. 842.

[200]Jason Kumar and Danny Marfatia. *Phys.Rev.* D88.1 (2013), p. 014035. arXiv: 1305.1611 [hep-ph].

[201]Paolo Gondolo and Graciela Gelmini. *Nucl.Phys.* B360 (1991), pp. 145–179.

[202]Oscar Macias and Chris Gordon. *Physical Review D* 89.6 (Mar. 2014), p. 063515.

[203]Dan Hooper, Ilias Cholis, Tim Linden, Jennifer M. Siegal-Gaskins, and Tracy R. Slatyer. *Physical Review D* 88.8 (Oct. 2013), p. 083009.

[204]Chris Gordon and Oscar Macías. *Physical Review D* 88.8 (Oct. 2013), p. 083521.

[205]Marco Cirelli, Gennaro Corcella, Andi Hektor, et al. *JCAP* 1103 (2011), p. 051.

[206]Torbjörn Sjöstrand, Stephen Mrenna, and Peter Skands. *Computer Physics Communications* 178.11 (June 2008), pp. 852–867.

[207]Joachim Kopp, Thomas Schwetz, and Jure Zupan. *Journal of Cosmology and Astroparticle Physics* 2010.02 (Feb. 2010), pp. 014–014.

[208]Hai-Yang Cheng and Cheng-Wei Chiang. *Journal of High Energy Physics* 2012.7 (July 2012), p. 9.

[209]D.C. Malling, D.S. Akerib, H.M. Araujo, X. Bai, S. Bedikian, et al. (2011). arXiv: 1110.0103 [astro-ph.IM].

[210]P. Klos, J. Menéndez, D. Gazit, and A. Schwenk. *Physical Review D* 88.8 (Oct. 2013), p. 083516.

[211]Christopher McCabe. *Journal of Cosmology and Astroparticle Physics* 2014.02 (Feb. 2014), pp. 027–027.

[212]Marat Freytsis and Zoltan Ligeti. *Physical Review D* 83.11 (June 2011), p. 115009.

[213]The ATLAS collaboration. *ATLAS-CONF-2013-048, ATLAS-COM-CONF-2013-056* (2013).

[214]The ATLAS collaboration. *ATLAS-CONF-2013-047, ATLAS-COM-CONF-2013-049* (2013).

[215]The ATLAS collaboration. *ATLAS-CONF-2012-104, ATLAS-COM-CONF-2012-143* (2012).

[216]The ATLAS collaboration. *ATLAS-CONF-2013-035, ATLAS-COM-CONF-2013-042* (2013).

[217]Ulrich Haisch, Felix Kahlhoefer, and James Unwin. *Journal of High Energy Physics* 2013.7 (July 2013), p. 125.

[218]Dieter Schildknecht. *Mod.Phys.Lett.* A29 (2014), p. 1430028.

[219]R. Keith Ellis, W. James Stirling, and B.R. Webber. *Camb.Monogr.Part.Phys.Nucl.Phys.Cosmol.* 8 (1996).

[220]I. Abt et al. *Phys.Lett.* B321 (1994), pp. 161–167.

[221]N. N. Nikolaev and B. G. Zakharov. *Zeitschrift für Physik C Particles and Fields* 49.4 (Dec. 1991), pp. 607–618.

[222]K Golec-Biernat and M Wüsthoff. *Physical Review D* 59 (1998), pp. 1–10.

[223]K Golec-Biernat and M Wüsthoff. *Physical Review D* 60 (1999), p. 114023.

[224]a.H. Mueller. *Nuclear Physics B* 558.1-2 (Oct. 1999), pp. 285–303.

[225]M. Hirai, S. Kumano, and T.-H. Nagai. *Physical Review C* 76.6 (Dec. 2007), p. 065207.

[226]L. Frankfurt and M. Strikman. *Physical Review D* 55.1 (Jan. 1997), pp. 98–104.

[227]J. Forshaw, G. Kerley, and G. Shaw. *Physical Review D* 60.7 (Sept. 1999), p. 074012.

[228]M. McDermott, L. Frankfurt, V. Guzey, and M. Strikman. *The European Physical Journal C* 16.4 (Sept. 2000), pp. 641–656.

[229]E Gotsman, E Levin, M Lublinsky, et al. *Journal of Physics G: Nuclear and Particle Physics* 27.11 (Nov. 2001), pp. 2297–2323.

[230]AH Mueller. *QCD Perspectives on Hot and Dense Matter* (2002), pp. 1–35. arXiv: 0111244v1 [arXiv:hep-ph].

[231]Krzysztof J. Golec-Biernat. *Acta Phys.Polon.* B35 (2004), pp. 3103–3114.

[232]K. Golec-Biernat. *Nuclear Physics A* 755 (June 2005), pp. 133–142.

[233]Prithwish Tribedy and Raju Venugopalan. *Nucl.Phys.* A850 (2011), pp. 136–156.

[234]A. Luszczak and H. Kowalski. *Physical Review D* 89.7 (Apr. 2014), p. 074051.

[235]F Hautmann and DE Soper. *Physical Review D* (2007). arXiv: 0702077v1 [arXiv:hep-ph].

[236]J. Bartels, K. Golec-Biernat, and H. Kowalski. *Physical Review D* 66.1 (June 2002), p. 014001.

[237]M.V.T. Machado. *The European Physical Journal C* 47.2 (May 2006), pp. 365–373.

[238]K. Golec-Biernat and M. Wüsthoff. *Physical Review D* 59.1 (Nov. 1998), p. 014017.

[239]K. De Winter et al. *Nucl. Instr. Meth.* A278 (1989), p. 670.

[240]T.A. Romanowski. *Acta Phys.Polon.* B16 (1985), pp. 179–193.

[241]M. Duffy, G. Fanourakis, R. Loveless, et al. *Physical Review D* 38.7 (Oct. 1988), pp. 2032–2055.

[242]E. Golowich and R. Robinett. *Physical Review D* 35.1 (Jan. 1987), pp. 391–393.

[243]Christopher Carone and Hitoshi Murayama. *Physical Review Letters* 74.16 (Apr. 1995), pp. 3122–3125.

[244]Christopher Carone and Hitoshi Murayama. *Physical Review D* 52.1 (July 1995), pp. 484–493.

[245]Sean Tulin. *Phys.Rev.* D89 (2014), p. 114008. arXiv: 1404.4370 [hep-ph].

[246]H. Leeb and J. Schmiedmayer. *Phys.Rev.Lett.* 68 (1992), pp. 1472–1475.

[247]S. Davidson, B. Campbell, and D. Bailey. *Physical Review D* 43.7 (Apr. 1991), pp. 2314–2321.

[248]A. Prinz, R. Baggs, J. Ballam, et al. *Physical Review Letters* 81.6 (Aug. 1998), pp. 1175–1178.

[249]A. Dolgov, S. Dubovsky, G. Rubtsov, and I. Tkachev. *Physical Review D* 88.11 (Dec. 2013), p. 117701.

[250]S. L. Dubovsky, D. S. Gorbunov, and G. I. Rubtsov. *Journal of Experimental and Theoretical Physics Letters* 79.1 (Jan. 2004), pp. 1–5.

[251]Hendrik Vogel and Javier Redondo. *Journal of Cosmology and Astroparticle Physics* 2014.02 (Feb. 2014), pp. 029–029.

[252]Chris Kouvaris and Ian M. Shoemaker. *Phys.Rev.* D90.9 (2014), p. 095011. arXiv: 1405.1729 [hep-ph].

[253]Felix Brummer and Joerg Jaeckel. *Phys.Lett.* B675 (2009), pp. 360–364. arXiv: 0902.3615 [hep-ph].

[254]Felix Brummer, Joerg Jaeckel, and Valentin V. Khoze. *JHEP* 0906 (2009), p. 037. arXiv: 0905.0633 [hep-ph].

List of Figures